Final Report

On

POLYMER CONCRETE JOINTS FOR PRECAST BRIDGE ELEMENTS IN ACCELERATED CONSTRUCTION

Sammelan Pokharel, MS

Mohamed A. Moustafa, PhD, PE

University of Nevada, Reno

University of Nevada, Reno
Department of Civil and Environmental Engineering, MS 258
1664 N. Virginia St.
Reno, NV 89557

Final Report Submitted to the New Mexico Department of Transportation (NMDOT)
under Contract No. C06415

December 2025

ABSTRACT

Accelerated Bridge Construction (ABC) relies on prefabricated bridge element systems (PBES) to reduce construction time and minimize traffic disruption. In such systems, closure joints play a critical role in ensuring structural continuity and long-term durability. Conventional cementitious closure materials often require extended curing times and may be susceptible to cracking, shrinkage, and durability-related degradation, which can compromise accelerated construction objectives. This study evaluates the feasibility of polymer concrete (PC) as an alternative closure joint material for longitudinal joints in prefabricated slab bridges.

A comprehensive experimental program was conducted in four interconnected phases to assess the mechanical, bond, thermal, and structural performance of PC under conditions representative of field applications. Phase I focused on material-level characterization of six commercially available polymer concrete products representing four polymer classes, including epoxy-based, polyester-based, polymethyl methacrylate (PMMA), and polyvinyl ester (PVE) systems. Test results demonstrated rapid early-age strength development across all PC types, with more than 50% of ultimate compressive strength and stiffness achieved within the first 24 hours. Among the evaluated materials, PMMA-PC and PVE-PC consistently exhibited higher compressive strength and modulus of elasticity compared to epoxy- and polyester-based systems.

Phase II investigated bond behavior between selected PC types and both reinforcing steel and conventional concrete. Direct pullout tests and flexural tests of spliced beams were performed to evaluate reinforcement development and splice performance. Results indicated that adequate bond strength and reinforcement development could be achieved within relatively short embedment lengths, particularly for PMMA-PC and PVE-PC. Surface preparation and primer application were found to significantly enhance bond performance at the PC–conventional

concrete interface.

Phase III evaluated the residual mechanical and bond properties of PC after exposure to thermal cycling and subzero temperatures. Test results demonstrated that PMMA-PC and PVE-PC retained satisfactory strength, stiffness, and bond performance following thermal exposure, indicating resilience under temperature variations relevant to bridge environments.

Phase IV assessed the structural behavior of large-scale prefabricated slab bridge specimens incorporating PC closure joints. Specimens were tested under realistic loading configurations to evaluate load transfer, stiffness response, cracking behavior, and water leakage. PC closure joints demonstrated structural performance comparable to conventional ultra-high-performance concrete joints, with failure governed by flexural behavior of the precast slabs rather than joint failure. Water leakage performance further highlighted the superior bond characteristics of PMMA-PC and PVE-PC systems.

Overall, the findings establish polymer concrete—particularly PMMA- and PVE-based systems—as a viable closure joint material for prefabricated slab bridges. The study provides experimental evidence supporting the use of performance-based material specifications, rational splice detailing, and construction practices necessary for successful field implementation in accelerated bridge construction.

TABLE OF CONTENTS

LIST OF TABLES

LIST OF FIGURES

LIST OF ACRONYMS

ABC: Accelerated Bridge Construction

ABC-UTC: Accelerated Bridge Construction – University Transportation Center

AASHTO: American Association of State Highway and Transportation Officials

ACI: American Concrete Institute

ASTM: ASTM International

ASCE: American Society of Civil Engineers

CA: Coarse Aggregate

CC: Conventional Concrete

CS: Compressive Strength

CTE: Coefficient of Thermal Expansion

DBT: Deck Bulb Tee

DOT: Department of Transportation

DSC: Differential Scanning Calorimeter

EPC: Epoxy Polymer Concrete

FA: Fine Aggregate

FHWA: Federal Highway Administration

HSS: High-Strength Steel

LRFD: Load and Resistance Factor Design

LVDT: Linear Variable Differential Transformer

MEKP: Methyl Ethyl Ketone Peroxide

MOE: Modulus of Elasticity

MOR: Modulus of Rupture

NMDOT: New Mexico Department of Transportation

PBES: Prefabricated Bridge Element System

PC: Polymer Concrete

PL: Proprietary Liquid

PMMA: Polymethyl Methacrylate

PMMA-PC: Polymethyl Methacrylate Polymer Concrete

PPC: Polyester Polymer Concrete

PUPC: Polyurethane Polymer Concrete

PVE: Polyvinyl Ester

PVE-PC: Polyvinyl Ester Polymer Concrete

T_g: Glass Transition Temperature

T55: Thermal Shock Cycling Between 55 °C and 0 °C

T110: Thermal Shock Cycling Between 110 °C and 0 °C

T-25: Constant Exposure at −25 °C

UHPC: Ultra-High Performance Concrete

UNR: University of Nevada, Reno

1 INTRODUCTION

1.1 Prefabricated Bridge Element System: Background and Problem Statement

According to the National Bridge Inventory and 2021 Infrastructure Report card by the American Society of Civil Engineers, 42% of the bridges in the United States are over 50 years old, which has increased from 39% in 2016. In addition to that, the same reports also state that 12% of highway bridges are over 80 years old, and the rate of reduction of structurally deficient bridges has been 0.1% annually in the past couple of years. Apart from these structurally deficient bridges, the same reports also claim that more than 94,000 bridges in the United States are functionally obsolete due to reasons like insufficient clearance and deficient road geometry [1], [2] .Structural and functional deficiencies in this many bridges, accompanied by the low rate of reconstruction or rehabilitation, have been a major challenge for bridge engineers. The number of structurally deficient bridges raises safety questions, while functionally deficient bridges have incurred a huge social cost, like increased traffic congestion. This problem has been further exacerbated by increased traffic flow every year.

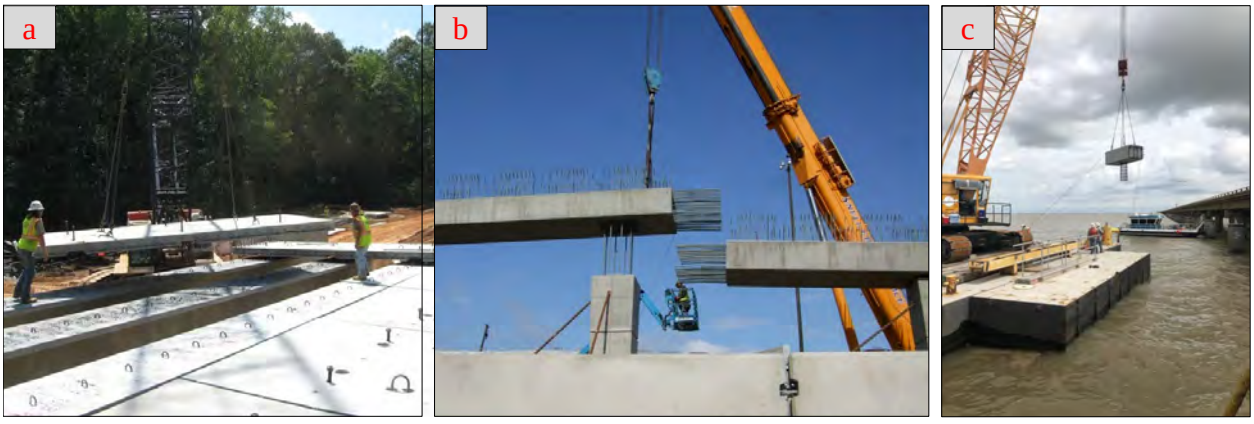

Figure 1.1. a-c) Prefabricated bridge deck, beam and bent cap being installed, respectively. “Courtesy of ABC-UTC”

In order to tackle this precarious situation, bridge engineers and researchers have been

trying to reduce the construction time and cost. One of the effective ways implemented for the construction of reinforced and prestressed concrete that has already been implemented in the past couple of decades is the use of the Prefabricated Bridge Element System (PBES). PBES is an innovative technology of bridge construction in which the elements of a bridge are constructed in a factory setting away from the bridge installation location and then transported and joined to one another on the site as shown in Figure 1.1. This system of bridge construction has numerous technical, economic, and social advantages. Technical advantages include reduced on-site construction time, high-quality control in the industrial construction setting, and improved safety due to minimization of exposure to construction hazards. Economically, this method saves construction costs by saving labor expenses. In addition to that, many Departments of Transportation are trying to use standard concrete sections similar to standard steel sections, which has opened the possibility of mass production of those standard concrete sections, ultimately leading to reduced construction costs. Socially, the PBES minimizes the public inconvenience of traffic congestion because of the reduced construction time.

A major problem that inherently arises in PBES construction is that the prefabricated bridge elements must be joined in the construction site and those joints form the weakest points in the structure. The durability and the overall structural performance of the bridge depend on the robustness of the joints. So, to ensure that, most of the recent bridge constructions with PBES use Ultra-High-Performance Concrete (UHPC), which has superior mechanical properties and durability, as the joint material. However, using UHPC comes with several challenges during the procurement, mixing, curing, and quality control phases. UHPC has high material and labor costs. Due to its steel fiber content, it must be mixed significantly longer than conventional concrete in a high-shear mixture. Although performed previously, the mixing process of UHPC in traditional

ready-mix concrete trucks has been found to be challenging due to the segregation of fibers. Additionally, the use of UHPC in very cold weather has also been found to be difficult due to crusting issues.

1.2 Slab-Type Bridges and PBES Alternative

Slab bridge is one of the simplest types of concrete bridges that have been used for a long time. In this type of bridge, the slab itself works as the primary load-carrying member and it does not have any additional beams or girders, which reduces the complexity of design and construction, ultimately reducing the cost. They are generally used in small to medium spans, typically ranging from 30 ft to 50 ft [3], where they are found to be most economical. However, some DOTs further limit their application at 35 ft [4]. Construction of slab bridges also has its demerits similar to all cast in situ bridge construction practices, like longer construction time, more on-site labor, lengthier disruption to traffic etc. In order to avoid those shortcomings, a PBES alternative to traditional slab bridges has been adopted by NMDOT, in which smaller panels of slabs, designed for easier installation and transportation, are prefabricated and joined together on site in either transverse direction, longitudinal direction, or both. This type of bridge is called “slab girder bridge” as shown in Figure 1.2 and the joint between the adjacent slabs is called closure joint.

Figure 1.2. Slab girder bridge construction in the United Kingdom [5]

As discussed earlier, similar to other prefabricated bridge construction, slab girder bridges have similar inherent drawbacks. With an inappropriate material used for the closure joint, longitudinal and transverse cracks can be formed along the joints between the slab panels. These cracks reduce the durability of the bridge by seepage of water into the joint reinforcement. More importantly, after the formation of these cracks, the load transfer mechanism between the slab panels is compromised. Once this occurs, the structural system transitions from the composite behavior, where live loads are distributed across the structure, to non-composite behavior, where the individual slabs are required to resist the live loads. Since the slabs are not designed to carry entirety of the live load independently, the overall load carrying capacity of the bridge decreases and necessitate load posting on the bridge.

In this context, this report primarily assesses the feasibility of using polymer concrete as a closure joint material for prefabricated bridge elements, with a major focus on its application as a closure joint material for longitudinal joints in slab girder bridges.

1.3 Polymer Concrete: Types and Selection

Polymer concrete is a matrix of fine and coarse aggregate bound together by polymer resin instead of cement paste in conventional concrete. Another major difference between polymer concrete and conventional cement-based concrete is that the hardening of conventional concrete is due to the hydration of cement while the hardening of polymer resin in PC is due to the reaction of the resin monomer with a hardener, which is also sometimes called an initiator. Various types of polymer resin are being used in polymer concrete and based on the primary chemical composition of the resins PC can be differentiated as polymethyl methacrylate polymer concrete (PMMA-PC), poly vinyl ester polymer concrete (PVE-PC), polyester polymer concrete (PPC), epoxy polymer concrete (EPC), polyurethane polymer concrete (PUPC) etc.

For this research study, commercially available PMMA-PC, PVE-PC, PPC and EPC were selected for use after carefully reviewing the literature and current practices of departments of transportation. These selected PCs are being used as bridge deck overlay material by various departments of transportation. The existing familiarity of various DOTs with these PCs is expected to facilitate the potential future application of PCs as closure joint material. Since these PCs are already being used as deck overlays, constructing both closure joints and overlay of the same material will allow streamlining of the construction by enabling both these work to be completed in a single effort, effectively reducing the construction time and cost.

1.4 Literature Review

Polymer concrete has been used and studied for structural applications for more than four decades. Some of the relevant studies performed on polymer concrete on material and component level as well as on structural level for application as bridge joints have been summarized and presented here after. In addition to the review of literature, the gap in existing information has also been analyzed at the end of each section, which serves as the motivation for this present study.

1.4.1 Mechanical Properties of Polymer Concrete

Vipulanandan et al. [6] studied the mechanical behavior of polyester and epoxy polymer concrete with varying curing temperatures between 22 °C to 110 °C, resin content between 10% to 20% of the total weight of concrete and glass fiber content up to 4% by weight of concrete. This study concluded that the strength and modulus of elasticity of concrete peaked at 14-16% resin content. In addition, the strength and flexural modulus were found to vary with curing temperature and addition of glass fibers increased both strength and toughness of polymer concrete. In a complimentary study [7], the same research group also examined the flexural properties of PPC under three points bending for different strain rates, resin content and method of preparation and

concluded that the effect of temperature has minimal effect on the optimum resin content but the flexural strength as well as stiffness of PPC reduces with increase in temperature. Additionally, both of this research concluded that compacted specimens have higher strength than the vibrated specimens at optimum resin content.

Recent work on PMM-PC has demonstrated its superior mechanical properties. Acharya et al. [8] studied the tensile strength of polymethyl methacrylate polymer concrete under different strain rates and concluded that the tensile strength of PMMA-PC is two to three times the tensile strength of conventional concrete and demonstrated that 16.90 MPa of tensile strength could be achieved with PMMA-PC loaded at the rate of 0.85 mm/s. Other studies[9], [10] on mechanical properties of PMMA-PC, when used as bridge deck joint, demonstrated that PMMA-PC could achieve a compressive strength up to 83.40 MPa, modulus of elasticity of 19.30 GPa, flexural strength of 20 MPa and direct tensile strength of 4.70 MPa.

Studies on polyester, epoxy and vinyl ester PC have also been performed. A 2005 study [11] focused on the mechanical properties of polyester polymer concrete showed that polymer concrete can achieve representative compressive strength in the first twenty-four hours, however it takes 16 days to develop full strength. The same study also demonstrated that polyester PC could achieve compressive strength of 102 MPa, modulus of elasticity of 30.49 GPa and flexural strength of about 26 MPa. A 2020 research paper [12] focused on optimization and characterization of epoxy polymer concrete demonstrated that the mechanical properties of polymer concrete can be influenced by resin content and filler content. In addition to that, the same study [12] proposed empirical equations relating modulus of elasticity, flexural strength, and tensile strength of epoxy polymer concrete to the compressive strength. These equations are used later in this study for comparison with the observed data. Vinyl ester PC in [13] has also been reported to achieve

compressive strength between 43.8-77.2 MPa, flexural strength between 18.2-21.8 MPa, and modulus of elasticity between 22.4-29.0 GPa.

In addition to the mechanical properties of polymer concrete, its durability properties have been highlighted as important parameter. In a 2007 study [14] , chemical resistance of two types of polyester PC was studied which demonstrated increased chemical resistance of both those types of PPC when fly ash was used and concluded those types have similar mechanical properties.
Most of these past studies focused on some selected properties of a single type of polymer concrete at a time. As these studies employed different instrumentation, specimen geometry, and testing protocol, the resulting data sets cannot be directly compared. Hence such inconsistencies make it difficult to evaluate the PC options, especially when the choice of resin plays a crucial role in determining the mechanical property of the PC[15].

The other gap in the past work is that there is a limited representation of commercially available PC intended for field applications. Moreover, continuous advancement in chemical engineering aspect of PC over the past decades further widened this gap, as previous research may not capture the properties of modern commercially developed products.

In addition, although the guiding document for the structural application of polymer concrete ACI 549.6R-19 summarizes the mechanical properties from previous studies but does not offer mathematical equations to determine the mechanical properties of polymer concrete [16]. The first phase of this study is performed in direct response to these gaps.

1.4.2 Bond behavior of polymer concrete

In prefabricated bridge construction with cast-in-place closure joints, the overall performance of the structural system depends upon the bond of the closure joint material with the precast conventional concrete and the reinforcing steel. Although there aren’t many previous studies on

the bond behavior of PC, motivations on the test methodology were obtained from similar studies on ultra high performance concrete (UHPC). Hence, some of the previous studies on bond behavior of UHPC have been presented hereafter followed by the limited research available on polymer concrete.

A 2012 study by Saleem et al. [17] studied the bond of UHPC with reinforcement and concluded that the required development length for #10 high strength steel (HSS) rebar is $12d_b$ and for #22 HSS rebar is $18d_b$. An extensive study [18] was conducted by the Federal Highway Administration on the bond behavior of UHPC with reinforcement which studied the effect of various parameters like embedment length, cover, spacing, and rebar types and recommended that a minimum embedment length of $8d_b$ must be provided for rebar #13- #25. The same study also recommended a minimum side cover of $3d_b$ and minimum bar clear spacing of $2d_b$. Notably, this study also concludes that non-contact lap splices in UHPC have greater bond strength than that of contact splices and attributed it to decreased contact between the rebar and concrete.

An investigation [19] conducted on the bond between conventional concrete and UHPC by Zhang et al. demonstrated that 19.4 MPa of interfacial shear strength could be achieved and concluded that higher interface roughness and higher strength of the substrate lead to higher slant shear strength A similar study by Feng et al. [20] also demonstrated that the bond between UHPC and conventional concrete could be improved by surface treatment processes like water blasting, underscoring the importance of surface preparation for closure joints.

The bond between PMMA-PC and reinforcement was investigated by Mantawy et al. [21]in the context of bridge closure joints through pullout and flexural tests. This study concluded that a minimum overlap of 4.1 times the bar diameter is required to achieve yield stress in spliced rebar. This development length requirement is particularly shorter than that required for

conventional concrete.

The promising bond between rebar and PMMA-PC reported in the previous work together with enhanced mechanical properties of PVE-PC and PMMA-PC underscores the need to further understand their bond behavior with reinforcing steel. Also, limited data on bond performance on PMMA-PC and PVE-PC with conventional concrete, motivated the second phase of this study which investigates the bond between these two types of PC with rebar and concrete. Moreover, for consistency and direct comparison, selected tests were also replicated with UHPC.

1.4.3 Thermal behavior of polymer concrete

Temperature variation plays a significant role in the long-term performance of bridge closure joints as it experiences daily and seasonal temperature variation along with some occasional extreme high and low temperatures depending on the location of the bridge. Some selected previous studies on thermal performance of conventional concrete in general followed by specific performance of polymer concrete has been presented in this section.

The effect of thermal variation on conventional concrete has been extensively investigated. Haddad and Abendeh [22] studied the tensile strength and concrete-rebar bond of plain and fiber reinforced concrete subjected to repeated thermal cycles between 25 °C and 150 °C. Their results showed that, after exposure to thermal cycles, the plain cement concrete exhibited up to a 45% reduction in bond strength and 28% reduction in split tensile strength. Moreover, the study also found that fiber reinforced concrete demonstrated greater resistance to thermal degradation, with comparatively lower losses in bond and tensile strength, than plain concrete. Khan et al. [23], [24] studied the influence of cyclic thermal loading on shear strength and concrete-rebar bond strength in reinforced concrete. They observed that 14 or fewer thermal cycles with peak temperature up to 200 °C caused an increase by 5-10% in bond and shear strength attributed to increased hydration,

general stiffening of cement gel and increase in surface force between gel particles due to removal of absorbed moisture. However, when subjected to 300 °C and 21 or more cycles, there was a reduction in both the parameters, likely due to dehydration and microcracking of cement paste.

A study by An et al. [25] on high performance concrete showed a reduction in compressive strength, splitting tensile strength and elastic modulus when subjected to 45 or more thermal cycles between 25 °C and 65 °C. Ma et al. [26] found that compressive strength of ultra-high performance concrete followed an increase - decrease - slight increase pattern when subjecting the samples to increasing number of thermal cycles from 0 - 300 cycles between 20 °C and 60 °C. In general, these studies on conventional cement based concrete show that, the effect of thermal variation depends upon temperature range, number of cycles and the very composition of the concrete, making it difficult to generalize the behavior without material specific evaluation under the intended thermal exposure condition.

A large body of early research dating back to late 20th century [27], [28], [29], [30], [31] on mechanical behavior of conventional concrete subjected to extreme cold conditions consistently show that the compressive strength, tensile strength, modulus of elasticity and rebar-concrete bond strength increase when tested at extreme cold conditions. However, the peak strain decreases with decrease in temperature causing brittleness. Huo et al. [32] reviewed these findings and noted that the compressive strength and the flexural strength of concrete typically peak at about -120 °C and -60 °C respectively. This strength enhancement has been primarily attributed to the freezing of pore water present in the cement matrix, a mechanism unlikely to occur in polymer concrete due to absence of moisture.

Thermal effects on mechanical properties of epoxy polymer concrete (EPC) and polyester polymer concrete (PPC) have been extensively studied under both steady-state extreme

temperature and temperature variations. Roh et al. [33] studied the mechanical properties of tire waste modified epoxy polymer concrete for application in repair of runways and concluded that the polymer concrete has higher coefficient of thermal expansion than conventional concrete and the bond strength of polymer concrete with conventional concrete depends upon the temperature of testing. Reis [34] observed a loss of more than 50% of compressive strength and flexural strength in epoxy and polyester polymer concrete when subjected to steady state temperature up to 90 °C and reported that the polyester polymer concrete has lower sensitivity to temperature than epoxy polymer concrete. Letsch [35] concluded that the effect due to higher temperature was relatively large in flexural strength and small in the compressive strength. Ribeiro et al. [36] observed a 75% drop in flexural strength of the epoxy polymer mortar when subjected to thermal cycles above the glass transition temperature while the same for polyester polymer mortar remained relatively stable.

Shokrieh et al. [37] found that the compressive strength of epoxy polymer concrete was largely unaffected by the thermal cycles, but the flexural strength dropped up to 21% on thermal cycles around glass transition temperature. Although significant effect of thermal cycles on polymer concrete has been observed across the studies, epoxy and polyester PC were found to have higher resistance to freeze thaw induced reduction in strength which is mainly attributed to impermeable microstructure of polymer resin, absence of moisture and enhanced bond with aggregate matrix [36], [38]. However, a long-term evaluation of performance of epoxy concrete overlay [39] showed that the bond strength of PC and conventional concrete degrades with a large number of freeze thaw cycles.

Despite the extensive work on the thermal behavior of EPC and PPC, relatively limited research of such kind has been focused on newer advanced PC types like polymethyl methacrylate

polymer concrete (PMMA-PC) and polyvinyl ester polymer concrete (PVE-PC). Earlier phases of this study showed promising mechanical and bond properties of PC, despite which their behavior under thermal cycles and extreme cold temperatures remains unexplored. To address this gap, the third phase of this present study investigates the residual mechanical and bond performance of PMMA-PC and PVE-PC as joint materials for accelerated bridge construction under service level and extreme temperature variation as well as extreme cold conditions.

1.4.4 Structural applications

In the context of structural application, with primary focus on accelerated bridge construction, a few studies have been conducted with PC as joint material. The majority of the studies [40], [41], [42], [43], [44] regarding the ABC connections have been focused on UHPC and they have verified the excellent structural performance of UHPC joints.

Focusing on PC applications, Abokifa and Moustafa [10] performed a comparative study on the performance of longitudinal PMMA-PC and UHPC closure joint for deck bulb tee (DBT) girders. For this study, slabs of dimensions 2.44 m x 2.13 m x11.24 cm with female -female diamond shaped shear key of 15.24 cm width were tested. The slabs were precast and joined later with PC and UHPC. The joint had non-contact lap spliced reinforcement with two additional lacer bars and was treated with a primer liquid to enhance the bond strength. Each test specimen was placed between two steel beams placed parallel to the joints mimicking the girder web and loaded with a hydraulic actuator adjacent to the field joint. From these tests, it was found that the peak load with PMMA-PC joint was lower than that with UHPC. However, PMMA-PC joint also remained elastic up to the AASHTO ultimate load. The study also found that interface cracking with PMMA-PC joint could occur at high load, but the joint would still be able to transfer the load significantly. Overall, the study demonstrated that PMMA-PC could be used as a cost-effective

alternative to UHPC for longitudinal bridge joint for deck bulb tee girder.

The same research group also performed similar study [9] for transverse field joint where the joint was kept perpendicular to the seat beams. In addition to lap spliced specimen, this study also tested specimens with looped rebar at the closure joint and concluded that PMMA-PC closure joint with loop splice can enhance the performance of transverse joint, especially the cracking behavior and demonstrated the viability of PMMA-PC as UHPC's alternative for transverse closure joints. Beyond the deck joints, PMMA-PC has been explored as grouting material for duct connection of seismic columns [45]. This study has demonstrated PMMA-PC's ability to withstand large inelastic deformation and adequate bond between the column and the foundation under lateral cyclic loading. In addition to this research, Thonstad and Donohoe [46] explored fiber reinforced polymer concrete and demonstrated its viability for demanding ABC applications and Mantawy et al. [21] specifically recommended PMMA-PC for bridge deck joint application.

Despite these advances, large scale structural studies with PC joints have been primarily focused on PMMA-PC. Other PC types, although available commercially and applied widely in non-structural applications, have not yet been studied for application in large scale bridge joints. Furthermore, the limited research on PMMA-PC closure joints focus on the top flange DBT girder, where the depth of closure joints is relatively smaller. This present research project focuses on extending this knowledge base to slab type bridges for the New Mexico Department of Transportation (NMDOT), where the slabs themselves act as the primary load carrying member, resulting in greater depth of the slab, therefore significantly deeper closure joint.

1.5 Research Objectives

The overall objective of this study is to evaluate the feasibility and performance of polymer concrete as closure joint material for precast bridge element system, with a particular emphasis on

its application in precast slab bridge. The study is structured to meet the following specific objectives:

- Objective 1. To evaluate, compare and enhance the basic material properties of commercially available polymer concrete products: The primary objective was to identify commercially available polymer concrete products which have a potential application as a closure joint material in prefabricated bridge element system, determining their mechanical properties, which can be helpful to assess their feasibility for integration into PBES. The secondary objective was to study the variation of modulus of elasticity of polymer concrete with variation in aggregate source and gradation and determine the gradation to obtain maximum modulus of elasticity.
- Objective 2. To evaluate the bond strength of selected polymer concrete materials with conventional concrete & rebar and compare the same for UHPC. One of the goals was to characterize the bond behavior of PMMA-PC, PVE-PC and UHPC with conventional concrete and study the effect of surface preparation and use of bonding agent on the bond strength. The second goal was to determine the lap splice length required for effective transfer of load between the bridge elements using simpler small-scale tests.
- Objective 3. To study the effect of temperature cycles and extreme temperature on the mechanical and bond properties of polymer concrete. The goal was to examine the resilience of polymer concrete under thermal variations, which are expected within the service life of a bridge as well as extreme temperature events.
- Objective 4. To study the behavior of the longitudinal joint of prefabricated slab bridge deck with polymer concrete as closure joint material. The main goal is to assess the feasibility of polymer concrete as closure joint material and compare the performance of four different

classes of polymer concrete shortlisted from previous experimental programs.

1.6 Research Methodology and Scope of Work

The research is structured in four phases to meet the objectives defined in the previous section. The methodology for each phase is provided next. In phase I, different types of polymer concrete that were being used for bridge deck overlay construction were selected, and their mechanical properties like compressive strength, modulus of elasticity, flexural strength, tensile strength, shrinkage, and abrasion resistance were determined in accordance with ASTM standard specifications. Interrelationship between these properties were established using statistical tools and compared with corresponding standard established relations for conventional concrete. To meet the secondary objective in phase I, PMMA-PC was selected and different gradations of local aggregate from Reno were used to construct the test samples, and the obtained results were compared with the same obtained using the aggregate provided along with the polymer resin by the manufacturer.

In phase II, the bond strength of two PCs and UHPC with conventional concrete was determined using the slant shear test as per the ASTM specification. Sand papering was performed on some of the specimens to study the effect of surface preparation, and primer liquids provided by the manufacturer were used in some PC specimens to study the effect of the use of bonding agent. In the second part of phase II, two tests were conducted, namely the direct pullout test and the flexural test of spliced beams. A parametric study was conducted with varying embedment length of rebar in cylindrical PC specimens to determine the required development length, and the findings of this study were used to develop flexural tests in which beams with spliced rebar were tested to refine those results for flexural applications.

In phase III, some of the studies from phases I and II were repeated after subjecting the test

samples to three types of thermal conditions: Thermal shock between 0°C to 55°C, 0°C to 110°C, and constant temperature of -25°C. Compressive strength, modulus of elasticity, flexural strength, bond with conventional concrete and bond with rebar of polymer concrete were evaluated at all three thermal conditions.

In phase IV, to study the performance of longitudinal closure joints in prefabricated slab bridge with polymer concrete, four large scale specimens were tested with four different types of polymer concrete.

1.7 Report Outline

This report discusses the viability of polymer concrete as a structural joint material for prefabricated bridge element systems. The work is organized into seven chapters. Chapter 1 introduces PBES and outlines the motivation for using PC as a joint material. The chapter also provides a brief introduction to PC followed by research objectives and the overall scope of the study. Chapter 2 presents the material and experimental methodology adopted in this research. This chapter outlines the details of material used, dimensions and details of specimens, the step-by-step procedure for the test performed, instrumentation used and the test matrix. Chapters 3, 4, 5, and 6 present the results and analyses from four phases of the project. Chapter 3 discusses material level testing focusing on the mechanical properties of PC. Chapter 4 explores the bond behavior of PC with reinforcing steel and conventional concrete. Chapter 5 addresses the mechanical and bond behavior of PC when subjected to service level and extreme thermal conditions. Chapter 6 evaluates the structural behavior of PC as closure joint material for PBES application. Finally, the major findings from all the phases of the study are summarized and concluded in chapter 7.

2 MATERIAL AND METHODOLOGY

This section consists of the details regarding the material used in this study, fabrication of the test specimens as well as the experimental setup used.

2.1 Material and mixing

2.1.1 Polymer concrete

Among the wide range of available polymer concrete products which are currently being used in non-structural applications, six different commercial proprietary products belonging to four classes of polymer concrete were selected as a potential application on the deck joints in Accelerated Bridge Construction. These products were two-Epoxy Polymer Concrete (EPC), two-Polyester Polymer concrete (PPC), one-Polymethyl Methacrylate Polymer Concrete (PMMA-PC) and one-Poly Vinyl Ester Polymer Concrete (PVE-PC). The two types of EPC and PPC were procured from different vendors. Since the products used in this research were proprietary, their exact chemical composition is not known. The quantity of the constituent of all the six types of polymer concrete and the resins used in this study is presented in Table 2.1and Figure 2.1 respectively.

Table 2.1：Description of constituents of PC and percentage by weight

PC type	Resin type	Hardener / Initiator	Fine Aggregate	Coarse Aggregate	Additional Material
EPC 1	PL (7.49%)	PL (3.21%)	Commercial (59.83%)	Commercial (29.47%)	None
EPC 2	PL (7.48%)	PL (7.48%)	Commercial (17.00%)	Commercial (42.52%)	Proprietary Powder (25.52%)
PPC 1	PL (10.69%)	MEKP (0.21%)	Commercial (59.40%)	Commercial (65.15%)	None
PPC 2	PL (15.00%)	MEKP (0.30%)	Commercial (28.80%)	Commercial (42.30%)	Proprietary Powder (13.60%)
PMMA-PC	PL (7.09%)	Blend of sand, filler, and benzoyl peroxide (61.94%)		Commercial (30.97%)	None
PVE-PC	PL (11.09%)	MEKP (0.22%)	Aggregate pre-mixed with basalt fiber (88.69%)		None

PL: Proprietary liquid MEKP: Methyl Ethyl Ketone Peroxide

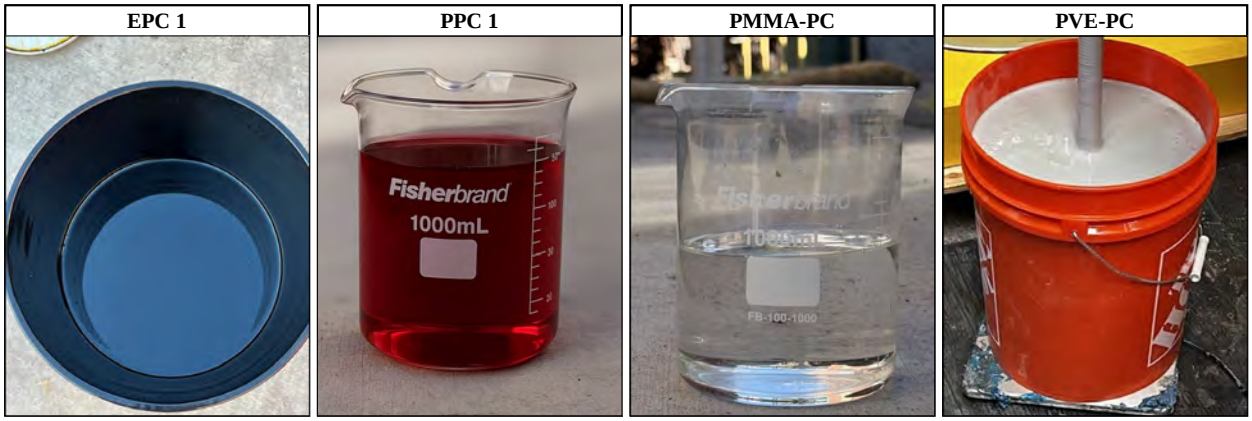

Figure 2.1. Resins used in different PC types

Mixing of the concrete was performed in buckets with the help of a double shaft paddle mixer. For all six types of PC, the resin and hardener/initiator were mixed for a manufacturer's recommended amount of time and then the dry components which include the aggregates, and the additional material were added gradually and mixed for a recommended amount or time or until homogeneous. Additional care was taken to avoid entraining the air into the concrete. The manufacturer's recommended mixing time for each type of concrete is presented in Table 2.2.

Table 2.2 : Recommended mixing time.

PC type	**Mixing time for Resin and Hardener**	**Mixing time after addition of dry components**
EPC 1	3 mins	Until homogeneous
EPC 2	3-5 mins	Until homogeneous
PPC 1	10 secs	1 min or until homogeneous
PPC 2	10 secs	Until homogeneous
PMMA-PC	Until homogeneous	1 min or until homogeneous
PVE-PC	10 secs	1 min or until homogeneous

2.1.2 Ultra-high-performance concrete

An economical version of cement Ultra-high-performance concrete (UHPC) which used locally sourced fine aggregates has been used as a reference material in the component level bond tests. The ingredients of the reference UHPC are UHPC powder (641 kg/m^3), fine sand (855 kg/m^3), cement (777 kg/m^3), steel fibers (157 kg/m^3), water-reducing admixtures (106 kg/m^3), and water

(126 kg/m^3). These ingredients were mixed in a high-shear mixer for about 15 minutes where dry components were agitated first followed by the addition of water and the admixtures gradually.

2.2 Methodology

The methodology used for this study is heavily experimental with investigations at material, component, and structural level. In addition to tests at ambient condition, additional tests were performed at the material and component level to characterize the behavior of PC under thermal conditions. The experimental methodology used in all four phases of this study is presented hereafter.

2.2.1 Material behavior of polymer concrete

The mechanical behavior of six commercial PC was characterized by performing six tests on the material level and based on these results the compressive behavior of one of the PC: PMMA-PC was studied using local construction material. The test methodology for these six tests is presented hereafter.

2.2.1.1 Compressive Strength

The compressive strength of PC was determined using two types of PC specimens: two inches cubes and cylinders with diameter of three inches and height of six inches. The compressive strength of PC cubes was determined according to ASTM C579-23 [47] with a loading rate of 6000 psi/min while that of cylinders were determined in accordance with ASTM C469-22 [48] at a loading rate of 35 psi/s. A small portion of the top of the cylinders were cut and then the top and bottom surfaces of the cylinders were grinded prior to testing to ensure a smooth contact with the compression testing machine. These specimens were tested in SATEC compression testing machine. Photographs of test setups and specimens after testing are presented in Figure 2.2.

2.2.1.2 Modulus of elasticity

The modulus of elasticity of all six PC types was determined in accordance with ASTM C469-22 [48] . A compressometer assembly, as shown in Figure 2.2, was used together with a data acquisition system to measure and record the axial deformation of the cylinder during the compressive strength test. The obtained results were then processed, and the modulus of elasticity was calculated as the slope of the best-fit line between the 10 % to 40 % of peak stress. This same methodology has also been used throughout this study to test the compressive strength and modulus of elasticity of companion cylinders in all component and structural level tests.

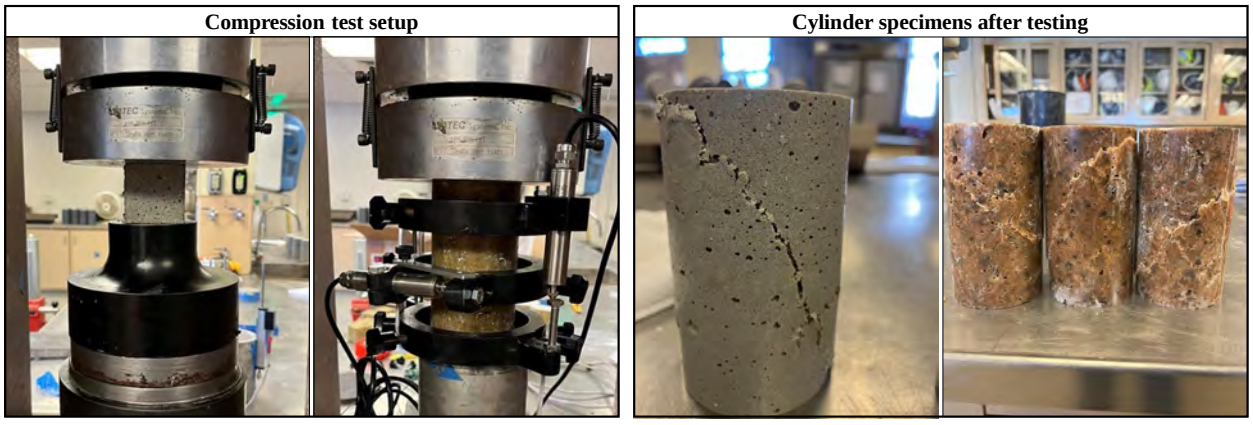

Figure 2.2. Compression test setup and specimens after testing

2.2.1.3 Flexural strength

The flexural strength test was performed in accordance with ASTM C78-22 [49] with a loading rate of 0.05 in/min. 3 in x 3 in x 12 in specimens were loaded at third points with a span of 9 in between the supports as shown in Figure 2.3. The deflection of the neutral axis at midspan was measured using a laser assisted system which was synchronized with the universal testing machine.

2.2.1.4 Tensile strength

The tensile strength of PC was determined using dog bone specimens with cross section area of 1 in x 1 in and gauge length of 3 in. The specimens were tested in an Instron universal testing

machine at the rate of 0.01 in/min as shown Figure 2.3. Elongation of the specimen between the gauge points during the test was measured with the help of laser assisted system.

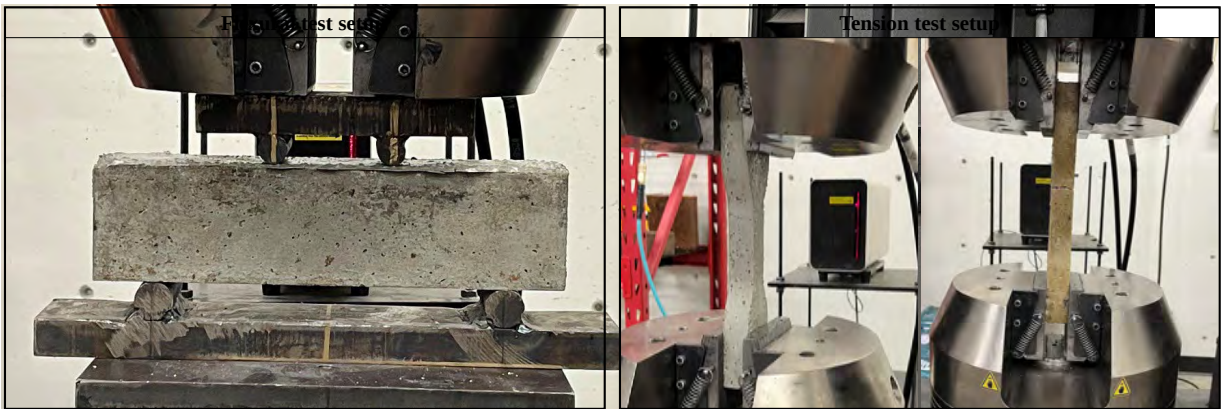

Figure 2.3. Flexural and tensile test setup

2.2.1.5 Shrinkage and abrasive resistance

Shrinkage test was performed in accordance with ASTM C531-18 [50]. 3 in x 3 in x 10 in specimen were cast with end studs. The length of the specimen was measured using a length comparator as soon as it is demolded which was used as a reference length for shrinkage calculations. The decrease in length of the specimen at seven and 28 days was measured using the comparator as shown in Figure 2.4 and the shrinkage was calculated accordingly.

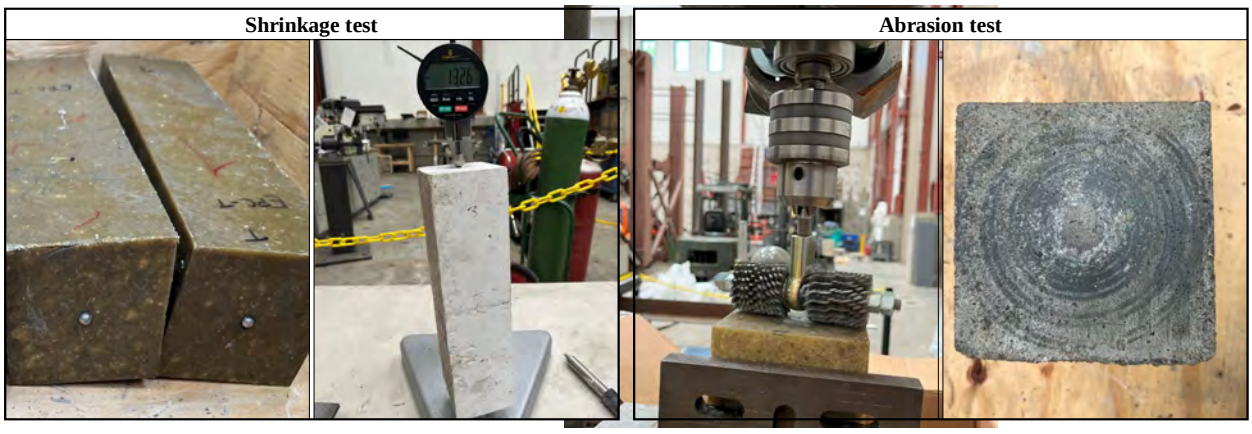

Figure 2.4. Shrinkage and abrasion test setup

Abrasion tests were performed in accordance with ASTM C944-19 [51]. The abrasion device as shown in Figure 2.4 was attached to a drill press which was modified to exert a constant

force of 22 lb. to the concrete specimen. The specimen was clamped as shown and was subjected to abrasion for 3 cycles of 2 minutes each and the weight loss after the third cycle was noted to the nearest 0.1gm. A summarized test matrix for the material level test has been presented in Table 2.3.

Table 2.3. Test matrix for material characterization of 6 types of polymer concrete.

Test	**Specimen dimension**	**Age of specimen**	**Number of specimens**
Compressive strength	Cube: 2 in	1,3,7, and 28 days	6
Compressive strength Modulus of elasticity	Cylinder: 3 in x 6 in (same specimens)	1,3,7, and 28 days	4
Flexural strength	Prism: 3 in x 3 in x 12 in	1,3,7, and 28 days	3
Tensile strength	Dog bones: C/S of 1 in x 1 in and gauge length of 3 in	1,3,7, and 28 days	3
Shrinkage	Prism: 3 in x 3 in x 10 in	7, and 28 days	4
Abrasion	Cube: 4 in	7, and 28 days	4

2.2.1.6 Effect of local aggregate and gradation on mechanical properties of PMMA-PC

In addition to the tests presented in the test matrix, compressive strength, and modulus of elasticity tests of eight different engineered mixes of PMMA-PC were also performed. For these tests, four cylinders of 3 in x 6 in specimens were tested at the age of 3,7, and 28 days. These mixes were prepared with local aggregate available at Reno, Nevada. Each of these eight mixes had different gradation of aggregate. These mixes are numbered from one to eight and the gradation curve for the aggregate used is shown in Figure 2.5. The aggregate gradation of mixes one, two, and three were suggested by the manufacturer. In all these three mixes, fine aggregate (FA) provided by the manufacturer was used. The coarse aggregate (CA) in mixes two and three were of the size 3/16 – 3/8 in and 3/8 – 3/4 in respectively whereas Mix 1 used no CA. Rest of the mixes five through eight are different combination of sizes of the coarse and fine aggregates. Mix 4 had a mixture of CA from mixes two and three i.e. CA size of 3/16 – 3/4 in. Mix 5 had CA of size 3/8 – 1/2 in

removed from Mix 4. Mixes six and seven were modifications to Mix 3 with CA size of 3/8 to 1/2 in and 1/2 in – 3/4 in, respectively. Mix 8 was a modification to Mix 1 with additional FA to make it well graded.

The aggregate used was procured from a local quarry and then washed, oven dried and sieved to get different sizes of aggregate. Required quantity of each size was mixed and tested to ensure the achievement of target gradation. The quantity of resin used for the mix one through eight were 8.70%, 7.09%, 6.26%, 6.61%, 6.61%, 6.26%, 6.26%, and 7.74% by total weight of the mix, respectively. The quantity of resin in mixes one, two, and three were also suggested by the manufacturer and the rest of them were interpolated based on the gradation. It should also be noted that the mix 2 uses the same aggregate gradation and mix proportions as the proprietary mix (referred as mix 2a in this document) used in the initial study.

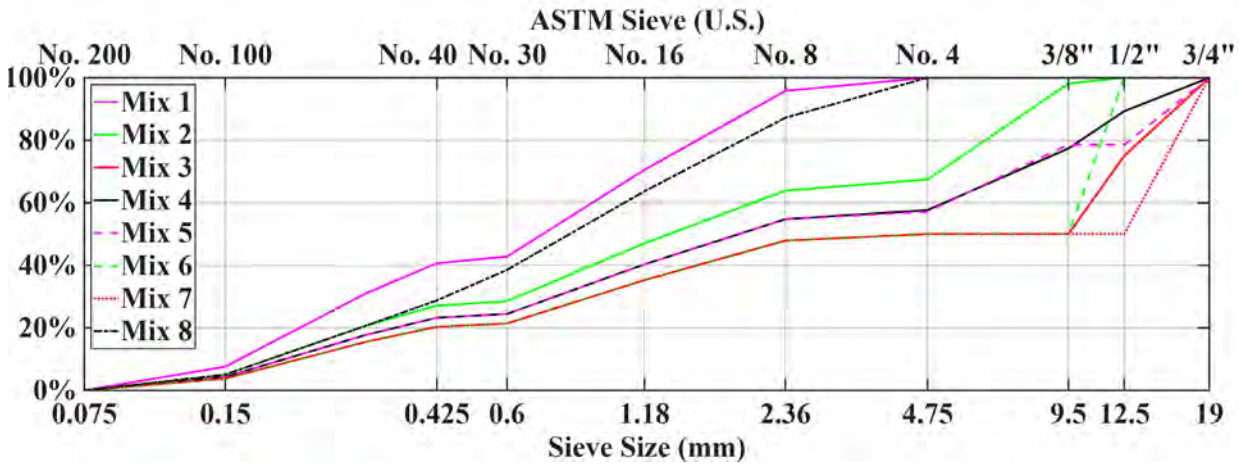

Figure 2.5. Particle size distribution curve of aggregate used in engineered mixes.

2.2.2 Bond behavior of polymer concrete

The bond behavior of two PC types: PMMA-PC and PVE-PC and reference UHPC was studied through three tests: bond strength on direct pullout, bond strength with rebar upon flexural loading, and bond with conventional concrete by slant shear test. The details of specimen fabrication, test methodology and test matrix for these three tests is presented in this section.

2.2.2.1 Bond with rebar upon direct pullout

The pullout performance of PC and reference UHPC was studied using three types of rebar: #4 grade 60, #5 Grade 60, and #4 grade 100. Five embedment lengths: two, four, six, eight, and ten times the diameter of the rebar were used for grade 60 rebar whereas embedment length of six, eight, ten, twelve, fourteen, and sixteen times the diameter of the rebar were used for grade 100 rebar. Three specimens were used for each combination of concrete type, rebar type, and embedment length. The UHPC samples were tested at the age of 28 days and the PC samples were tested at the age of 7 days. A summarized test matrix of the pullout tests has been presented in Table 2.4.

Table 2.4. Test matrix for pullout specimens.

Material	Test age	Rebar grade	Rebar size	Embedment length	Number of samples
PMMA-PC	7 days	60	#4	2, 4, 6, 8, and 10 times rebar diameter	3 each
			#5	2, 4, 6, 8, and 10 times rebar diameter	3 each
		100	#4	6, 8, 10, 12, 14, and 16 times rebar diameter	3 each
PVE-PC	7 days	60	#4	2, 4, 6, 8, and 10 times rebar diameter	3 each
			#5	2, 4, 6, 8, and 10 times rebar diameter	3 each
		100	#4	6, 8, 10, 12, 14, and 16 times rebar diameter	3 each
UHPC	28 days	60	#4	2, 4, 6, 8, and 10 times rebar diameter	3 each
		100	#4	6, 8, 10, 12, 14, and 16 times rebar diameter	3 each

These specimens were cast on a specially crafted table consisting of drilled holes to house and hold the rebar in an appropriate position such that the desired embedment length could be achieved. 6 in x 12 in cylinder molds were drilled in the bottom and placed on top of the rebars,

doing so helped to achieve a flat bearing surface on the specimen. Concrete was cast in the molds, de-molded after 24 hours, and cured at room temperature till testing. The setup for casting and testing of the specimens is presented in Figure 2.6. A steel encasing was used which was gripped by the lower head of the Instron universal testing machine and the upped head was used to grip the rebar. A laser-assisted extensometer was used which measured the extension of the rebar between the bearing surface of the concrete and a reflective tape attached to the rebar near the loading grips which measured the sum of rebar extension and slip of the rebar from the concrete. The rebar was pulled out of concrete at a rate of 0.19 in/min till the load dropped by 40% of the maximum load.

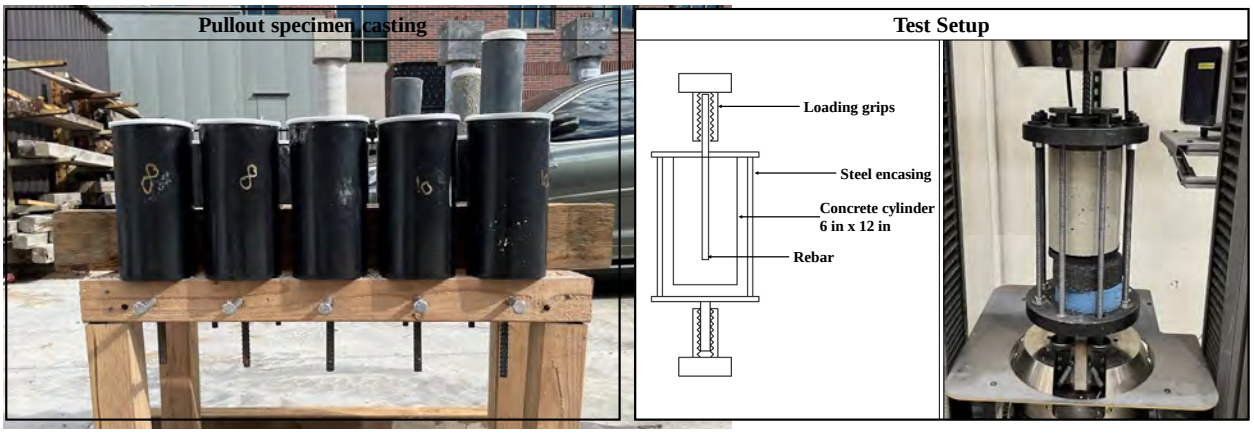

Figure 2.6. Setup for casting and testing of pullout specimens.

2.2.2.2 Bond with rebar upon flexural loading

The validity of results obtained from the direct pullout test in the case of flexural members was evaluated by testing beams of size 6 in x 6 in x 21 in consisting of #4 rebars spliced at the midspan with splice length obtained from the direct pullout test. The PC beams were constructed with splice lengths of eight, ten, and twelve times the diameter of the rebar whereas the UHPC beams were constructed with splice lengths of eight times the rebar diameter. The spacing between the rebars was set to one-fifth of the spliced length, which is the maximum spacing suggested by the AASHTO LRFD bridge design specifications [52]. Three additional beams with $8d_b$ splice length

for each material were also constructed with contact splice to study the effect of rebar contact. The results obtained from these tests were compared against control beams of corresponding material with continuous rebar running throughout the length of the beam. 1 in ($2d_b$) clear cover was provided for all the specimens. A representative figure of reinforcement details in spliced non-contact specimen and control specimen has been shown in Figure 2.7. Additionally, some of the beams with $8d_b$ spliced lengths and with continuous rebars were equipped with strain gauges to measure the strain in the rebars. The tests were performed at the age of seven days and 28 days for PC and UHPC, respectively. A summarized test matrix in terms of the number of specimens for each case has been presented in Table 2.5.

Table 2.5. Test matrix for splice length test presenting the number of specimens for each case.

Concrete type	**Control**	**Spliced**			
		$8d_b$ non-contact	**$8d_b$ contact**	**$10d_b$ non-contact**	**$12d_b$ non-contact**
PMMA-PC	2+3*	2+3*	3	3	3
PVE-PC	2+3*	2+3*	3	3	3
UHPC	2+3*	2+3*	-	-	-

* With strain gauge

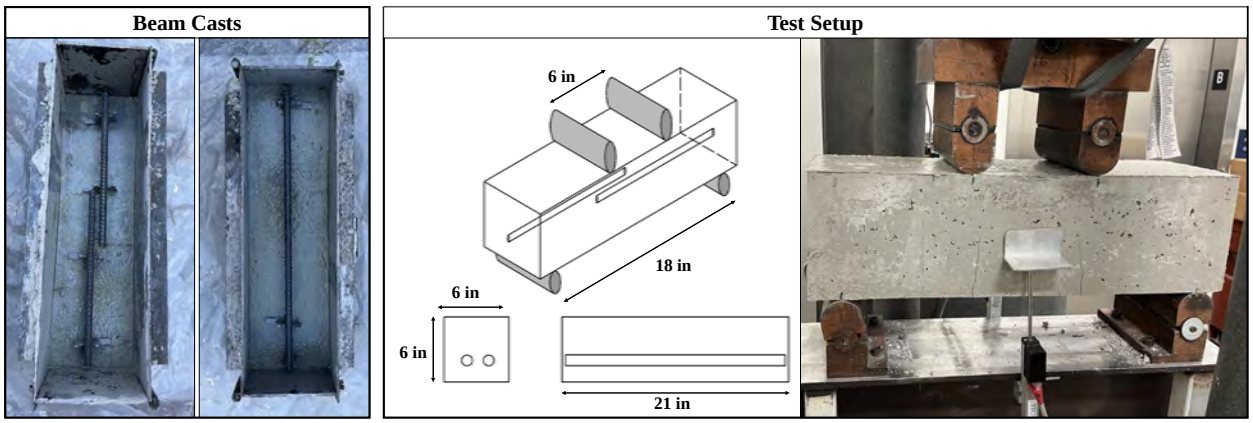

Figure 2.7. Setup for casting and testing of spliced and control beams.

All the beams were cured at room temperature and then tested in the Tinius Olsen Compression testing machine with a setup as shown in Figure 2.7. Two LVDTs were attached to the side face at the mid-depth of the beam to measure the midspan deflection. The specimens were

loaded at a rate of 0.04 in of deflection per minute till failure and the load, the LVDT readings, and the strain gauge readings when applicable were continuously recorded with the help of a data acquisition system.

2.2.2.3 Bond with conventional concrete

The bond of PC and UHPC with conventional concrete was evaluated using slant shear tests conducted in accordance with ASTM C882 [53]. As suggested by the ASTM standard, dummy sections of dimensions depicted in were prepared and inserted in standard cylindrical molds measuring 3 in x 6 in. Conventional concrete (CC) was mixed and cast in such cylindrical mold to form cylindrical wedge pieces of CC. The CC wedge pieces were then cured at 100% relative humidity and room temperature for 28 days. To investigate the effect of surface preparation on the bond strength, half of the wedge pieces were treated with sandpaper of grade 80 followed by grade 150. These grades of sandpaper were chosen based on industry practice commonly followed to prepare the concrete surface for the application of epoxy coating for waterproofing, which ensures proper bonding.

To further study the effect of the bonding agent, a proprietary primer supplied by the manufacturer of corresponding polymer resin was applied to some CC wedge pieces both sandpapered as well as left as it is. The application of the bonding agent adhered to the manufacturer's recommendation of 0.0125 gallon per sq ft of concrete surface. The prepared CC wedges were reinserted into the cylindrical molds and PC or UHPC were cast into the mold to get a final test specimen. The UHPC and PC specimens were cured for 28 and seven days before testing. The slant shear test was conducted using a Satec compression testing machine and the peak load at failure was recorded for each specimen and the corresponding shear stress developed along the interface was calculated. The details of test specimen and setup is presented in Figure 2.8 and

the summarized test matrix is presented in Table 2.6.

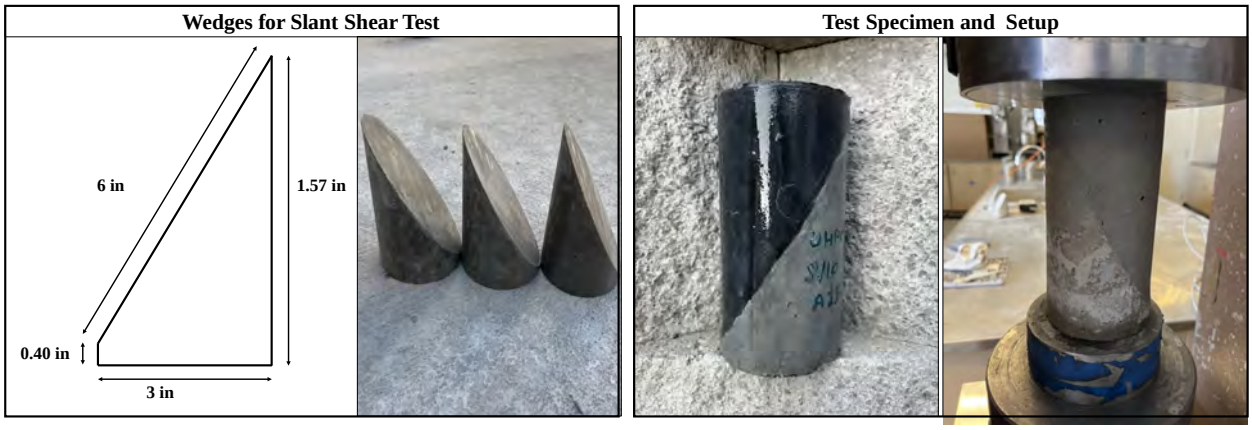

Figure 2.8. Details of slant shear test specimens and test setup

Table 2.6. Test matrix for slant shear test presenting the number of specimens for each case.

	Without surface preparation		With surface preparation	
	With primer	**Without primer**	**With primer**	**Without primer**
PMMA-PC	4	4	4	4
PVE-PC	4	4	4	4
UHPC	-	4	-	4

2.2.3 Thermal properties and performance of polymer concrete

2.2.3.1 Thermal properties of polymer concrete

The thermal properties of PC were first characterized to design the experimental methodology for characterizing the thermal performance of PC. In polymer-based materials, glass transition temperature (Tg) represents the critical temperature at which the polymer transitions from glassy to rubbery state. Similarly, the coefficient of thermal expansion governs the magnitude of thermally induced stresses in PC- Conventional concrete joint.

The glass transition temperature of the polymers was determined using TA Instruments Differential Scanning Calorimeter (DSC). A small sample obtained by scraping a fully set polymer concrete sample was precisely weighed and placed in a standard aluminum pan. The pan consisting of the sample and an empty reference pan were hermetically sealed and placed in the DSC cell. The DSC

cell was then filled with Nitrogen gas, and a multi-step temperature profile was applied through a computerized system. The pans were first let to obtain thermal equilibrium at 25 °C and then heated to 300 °C at the rate of 10 °C/min and then cooled to 25 °C. This cycle between 25 °C and 300 °C was repeated twice. The difference between the heat energy required to raise the temperature of the sample and that of the reference pan also known as the differential heat flow was measured during the second cycle. The measured heat flow was plotted against the temperature and the first step in the heat flow was noted and the midpoint of heat flow step change was determined as the glass transition temperature. Three trials were performed for each material and in doing so the, the glass transition temperature of PMMA-PC and PVE-PC was determined to be 66±1 °C and 60 ±2 °C. It should be also noted that the PC samples used to obtain this glass transition temperature was not a pure polymer sample typically used to determine perform thermal analysis on polymers rather was an actual scrape of polymer concrete potentially laced with impurities like sand and fine silica powder.

Based on the obtained glass transition temperatures, two temperatures 55 °C and 110 °C were determined as the upper limit for thermal shock cycles representing service level and extreme environmental conditions.

The coefficient of thermal expansion (CTE) of PMMA-PC and PVE-PC was determined in accordance with ASTM C531-18 [50]. For each material, four Prismatic beams of dimension 3 in x 3 in x 10 in were cast with embedded steel end studs with coefficient of thermal expansion of 1.60×10^{-5} mm/mm/°C. These PC specimens were stored in room temperature for one year to eliminate any shrinkage effects were prior to CTE measurement. Same specimens as well as length comparator that was used for determining the shrinkage of PC were used for this purpose.

For determining the CTE, the original length of the specimens was first measured by using a length

comparator of precision 0.001 mm at temperature of 23 °C as shown in **Error! Reference source not found.**b and c. The specimens were then kept in a hot air oven maintained at 100 °C for 24 hours and their lengths were measured at the elevated temperature. The heating cooling process was repeated until identical measurements were produced at 23 °C as specified by ASTM C531 to confirm that no additional shrinkage was taking place.

The contribution of the end studs in the length change was accounted for using their CTE. The change in lengths obtained in the last cycle were then used to determine the CTE of PC specimens. Based on these measurements, the CTE of PMMA-PC and PVE-PC was found to be (2.97 ± 0.05) x 10^{-5} /°C and (2.15 ± 0.07) x 10^{-5} /°C respectively.

2.2.3.2 Thermal performance of polymer concrete

Building on the measured thermal properties of PC characterized in the previous section, the thermal performance of PC was evaluated by studying the residual mechanical and bond strengths of PC when exposed to thermal conditioning. Four tests namely compressive strength test, flexural strength test, pullout test and slant shear tests were performed after subjecting the test specimens to three thermal regimes: thermal Shock between 55° C to 0° C (T55), thermal shock between 110° C to 0° C (T110) and a constant freezing temperature of -25°C (T-25). The results from these conditions were compared to baseline tests conducted at room temperature without any exposure to adverse thermal conditions.

The upper limit of T55 and T110 cases were selected based on the glass transition temperatures (T_g) of the PMMA and PVE polymer samples, T55 representing the service level exposure below the glass transition temperature while T110 representing extreme thermal conditions well above the glass transition temperature. The temperature range of these thermal shock cycles was determined based on the bridge design recommendation in the state of New

Mexico. In contrast, the constant -25°C was selected to mimic extreme cold environment representative of potential field exposure.

In both T55 and T110 cases, the specimens were initially heated in a hot air oven to respective maximum temperature of 55°C and 110°C as shown in Figure 2.9. The temperature was monitored and recorded with two thermocouples, one embedded in the core of specimen and one attached to the surface of the specimen. The pullout test specimen being the largest among all specimens used was selected for monitoring the temperature under the assumption that the rest of the smaller specimens achieved thermal equilibrium faster than the instrumented specimen.

Figure 2.9. Specimens under thermal conditioning

The heated specimens were immersed into ice water bath maintained at 0° C immediately after removing from the oven where the temperature was monitored similarly as shown in Figure 2.9. Similarly, once the thermal equilibrium was maintained at 0°C, the specimens were promptly transferred to the oven pre heated to 55°C or 110°C. This process of subjecting the specimen to extremely rapid thermal variation is known as thermal shock. Figure 2.10 shows the temperature profile measured at the surface and the core of the monitored specimens during heating and cooling period. For both T55 and T110 conditions, the specimens were subjected to 10 such heating and cooling thermal shock cycles.

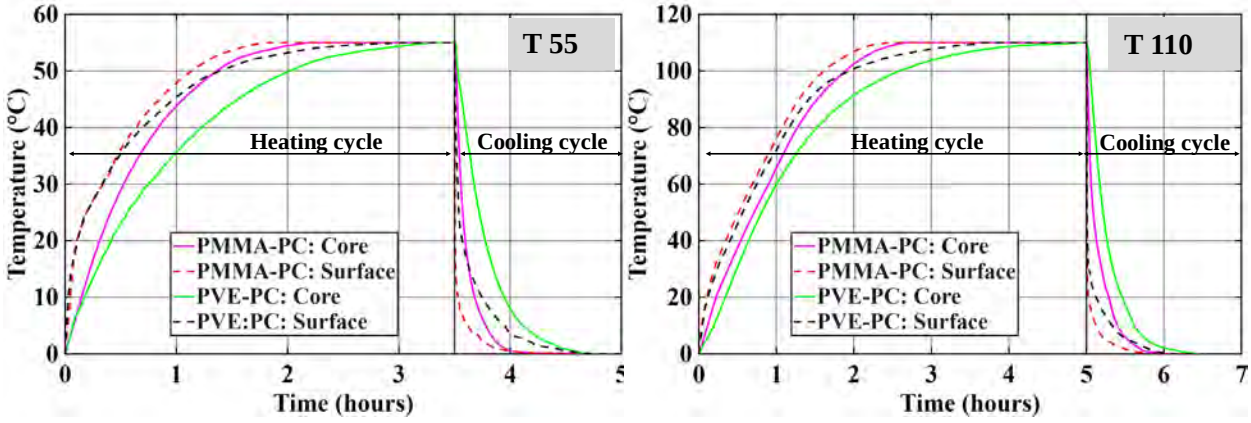

Figure 2.10. Temperature profiles of monitored specimens' core and surface during the thermal cycles.

Table 2.7. Test matrix to study the behavior of polymer concrete under thermal stresses.

Test Type	Specimen type and dimension	Test sets	Specimen per test set
Compressive strength	Cylinder of 3 in x 6 in	Day 7 (Early age reference), Test day (Late age reference), T55, T110, T-25	4
Flexural strength	Beam of 3 in x 3 in x 12 in		3
Bond strength with concrete	Slant shear test cylinder of 3 in x 6 in		With primer: 3 Without primer: 3
Bond strength with rebar	#4 rebar embedded for 4 in in PC cylinder of 6 in x 12 in	Day 7 (Early age reference), T55, T110, T-25	3

For the third temperature condition of T-25, the specimens were kept in a freezer maintained at constant -25°C for a period of two weeks and tested within a period of 10 minutes after removing from the freezer. Thermocouple measurements confirmed that there was no change in core temperature during this interval. However, the surface temperature increased up to -22°C in some specimens by the end of the test. The test matrix consisting of the details of the test specimen and their numbers has been presented in Table 2.7.

2.2.4 Structural performance of polymer concrete

In order to study the structural performance of polymer concrete when used as longitudinal closure joint material in bridge decks, four bridge deck slabs were constructed and tested. The details of

the specimen design, construction, test setup, and instrumentation is presented hereafter.

2.2.4.1 Specimen design

Four bridge deck slabs were constructed, each identical in geometry as well as reinforcement but with a different type of polymer concrete in the longitudinal closure joint. The slabs were designed in accordance with the AASHTO LRFD bridge design specification using the equivalent strip method. The prototype configuration was selected to meet the constraints of laboratory space as well as the capacity of the testing system.

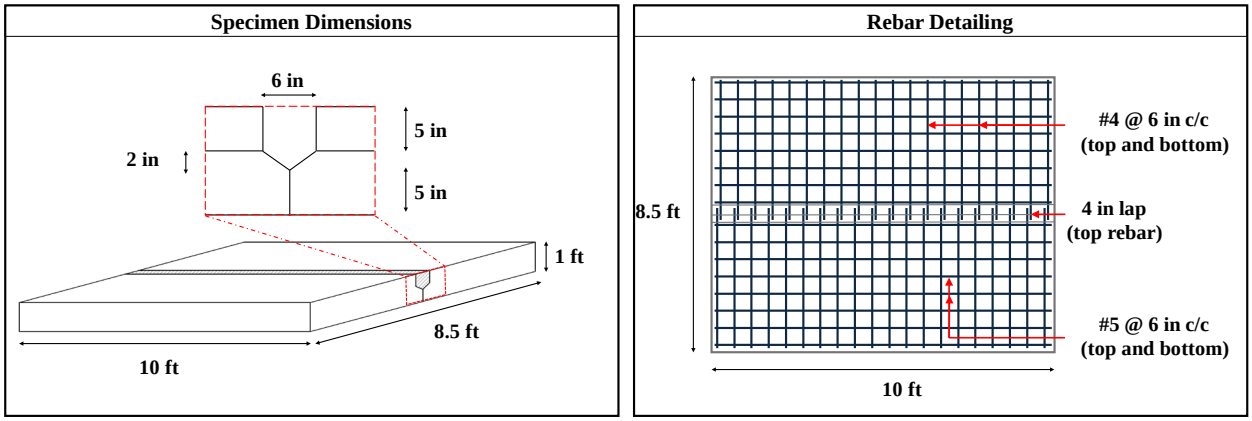

Figure 2.11. Details of test specimen

The test specimens were designed to be stronger in the longitudinal direction so that the performance of the joint can be evaluated at a higher load. Longitudinal reinforcement consisted of #5 rebars spaced at 6 in center to center along with transverse #4 rebars at the same spacing to form the bottom mesh. The top mesh was identical to the bottom one with the transverse rebar extended 5 in towards the joint face. A clear cover of 1 in and 2 in was maintained for the bottom and top mat, respectively. A non-contact lap splice length of 4 in was provided in the top transverse rebars at the joint which was equivalent to eight times the diameter of rebar. Each test specimen measured 10 x 8.5 x 1 ft with a longitudinal joint 6 in wide kept parallel to the longer dimension of the specimen. The slab geometry, joint configuration and the details of reinforcement are

presented in Figure 2.11 .

Four commercial PCs were selected for this study based on the material and component level tests as a potential closure joint material in Accelerated Bridge Construction (ABC) applications. These included polymethyl methacrylate polymer concrete (PMMA-PC), polyester polymer concrete (PPC), epoxy polymer concrete (EPC), and polyvinyl ester polymer concrete (PVE-PC). The same PMMA-PC and PVE-PC material were used throughout all phases of this study while the EPC and PPC correspond to EPC 1 and PPC 1 used in the material level study.

2.2.4.2 Material and construction.

The deck slabs were constructed at a commercial precast facility at Sparks, Nevada using a standard concrete mix proportioned to achieve a target compressive strength of 5000 psi at 28 days and standard ASTM A615 grade 60 rebar as reinforcement. Photographs from the slab construction phase are presented in Figure 2.12aand b. The slab panels were cured under ambient outdoor conditions in the precast yard until they reached a handling strength. At an approximate age of 7-14 days, the panels were transported to the fabrication yard at University of Nevada Reno where they were aligned to place polymer concrete in the joint.

Prior to placement of polymer concrete, the joint surface of the conventional concrete slab panels was cleaned of any dust and debris followed by application of the primer as shown in Figure 2.12c and d. PMMA-PC, PPC and PVE-PC were provided with a separate set of primer and their corresponding hardener whereas the same resin hardener combination was used for EPC. Although each of these primers had a recommended application rate, the primer was applied with a paint brush until the surface was saturated, that is when the primer stopped adhering to the surface and began to flow.

Following the application of primer, PC was placed in the joint after 10-15 minutes without

any mechanical vibration relying on the inherent flowability of the mix supported by light tamping as shown in Figure 2.13. All PC products were procured from the manufacturer and used as per their recommendation. The general composition and the mixing procedure of the PC material used has already been discussed in the material and mixing section in chapter 2.

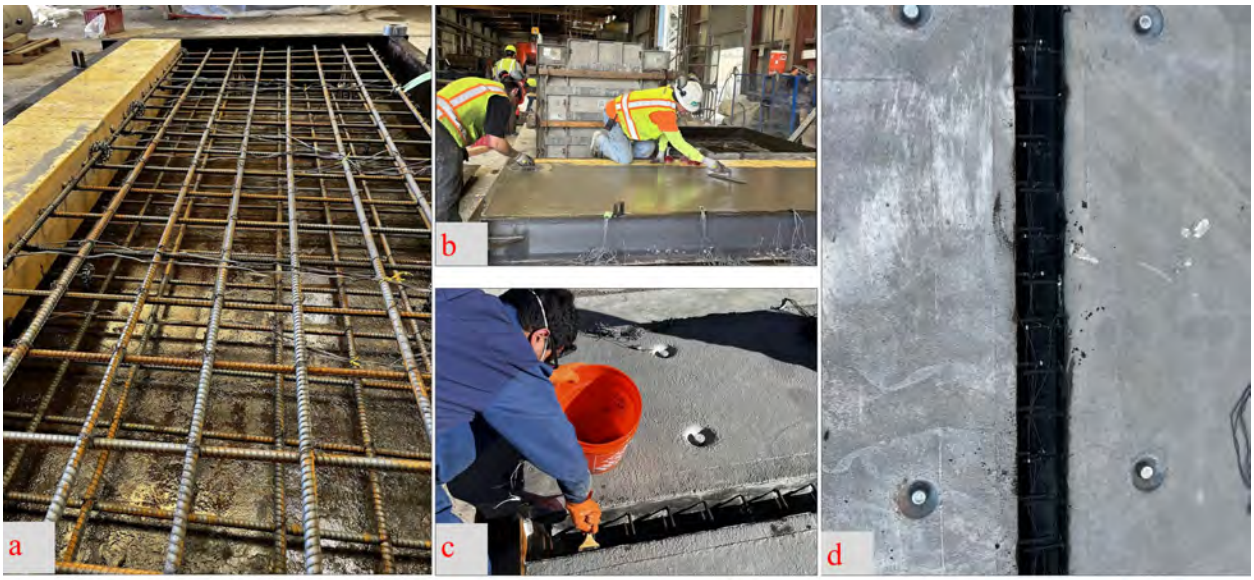

Figure 2.12. a) Reinforcement mat ready for casting b) Top surface finishing c) Application of primer d) Slabs ready for closure pour

Figure 2.13. PC mixing and closure pour.

2.2.4.3 Test setup

The slabs were tested on the strong floor in the Earthquake Engineering Laboratory at the University of Nevada Reno. Each specimen was simply supported on elastomeric pads 2 in thick,

placed on two steel beams with a center-to-center span of 9 ft between the elastomeric pads. These elastomeric pads were provided to allow free rotation and eliminate restraint induced moments at the supports and to avoid risk of stress concentrations.

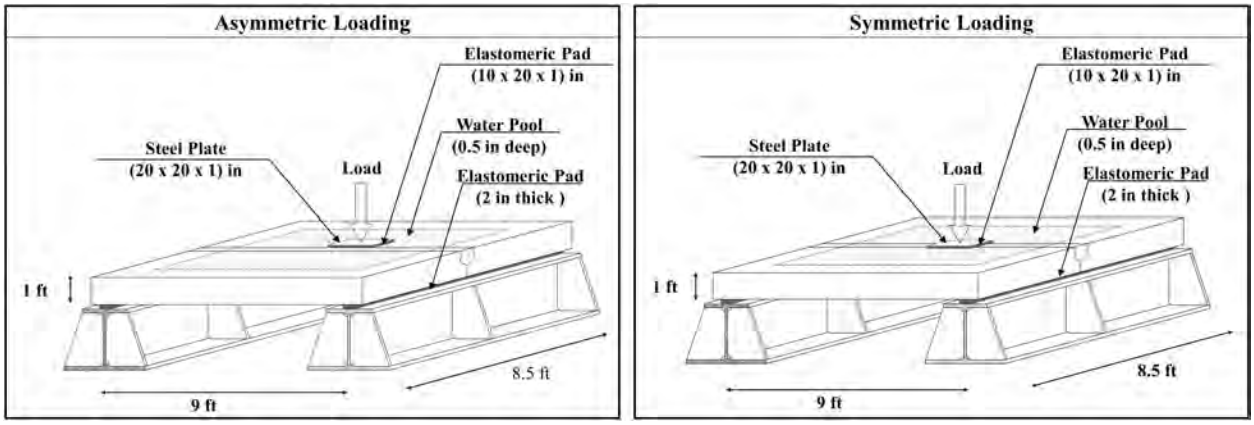

Figure 2.14. Schematic test setup with asymmetric loading adjacent to the joint and symmetric loading on top of joint

Vertical load was applied using a 220 kips hydraulic actuator through a steel loading plate of 20 x 20 x 1 in, with an elastomeric pad of size 10 x 20 x 1 in placed directly below the loading plate. The elastomeric pad was used to simulate the AASHTO wheel load. For the PMMA-PC and PPC specimens, the load was applied adjacent to the joint towards the east side at midspan, while for EPC and PVE-PC specimens, the load was applied symmetrically at midspan, directly over the center of the joint. The schematic test setup for both the loading cases have been shown in Figure 2.14 and the actual setup of the lab has been shown in Figure 2.15.

These two loading setups were adopted to study distinct aspects of joint behavior. The asymmetric loading adjacent to the joint was intended to replicate the conditions where the wheel load is transferred from one slab to another, inducing shear forces and differential deflection at the joint. In contrast, the symmetric loading above the joint simulated the case when wheel load is applied directly at the joint material, subjecting the closure material to flexural and shear stresses.

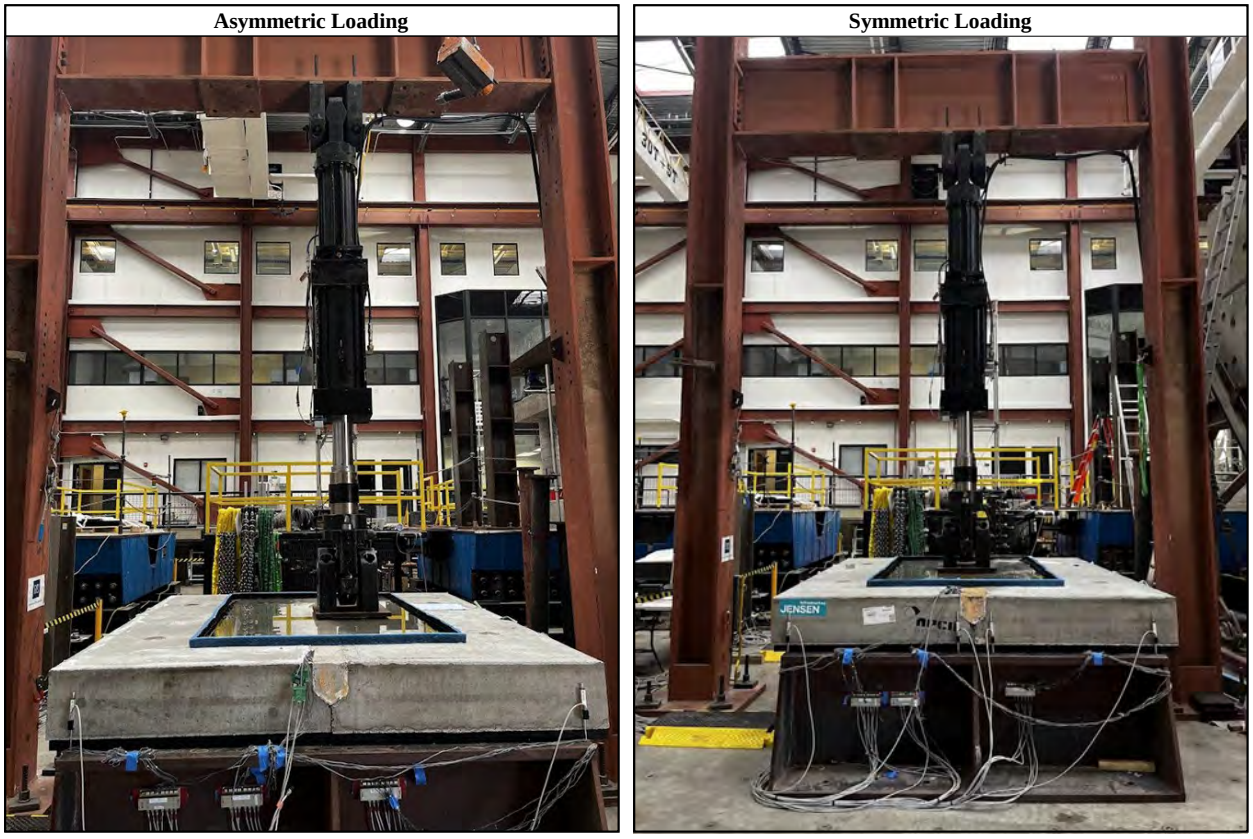

Figure 2.15. Actual test setup with asymmetric loading adjacent to the joint and symmetric loading on top of joint

2.2.4.4 Instrumentation plan

Instrumentation was installed to monitor and record the global response of slabs, strains in the reinforcement, and the joint performance. Vertical deflections were measured using 12 string potentiometers, with a special emphasis on the locations adjacent to the joint. A total of 42 strain gauges were installed on the longitudinal and transverse rebars near the joint to capture the rebar strains at various load levels. The layout of the strain gauges and string potentiometers are presented in Figure 2.16 and Figure 2.17 respectively.

The integrity of bond between the PC and CC in the slab throughout the loading was monitored by checking the water tightness during the test. A shallow pool of water, approximately 0.5 in, was maintained on top of the slabs. The leakage was monitored using four moisture sensors

located along the joint, two embedded within the closure material and two positioned between the adjacent flat faces of the slabs below the joint, connected to the data acquisition system. However, this approach was found to be unreliable, likely due to the polymer resin coating the sensor surfaces. Nevertheless, visual inspection was adopted as primary assessment method, supplemented by continuous video recording using a camera mounted beneath the test slab.

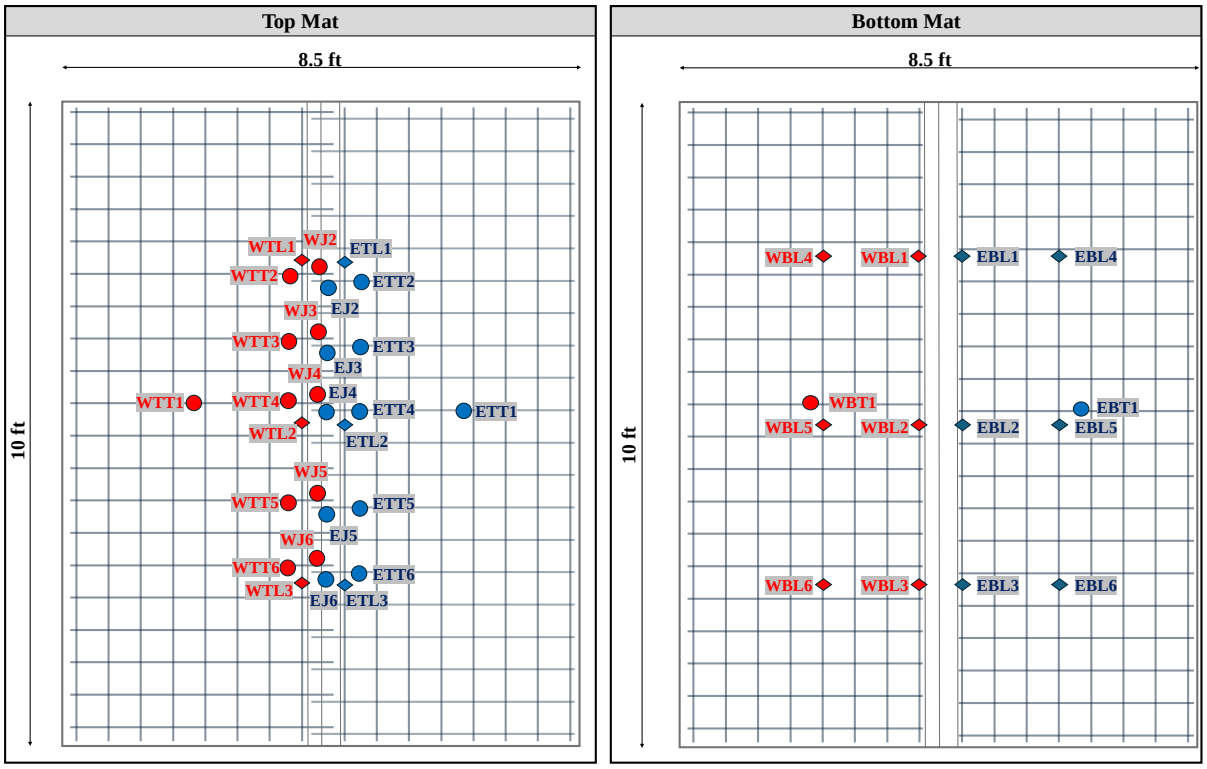

Figure 2.16. Distribution of strain gauges in the top and bottom mat

2.2.4.5 Loading protocol

The loading protocol was designed to replicate service and ultimate limit states in accordance with AASHTO LRFD Bridge design specifications, while also characterizing the post peak failure mechanism. The initial four cycles were force controlled to permit precise application of the code based loads. The first two cycles were applied to 30 kips representing the service load followed by the next two cycles to 50 kips representing the design ultimate load. The loading rate of these cycles was maintained at 5 kips/min.

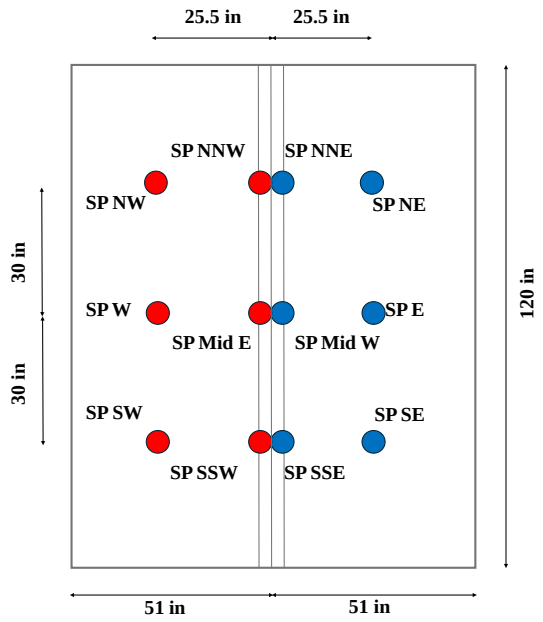

Figure 2.17. Location of string potentiometers

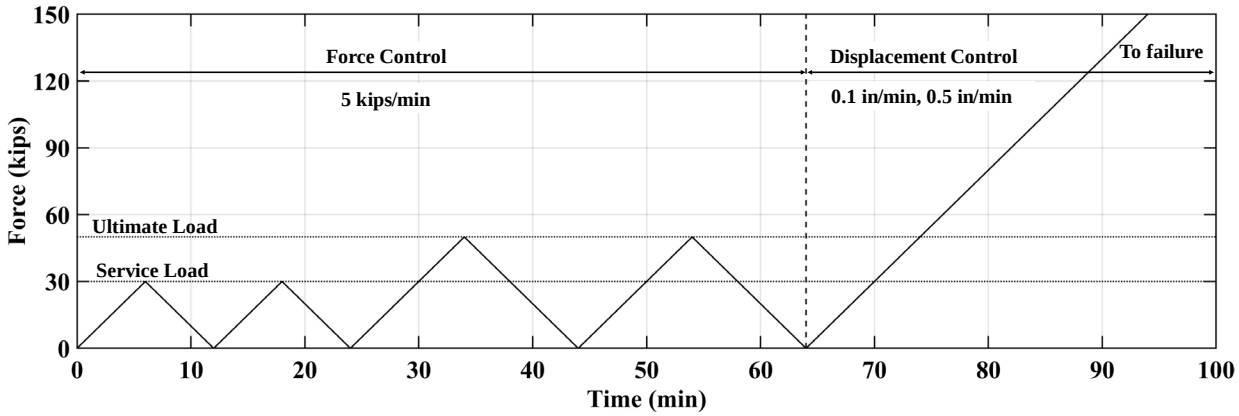

Figure 2.18 Loading Protocol

After the cyclic loading, a displacement control monotonic load was applied at 0.1 in/min until the onset of major water leakage. In order to inspect the specimen to avoid instrumental damage, the specimens were unloaded at this point. The specimens were then reloaded under displacement controlled at five times the original rate, 0.5 in/min and tested until failure. The displacement control loading was chosen for this phase to ensure stable progression of load and to reliably document the post peak response involving reinforcement yielding and crack propagation. The loading protocol has been presented in Figure 2.18. A summarized test matrix has been presented in the next section.

2.2.4.6 Test matrix

A total of four slabs with polymer concrete longitudinal closure joints were constructed and tested in this study. Each specimen was identical to each other in terms of geometry, reinforcement details, and support configuration, with the variables being the PC type used and loading configuration. For brevity, the specimens are named after the PC type used in the joint. A summarized test matrix has been presented in Table 2.8.

Table 2.8. Test matrix for large scale test

Specimen ID	Joint Material	Primer Used	Load configuration
PMMA-PC	Polymethyl methacrylate polymer concrete	Separate set of primer and hardener	Asymmetric: Load adjacent to the joint
PPC	Polyester polymer concrete	Separate set of primer and hardener	Asymmetric: Load adjacent to the joint
EPC	Epoxy polymer concrete	Same resin and hardener as concrete	Symmetric: Load centered at the joint
PVE-PC	Polyvinyl ester polymer concrete	Separate set of primer and hardener	Symmetric: Load centered at the joint

3 RESULTS AND ANALYSIS: MATERIAL BEHAVIOR OF POLYMER CONCRETE

The experimental results of the material tests of six different types of PC followed by their assessment and the results of the test of eight different engineered mixes of PMMA-PC are presented in this section.

3.1 Experimental results

3.1.1 Compressive strength

The compressive strength (CS) of PC cubes and cylinders at specimen age of one, three, seven and twenty-eight days are shown in Figure 3.1 and Figure 3.2 respectively. From these figures, it can be seen that PMMA-PC and PVE-PC have relatively higher CS than other types of PCs at all ages with 10102 psi and 9697 psi being the highest CS of PMMA and PVE-PC cubes at the age of day 28.

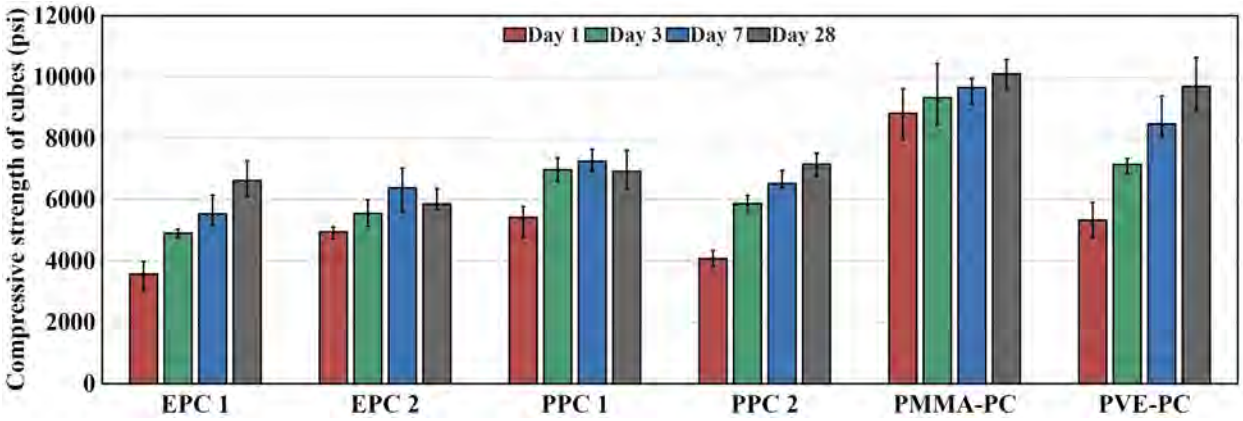

Figure 3.1. Compressive strength of PC cubes

It can also be observed that all types of polymer concrete cubes and cylinders have a CS greater than 3500 psi when tested after 24 hours of casting. The strength progression based on average cube and cylinder strength has been presented in Figure 3.3. In this figure it can be observed that all the types of polymer concrete do not have same strength gain pattern over the course of 28 days. For example, PMMA-PC and PVE-PC despite having comparable CS at the

age of 28 days, PMMA-PC gains 89.67% of it on day one and PVE-PC gains 58.49% of it during the same time. However, all six PCs have at least 58.50% strength gain within the first 24 hours with a maximum of 92.50% in the case of EPC 2.

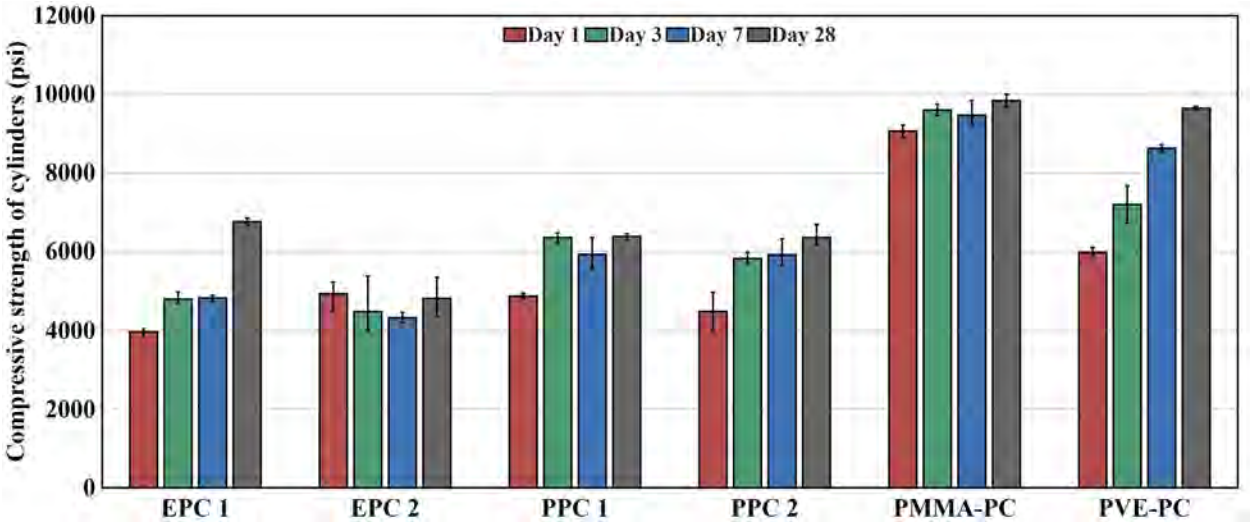

Figure 3.2. Compressive strength of PC cylinders

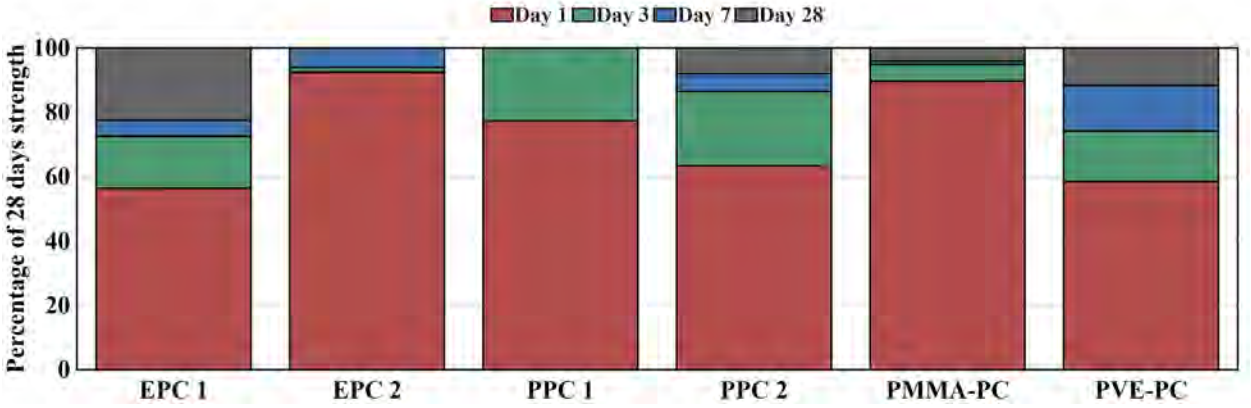

Figure 3.3. Strength progression of PC specimens

3.1.2 Modulus of elasticity

Figure 3.4 and Figure 3.5 show the compressive stress strain behavior obtained from the test of PC cylinders and the modulus of elasticity (MOE). The progression of modulus of elasticity over the course of 28 days follows a similar trend like compressive strength. All the PC have at least 58.61% of 28 days MOE developed within the first 24 hours. Also, like compressive strength, PVE-PC and PMMA-PC have the highest MOE of 2652 ksi and 2501 ksi at the age of day 28.

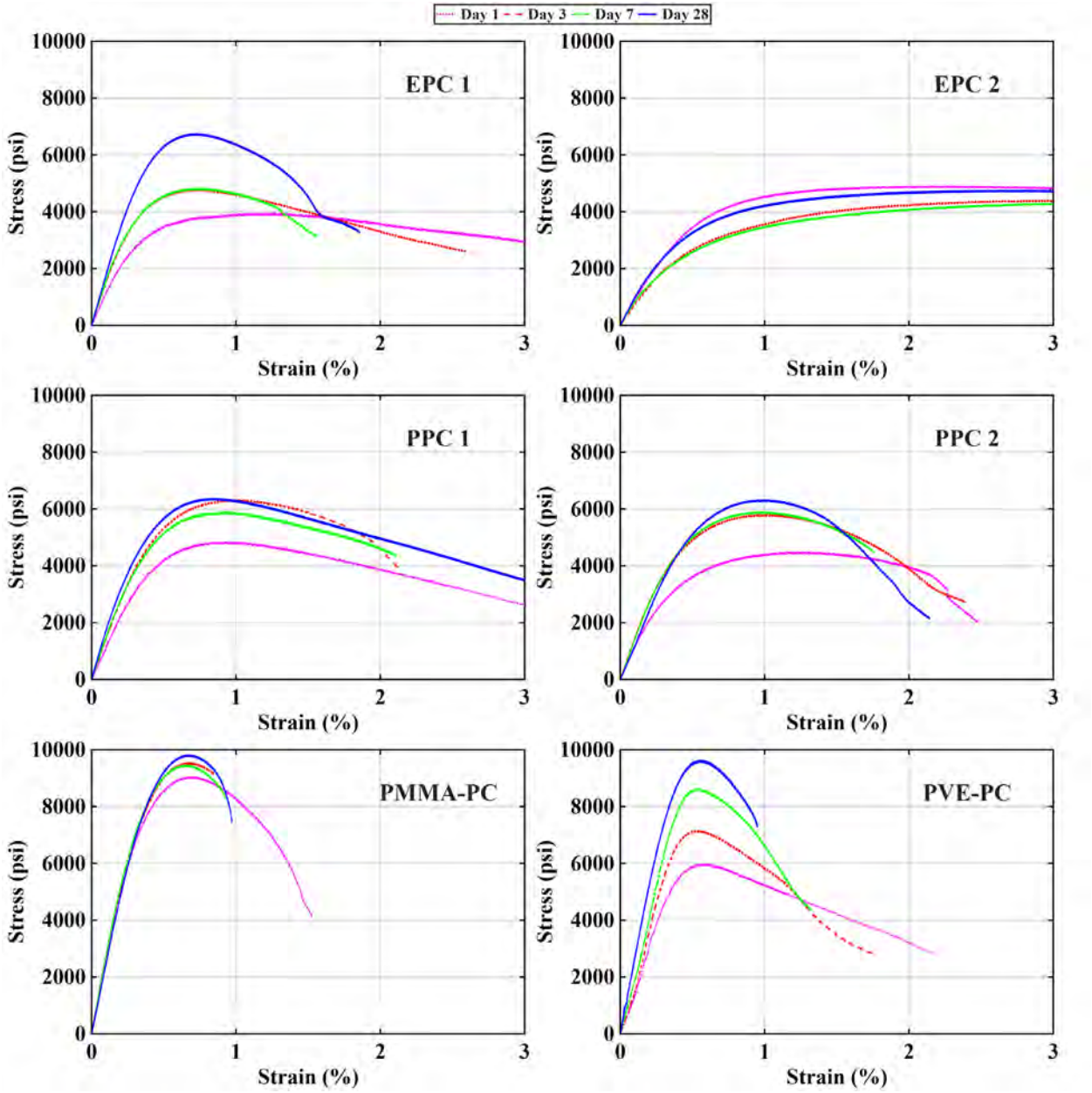

Figure 3.4. Compressive stress-strain behavior of polymer concrete cylinders

It can also be observed that the compressive stress-strain behavior of two PCs of same class may not be identical. For example, EPC 1 and EPC 2, despite having equal quantity of resin of the same class, have different stress strain relationships. The MOE of EPC 1 has been found to be 1764 ksi at 28 days whereas the same for EPC 2 is 843 ksi. Similarly, in the case of polyester polymer concrete, although having a comparable CS, the MOE of PPC 1 is found to be 1620 ksi

at 28 days whereas the same for PPC 2 is 1230 ksi.

Examining the post peak behavior of all the PCs, EPC 2 shows abnormal post peak behavior. EPC 2 has a sustained load capacity for a prolonged period unlike other five PCs. It should be noted that the 3% strain shown in the graph does not represent the ultimate strain capacity of EPC 2. The compressive strength test was continued up to approximately 5% strain, the upper limit of measurement of the LVDT used in the compressometer, where this behavior continued.

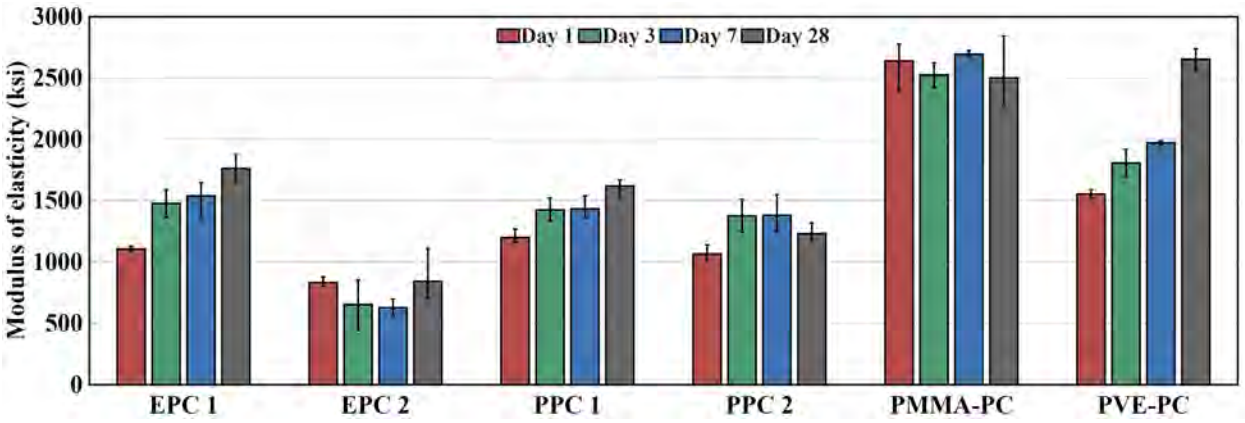

Figure 3.5. Modulus of elasticity of PC

3.1.3 Flexural strength

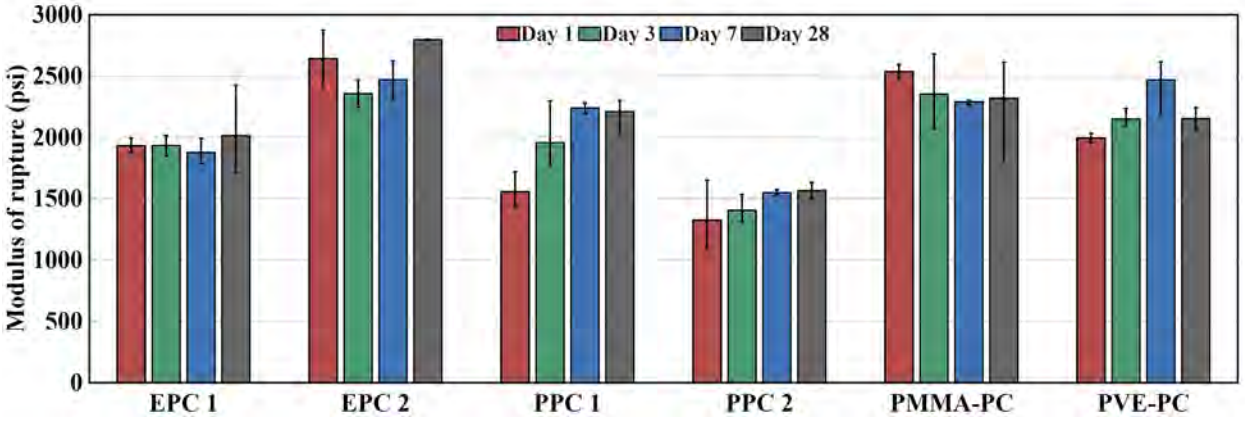

Figure 3.6. Modulus of rupture of 6 PC types

The force deflection behavior of polymer concrete beam subjected to four-point bending is

shown in Figure 3.7. The modulus of rupture for each case has been calculated and shown in Figure 3.6 . It can be observed that the flexural stiffness of all the PC types generally increased with age. It can also be observed that, similar to compression loading, EPC 2 shows a higher flexural deflection at failure compared to all other types of PC. However, it can also be observed there is no significant increase in modulus of rupture (MOR) with age in all types of PC except for PPC 1. Among the PC types, EPC 2, despite having the least compressive strength at the age of 28 days, has the highest MOR of 2796 psi.

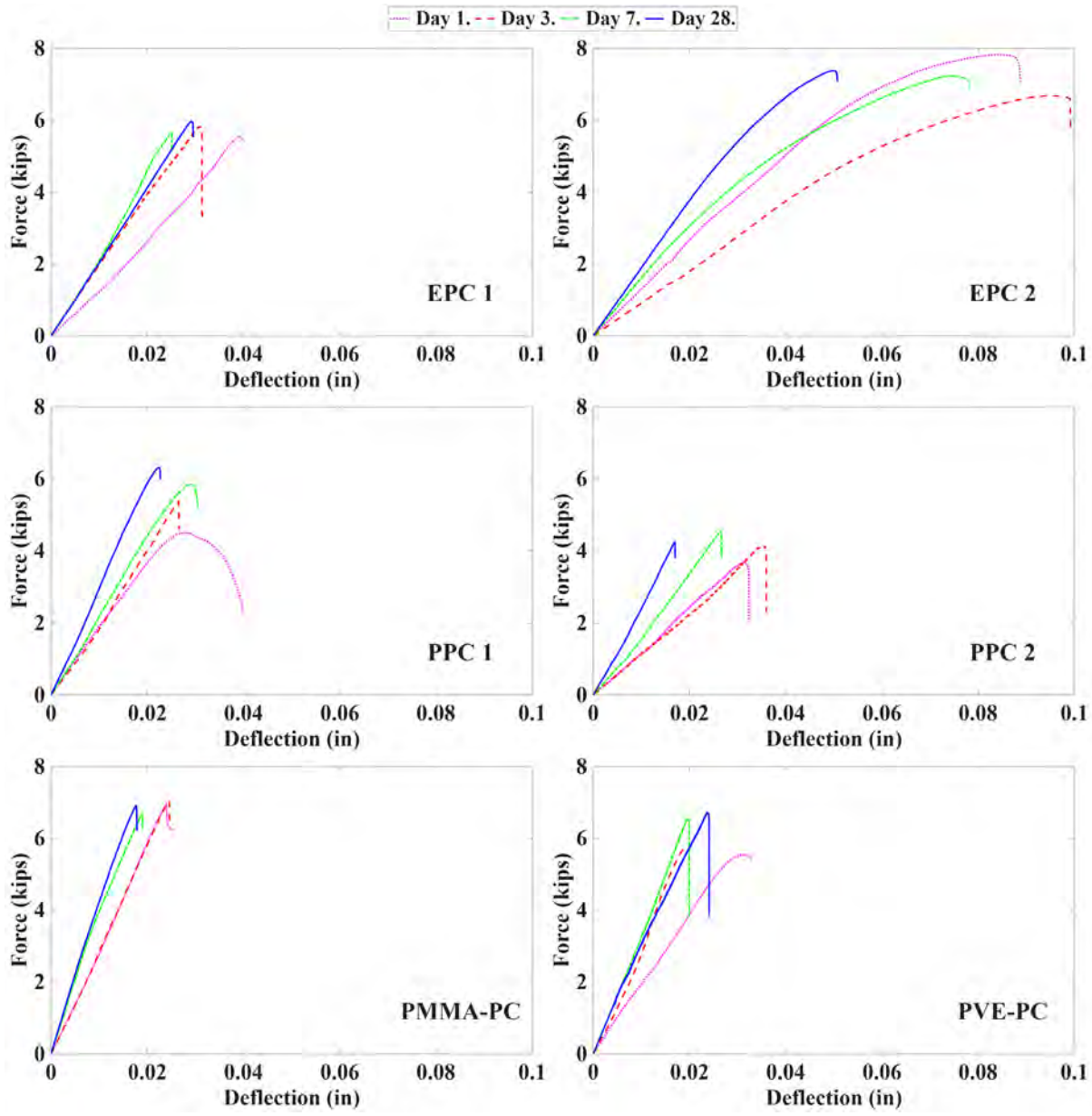

Figure 3.7. Force-Deflection relationship of PC beams subjected to flexure.

3.1.4 Tensile strength

The average tensile stress – strain relationship so obtained has been presented in Figure 3.8 and the average tensile strength has been summarized in Figure 3.9. These figures show that the tensile strength usually increases with the age of PC; however, majority portion of the tensile strength is achieved within the first 24 hours. In addition to that, it can also be observed that PC can achieve a minimum direct tensile strength of 987 psi during that period. At the age of 28 days, PVE PC has

the highest tensile strength of 1722 psi. The tensile stress-strain relationship of PCs at the age of 28 days has been presented in Figure 3.8 which shows that the tensile stiffness of PC is in the ascending order of EPC followed by PPC, PMMA-PC and PVE-PC.

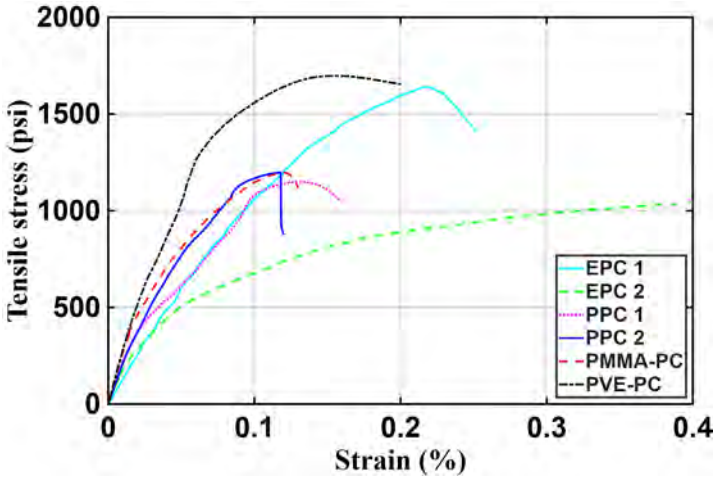

Figure 3.8. Tensile stress-strain relationship of PC dog bones

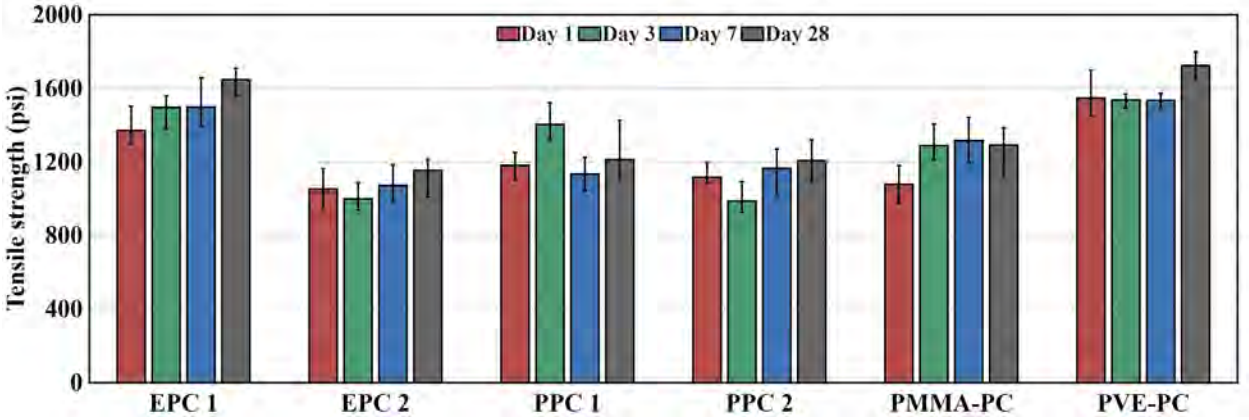

Figure 3.9. Tensile strength of PC dog bones

3.1.5 Shrinkage and abrasion

The percentage shrinkage of PC at the age of seven and 28 days is shown in Figure 3.10 Both seven- and 28-days shrinkage are calculated considering the length of sample during demolding at around 24 hours as initial length. From the figure it can be observed that PMMA-PC has the least shrinkage and EPC 2 has the highest shrinkage of 0.09%. It can also be seen that the rate of

shrinkage is higher in the first seven days compared to the period of seven to twenty-eight days.

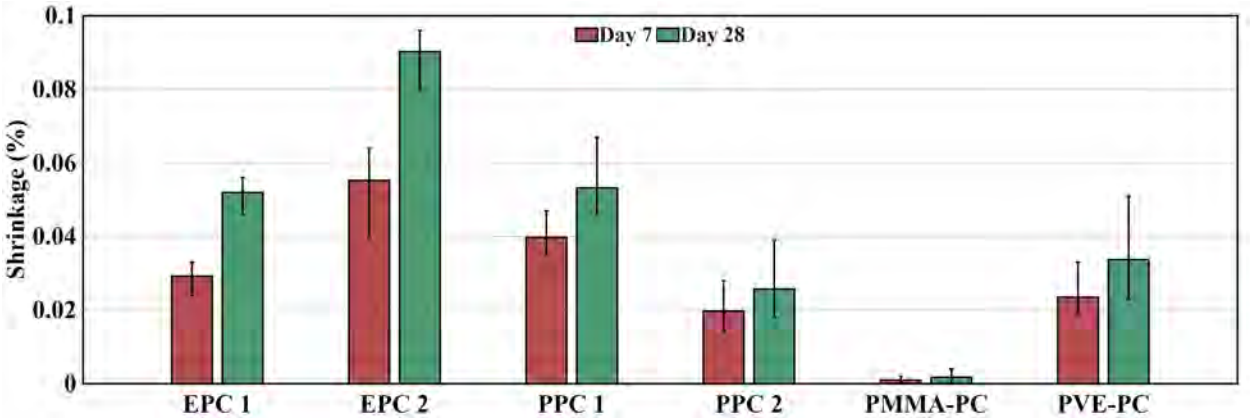

Figure 3.10. Shrinkage of PC

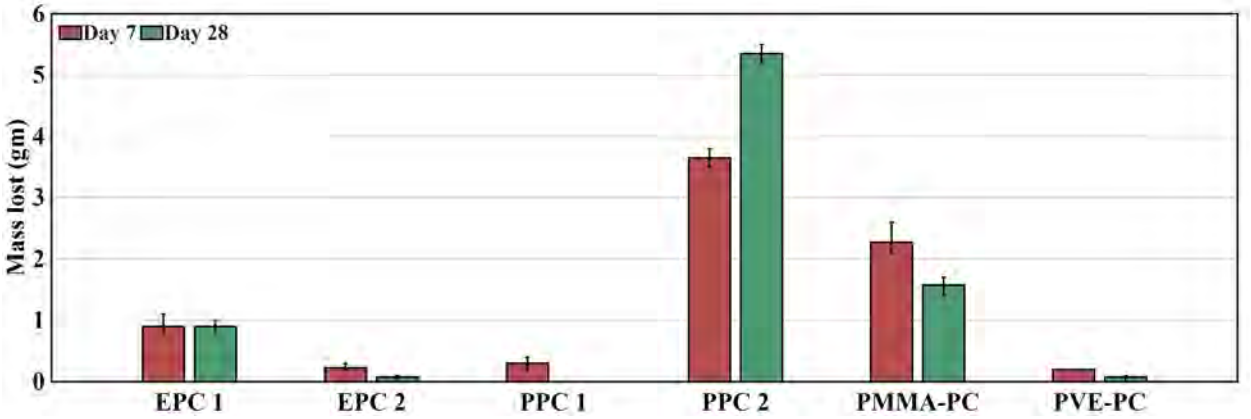

Figure 3.11. Abrasion of PC presented in terms of mass lost.

The mass lost when PC samples were subjected to abrasion is presented in Figure 3.11. PPC 2 has been found to have the least resistance to abrasion followed by PMMA-PC. It can also be observed that the abrasive resistance is usually higher at 28 days than that in seven days. However, in the case of PPC 2 the abrasive resistance is found to be lower at 28 days than at seven days for unknown reasons.

3.2 Assessment and proposed empirical equation.

In this section general equations are proposed to relate mechanical properties of polymer concrete to its compressive strength of polymer concrete. These relationships are not meant to be universally

precise, as a large variation exists across the classes and types of polymer concrete. Rather, the objective of this exercise was to provide a broad guideline that presents a typical trend and offers practical estimate for design purposes.

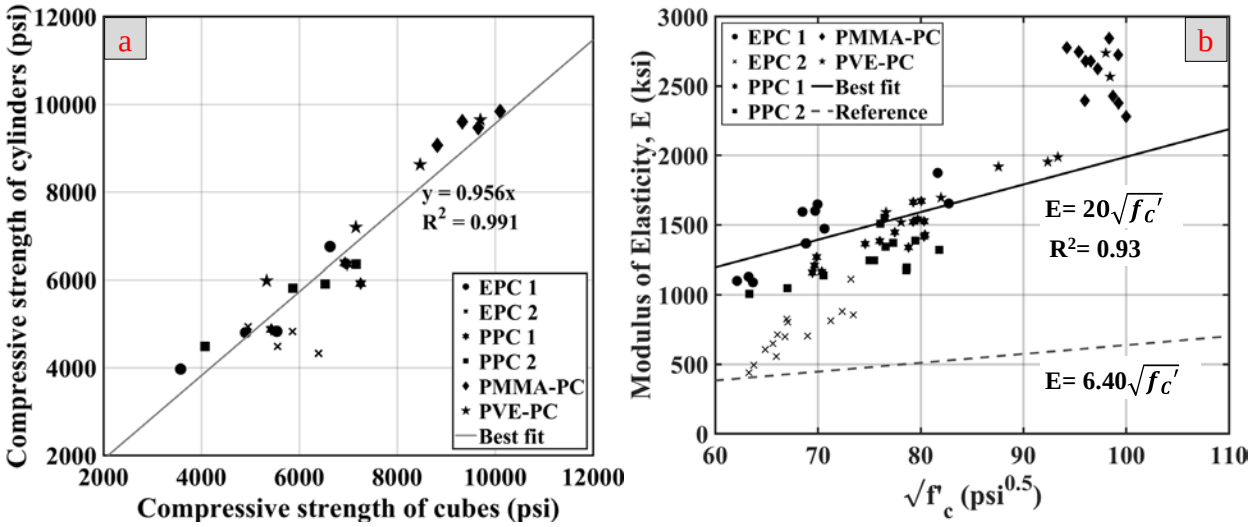

Figure 3.12.a) Proposed relation between compressive strength of PC cylinders and cubes. b) Proposed relationship between modulus of elasticity and compressive strength of PC

A scatter plot of the compressive strength of PC obtained from 3 in x 6 in cylinder against that obtained from 2 in cubes is presented in Figure 3.12a. A regression model was fit, and a line of best fit was obtained as shown in the same figure which shows that the compressive strength obtained from using 3 in x 6in cylinders can be approximated as 0.956 times the strength obtained by using 2 in cubes.

The modulus of elasticity (MOE) of all the PC samples is plotted against the square root of their compressive strength in Figure 3.12b. An equation provided by a previous study by Ferdous Et al. on epoxy polymer concrete relating to the MOE with compressive strength is also plotted for reference. On comparing the obtained MOE with the previous study, the observed MOE values are higher than the predicted values. The MOE of EPC 2 is closer to that predicted by the previous study but the same cannot be said for EPC 1.

Also, a curve of best fit which gives the relationship between MOE and CS of PC has also

been plotted and its equation has been presented in Figure 3.12b, which shows that MOE of PC (in ksi) can be approximated as 20 times the square root of the compressive strength (in psi). This equation, when compared to the standard relationship in the case of conventional concrete shows that the modulus of elasticity of polymer concrete is lower than that of conventional concrete of same strength.

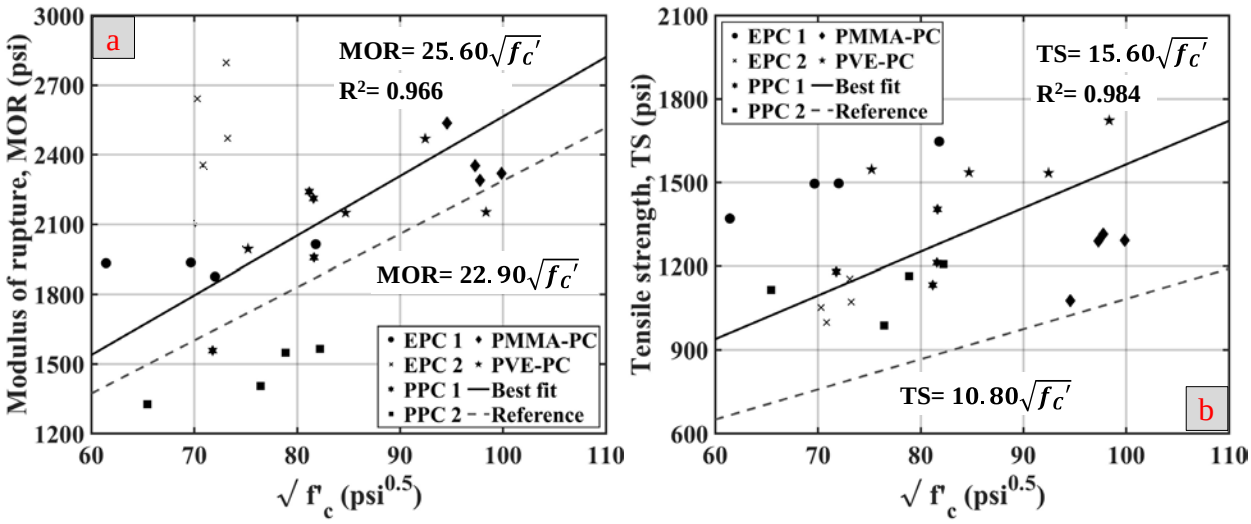

Figure 3.13. Proposed relation between a) Modulus of rupture and b) Tensile strength of PC with its compressive strength Effect of local aggregate and gradation on mechanical properties.

The modulus of rupture (MOR) of all the PCs has been plotted against the square root of their corresponding compressive strength in Figure 3.13a. In this figure, a relationship proposed by a previous study on epoxy polymer concrete has also been shown. A curve of best fit has also been plotted which shows that the MOR of PC, in psi, can be approximated to 25.60 times the square root of its compressive strength, in psi. The previous study by Ferdous Et al. proposed MOR of epoxy polymer concrete as 22.90 times the square root of compressive strength which slightly underestimates the MOR.

The tensile strengths (TS) of PC have been plotted against the square root of compressive strength in Figure 3.13b. A regression model was fit between the TS and square root of the compressive strength, and the obtained curve of best fit is shown in the figure. Additionally, a

relationship proposed by Ferdous Et al. has also been plotted as a reference. From this figure, the TS of PC can be approximated as 15.60 times the square root of compressive strength. On comparing the obtained TS with the previous study, the obtained TS are higher than those predicted by the previously proposed relation.

3.3 Effect of local aggregate and gradation on properties of PMMA-PC

The compressive strength and modulus of elasticity of PMMA-PC with local aggregates are presented in Figure 3.14 and Figure 3.15 respectively. Among the manufacturer's recommended mixes with locally sourced aggregate (mixes 1-3), Mix 3, which contained the largest size of coarse aggregate (CA), has the highest compressive strength as well as modulus of elasticity, with 13,185 psi and 4072 ksi at the age of 28 days, respectively. In contrast, Mix 1, prepared without any coarse aggregate, has lowest compressive strength of 9845 psi.

A comparison of Mix 2 (with locally sourced CA) and Mix 2a (with commercial CA) highlights the influence of aggregate source on the mechanical properties of PMMA-PC. Mix 2 has a 28 days compressive strength of 11,548 psi, which is 17.40% higher than that of Mix 2a while it has a modulus of elasticity of 3,178 ksi, which is 27.1% greater than Mix 2a.

Mixes 4, 5, 6, and 7, which were modifications to Mix 2 and 3, exhibited twenty-eight days compressive strength from 11000 to 12,000 psi and modulus of elasticity of 2950 to 3450 ksi. These values are comparable to those of Mix 2 but lower than that of Mix 3. Similarly, Mix 8, which was a well graded modification of Mix 1, has twenty-eight days strength and modulus of elasticity of 9608 psi and 2107 ksi, both lower than those of Mix 1.

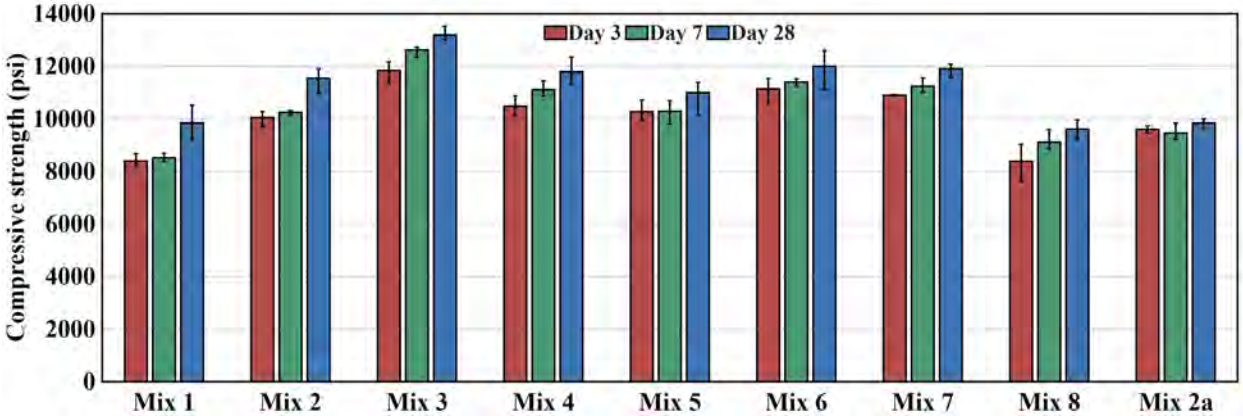

Figure 3.14. Compressive strength of different PMMA-PC mix

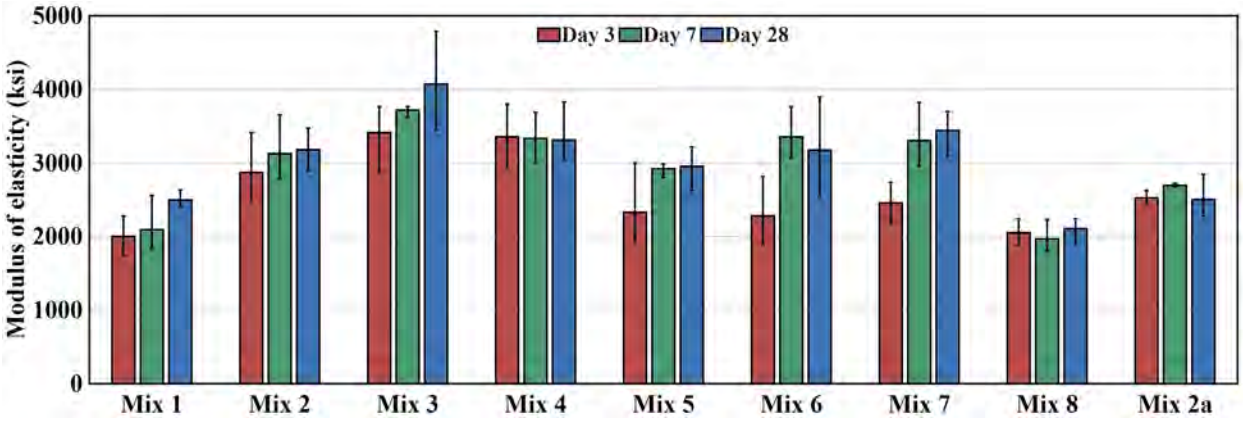

Figure 3.15. Modulus of elasticity of different PMMA-PC mix

4 RESULTS AND ANALYSIS: BOND BEHAVIOR OF POLYMER CONCRETE

This chapter presents the experimental results of tests conducted to evaluate the bond strength of PMMA-PC and PVE-PC in structural applications. Three types of bond strength were evaluated namely bond strength with rebar upon direct pullout, bond strength with rebar upon flexural loading through test of PC beams with spliced reinforcement, and bond strength with conventional concrete subjected to different surface preparation. This chapter concludes with analyses of these results and practical recommendations for PC applications as joint material in bridge and other structural construction.

4.1 Experimental results

4.1.1 Bond with rebar upon direct pullout

Figure 4.1 shows the maximum rebar stress during the pullout test with grade-60 rebar and Figure 4.2 and Figure 4.3 shows the average stress-strain relationship during the pull-out test in PC and UHPC respectively. A line representing the nominal yield stress of 60 ksi has also been plotted for reference. Four distinct modes of failures were identified namely: rebar rupture (R), rebar pull out with a conical failure surface (C), rebar pull out with split in concrete (S), and mixed failure involving both conical and split failure (M) as shown in Figure 4.4 and the number of specimens in each category corresponding to the failure mechanism has been presented in Table 4.1.

From these figures, it can be observed that with the embedment length of two times the diameter of the rebar ($2d_b$), both the PCs and UHPC had a similar bond strength and all the specimens failed with rebar pullout. All the PC specimens with #4 rebar had conical failure surfaces while some of the PC specimens with #5 rebar and all the UHPC specimens had splitting failure accompanied by rebar pullout. On increasing the embedment length to $4d_b$, the bond strength with UHPC was higher than the two PCs. Also, at $4d_b$, the rebar embedded in UHPC could

achieve nominal yield stress whereas not all rebars embedded in PCs could achieve nominal yield stress. The same observation can also be made in the stress-strain relationship curves. The failure mechanism at $4d_b$ was the same as that in $2d_b$.

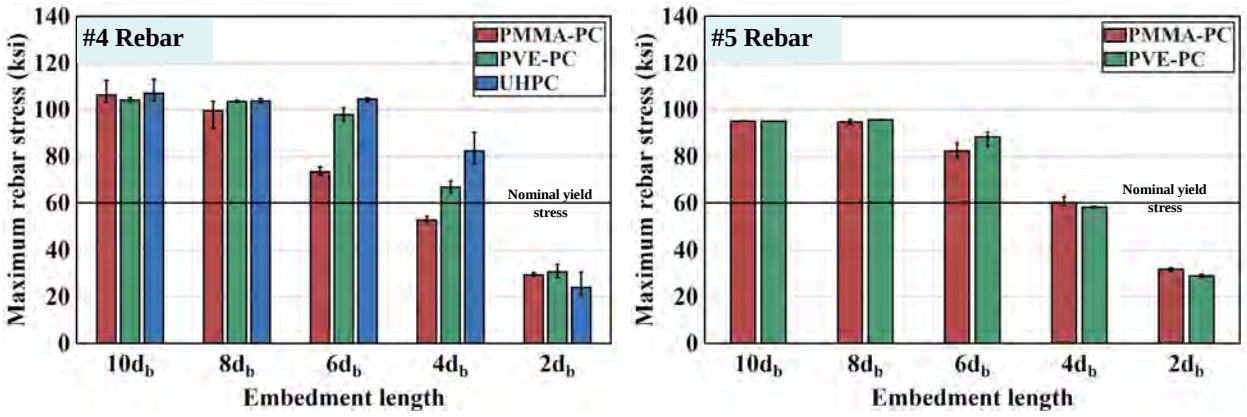

Figure 4.1. Maximum bar stress during pullout test with grade-60 rebar

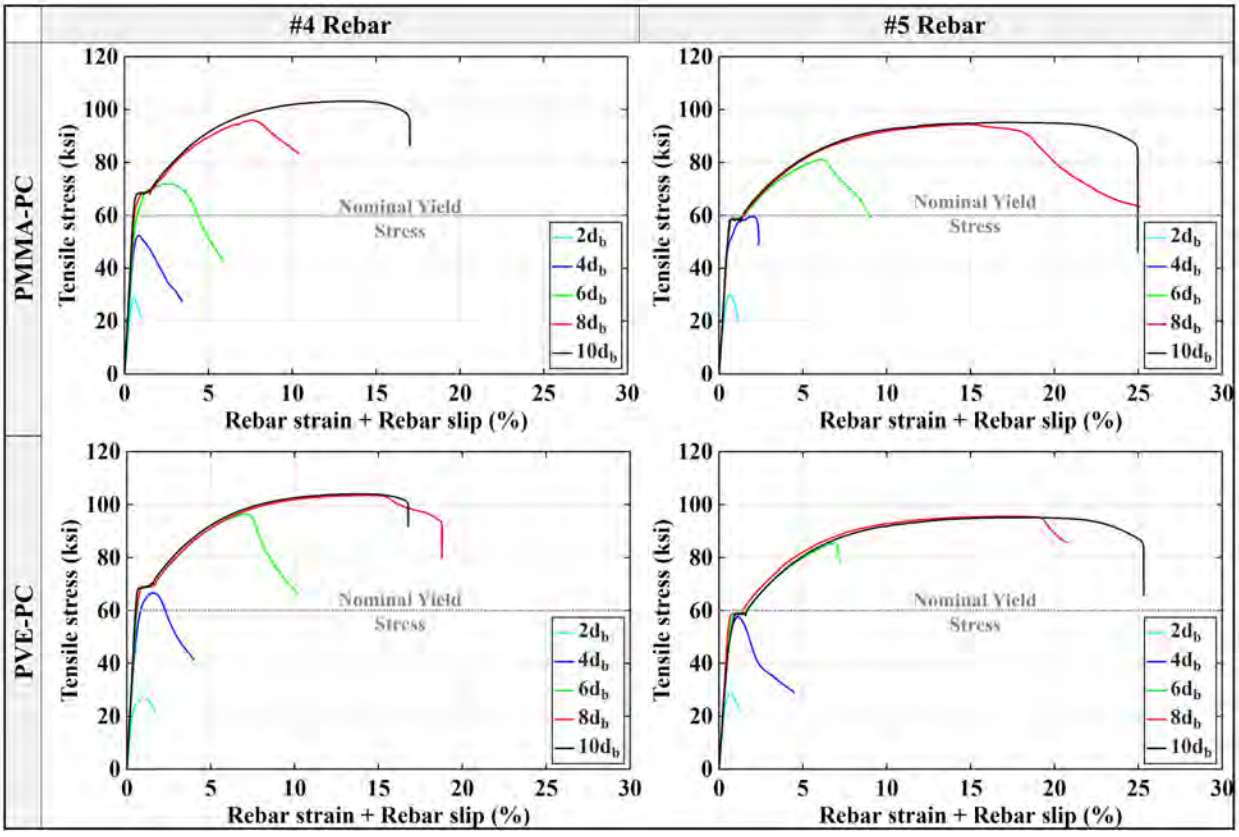

Figure 4.2. Tensile stress vs loading head displacement during pullout test in PC

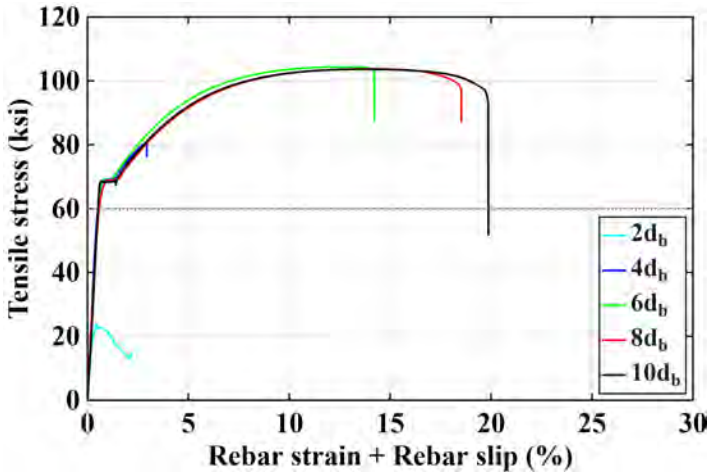

Figure 4.3 Tensile stress vs loading head displacement during pullout test in UHPC.

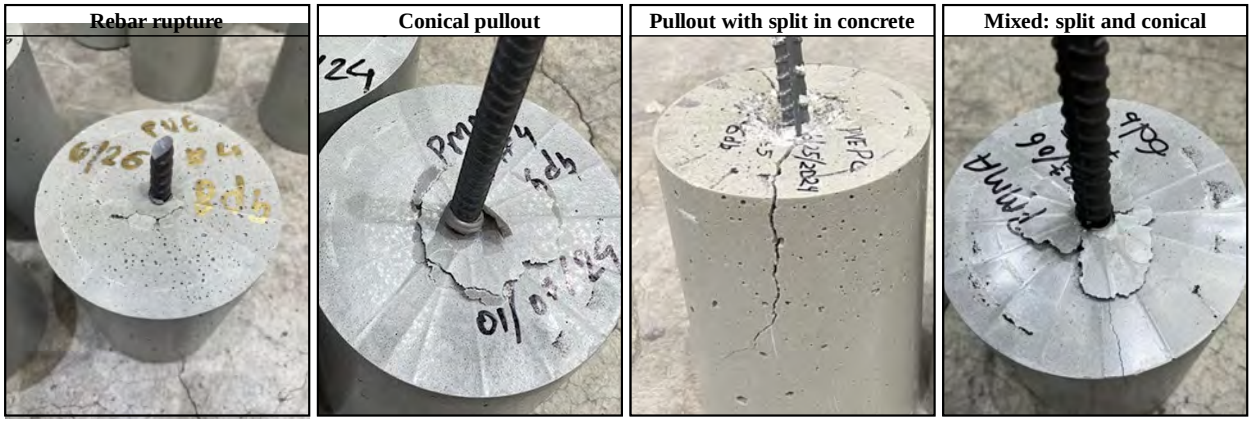

Figure 4.4. Failure mechanism during pullout tests

Table 4.1. Number of pullout specimens of grade-60 rebar corresponding to the failure modes

Embedment length	PMMA-PC								PVE-PC								UHPC			
	#4				#5				#4				#5				#4			
	R	C	S	M	R	C	S	M	R	C	S	M	R	C	S	M	R	C	S	M
10d_b	3	-	-	-	3	-	-	-	3	-	-	-	3	-	-	-	3	-	-	-
8d_b	1	2	-	-	1	2	-	-	2	1	-	-	2	1	-	-	3	-	-	-
6d_b	-	3	-	-	-	1	-	2	-	3	-	-	-	1	2	-	3	-	-	-
4d_b	-	3	-	-	-	1	2		-	3	-	-	-	-	2	1	-	-	3	-
2d_b	-	3	-	-	-	2	1	-	-	3	-	-	-	-	1	2	-	-	3	-

At 6d_b and higher embedment length, the stress in the bar embedded in UHPC reached its ultimate strength with rebar rupture whereas in the case of PCs with 6d_b the rebar yielded but failed to reach the ultimate stress. The failure mechanism was rebar pullout with conical failure surface for #4

rebars in both the PCs whereas concrete splitting was observed in some #5 specimens. At embedment length of $8d_b$ and higher, most of the samples were able to achieve the ultimate strength of rebar, however, the mode of failure was a mix of rebar rupture and pullout with a conical failure surface for $8d_b$ which improved to all the samples failing in rebar rupture at $10d_b$.

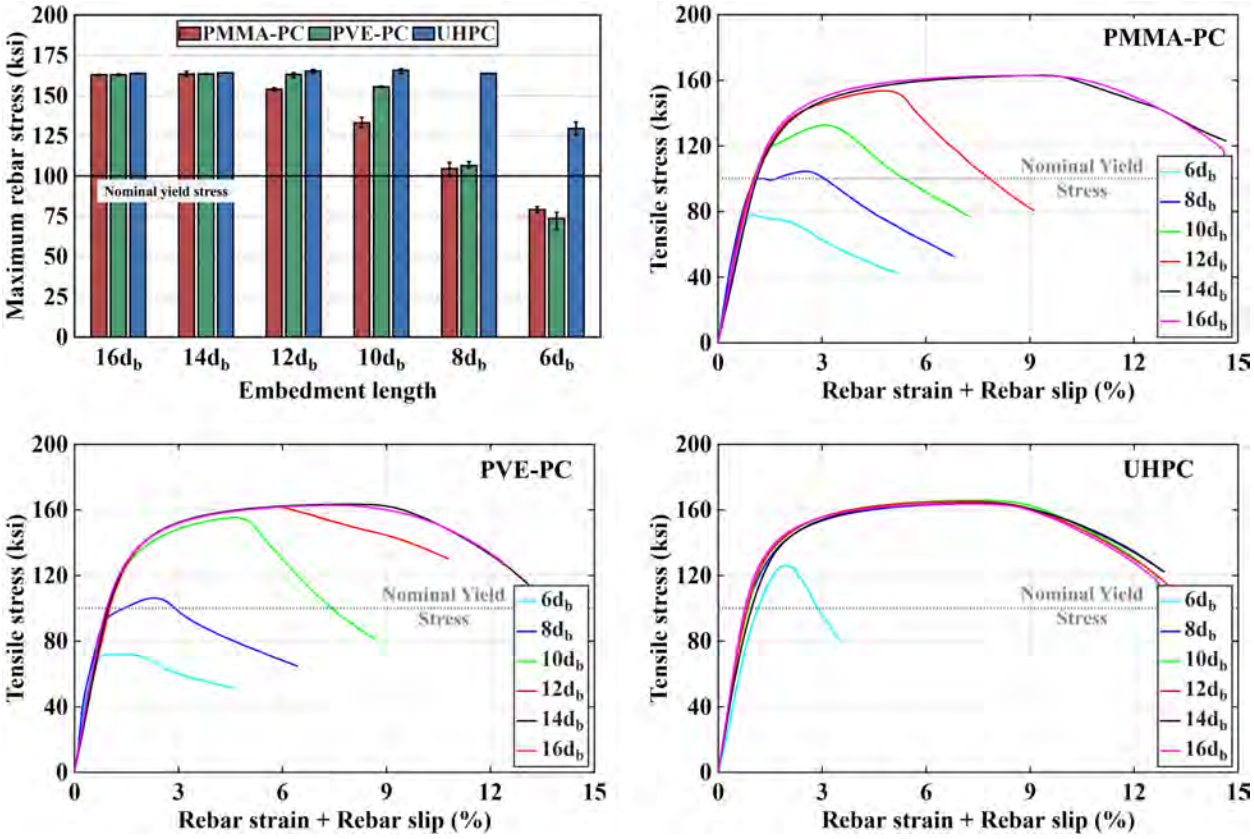

Figure 4.5 Summary of maximum stress in rebar and tensile stress vs loading head displacement during pullout test with grade-100 rebar

Similarly, the peak rebar stress and the stress-strain relationship during the pull-out tests with grade 100 rebar are presented in Figure 4.5 and the summary of the failure mechanism is presented in Table 4.2. In Figure 4.5a, the nominal yield stress of 100 ksi is plotted for reference. From these figures, it can be observed that rebar embedded in both PMMA-PC and PVE-PC can achieve nominal yield stress with the minimum embedment of $8d_b$ and ultimate stress with minimum embedment lengths of $14d_b$ and $12d_b$, respectively. It can also be observed that the required

embedment length for yield and ultimate stress for UHPC is less than $6d_b$ and $8d_b$, respectively. On observing the failure mechanism, PMMA PC, despite achieving ultimate tensile stress at $14d_b$, failed due to rebar pullout with a conical failure surface. Similar to grade-60 rebars, the failure of the UHPC specimen with inadequate embedment length was due to rebar pullout with split in the concrete.

Table 4.2. Number of pullout specimens of grade-100 rebar corresponding to the failure modes

Embedment length	PMMA-PC			PVE-PC			UHPC		
	R	C	S	R	C	S	R	C	S
16d_b	3	-	-	3	-	-	3	-	-
14d_b	-	3	-	3	-	-	3	-	-
12d_b	-	3	-	1	2	-	3	-	-
10d_b	-	3	-	-	3	-	3	-	-
8d_b	-	3	-	-	3	-	3	-	-
6d_b	-	3	-	-	3	-	-	-	3

4.1.2 Bond with rebar upon flexural loading

The results of the bond test of PMMA-PC and PVE-PC and reference UHPC with reinforcing steel under flexural loading has been presented in this section. The results of the flexural tests are organized into three subtopics: the effect of different splice lengths, the comparison between beams with rebars placed in direct contact and those spaced at the maximum distance permitted by code, and the unintended yet observed effect of rebar instrumentation on the bond behavior.

4.1.2.1 Effect of splice length

The ultimate strength of the control and spliced PC and UHPC beams subjected to flexural loading and the average force-deflection are shown in Figure 4.7 . In these figures, the failure modes: Rebar rupture(R), and Rebar slippage (S) for each type of beam are also shown at the end of each curve. A typical example of rebar rupture and slippage is shown in Figure 4.6. The major difference observed during the test between the control and the spliced beams was that the control beams had

a single crack at the midspan of the beams whereas some of the spliced beams had two cracks developed at the two ends of the splice. In Figure 4.6, the crack pattern developed in the soffit of all the beams failed with rebar slippage is shown. In beams that failed with rebar slippage, a diagonal crack was formed between two transverse cracks formed at the end of the splice length. This shows that rebar slippage occurred when the concrete around the rebar failed to transfer the tensile stress from one rebar to another.

From Figure 4.7, it can be observed that the average ultimate load capacity of the control PMMA-PC beam was 34.93 kips, while the same for spliced beams with splice lengths of $8d_b$, $10d_b$, and $12d_b$ were 28.35 kips, 31.71 kips, and 30.76 kips respectively. It can also be observed that all the spliced PMMA-PC beams failed with rebar slippage and could not achieve the ultimate load as well as the displacement capacity of the control beam.

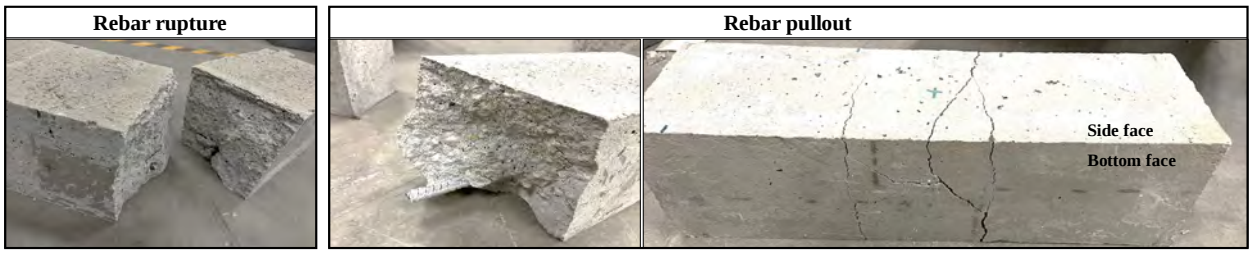

Figure 4.6. Failure mode of beam specimens

The average ultimate load capacity of the control beam and the spliced PVE-PC beams with splice lengths 8, 10, and 12 d_b were 43.10, 30.13, 40.69, and 41.75 kips, respectively. Notably, all the beams except the one with $8d_b$ splice length failed with rebar rupture. Additionally, spliced beams with splice lengths of $10d_b$ and $12d_b$ had greater ultimate deflection than that of the control beams. The primary reason for the higher deflection of the spliced beams compared to the control beam lies in the failure pattern of the beams as shown in Figure 4.6. The control beams failed with a single crack in the midspan whereas the spliced beams failed with two cracks at the ends of the spliced section which increased the length of the rebar section in the crack width region, thereby

increasing the cumulative amount of tensile deformation the rebars could undergo before rupture which ultimately caused the higher ultimate deflection in the spliced beams.

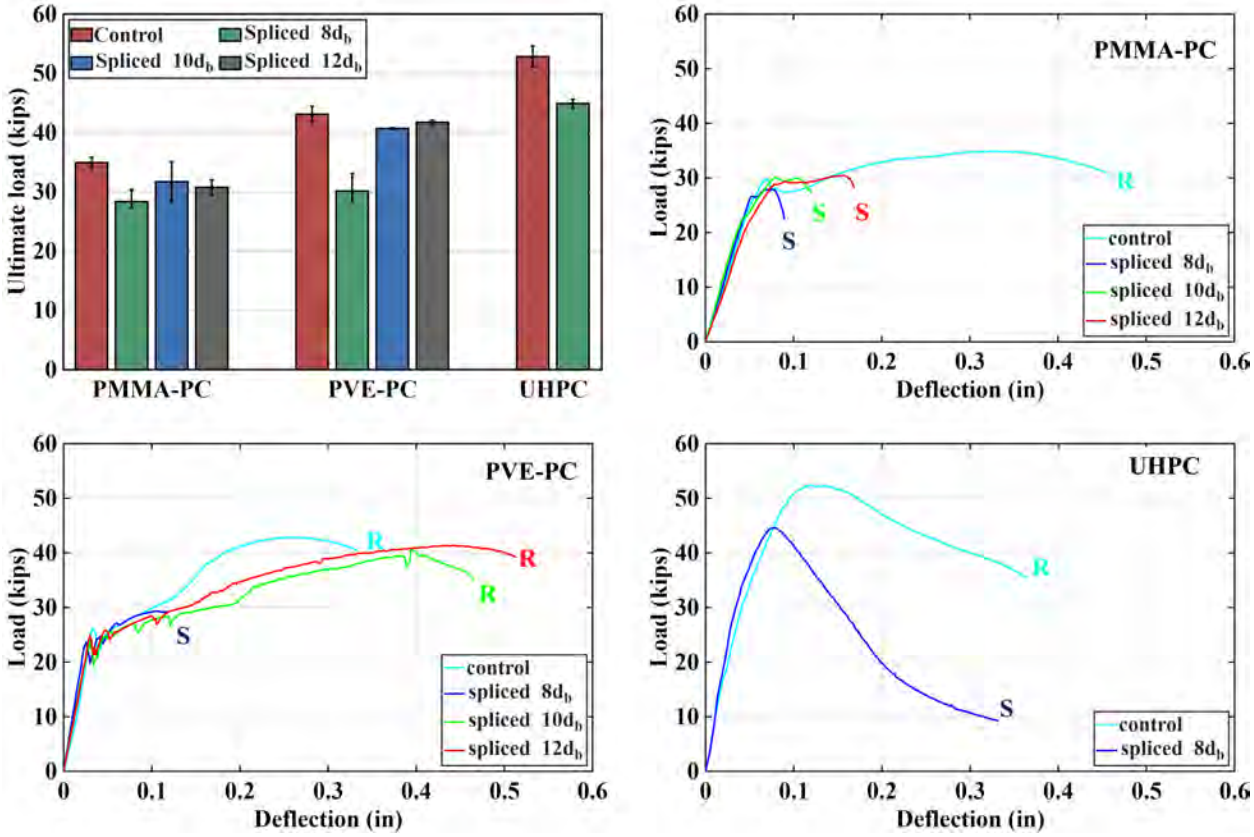

Figure 4.7. Ultimate load capacity and force deflection relationship of spliced beams and their control counterparts\

In the case of reference UHPC beams, the ultimate load capacity of control and spliced specimens were found to be higher than that of corresponding PC beams. The notable difference in the UHPC beams is that there was no drop in the force after the development of crack in both control and spliced cases.

4.1.2.2 Effect of contact of spliced reinforcement

A comparison of the ultimate load capacity and the force deflection relationship of spliced beams with contact and non-contact splicing of length 8db has been presented in Figure 4.8. In these figures, it can be observed that the ultimate load capacity of PVE-PC beams increased to 37.12

kips when the spliced rebars were in contact with each other from 30.14 kips when the spliced rebars were placed at the maximum permissible limit set by the ACI standards. However, this increased ultimate strength was still less than that of the control beam. In the case of PMMA-PC beams, there was no significant change in the ultimate load capacity in those two cases. The ultimate load capacity of PMMA beams were 28.35 kips and 29.08 kips for non-contact and contact splices, respectively. Similarly, the ultimate deflection of the PVE-PC beam also increased with contact splice but didn't change in the case of PMMA-PC beams. Additionally, the failure of all the specimens with both contact and non-contact splice was due to rebar slippage.

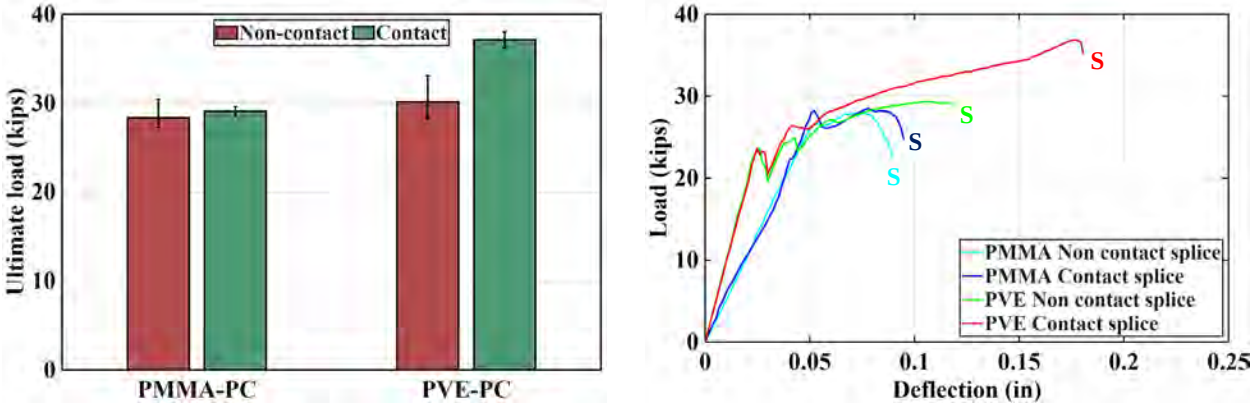

Figure 4.8. Ultimate load capacity and force deflection relationship in contact and non-contact spliced PC beams with splice length of $8d_b$.

4.1.2.3 Effect of rebar instrumentation and strain results

Figure 4.9 shows the effect of using strain gauges on the control and spliced rebars with splice length of $8d_b$ when tested under flexural loading. In these figures, it can be observed that the ultimate strength of both control and spliced PMMA-PC specimens decreased from 34.93 kips and 28.36 kips to 33.13 kips and 25.74 kips respectively when the strain gauges were used. This decrease in the ultimate strength capacity can be associated with the reduced bond between the rebar and PC due to the strain gauges. Similar observations can be made for the PVE-PC beams where the ultimate strength of control and spliced beams reduced from 43.10 kips and 30.14 kips

to 37.18 and 23.54 kips, respectively. Similarly, the ultimate strength of spliced UHPC beams decreased from 44.92 kips to 37.67 kips. On the contrary, the ultimate strength of control UHPC beams remained constant at 52.70 kips.

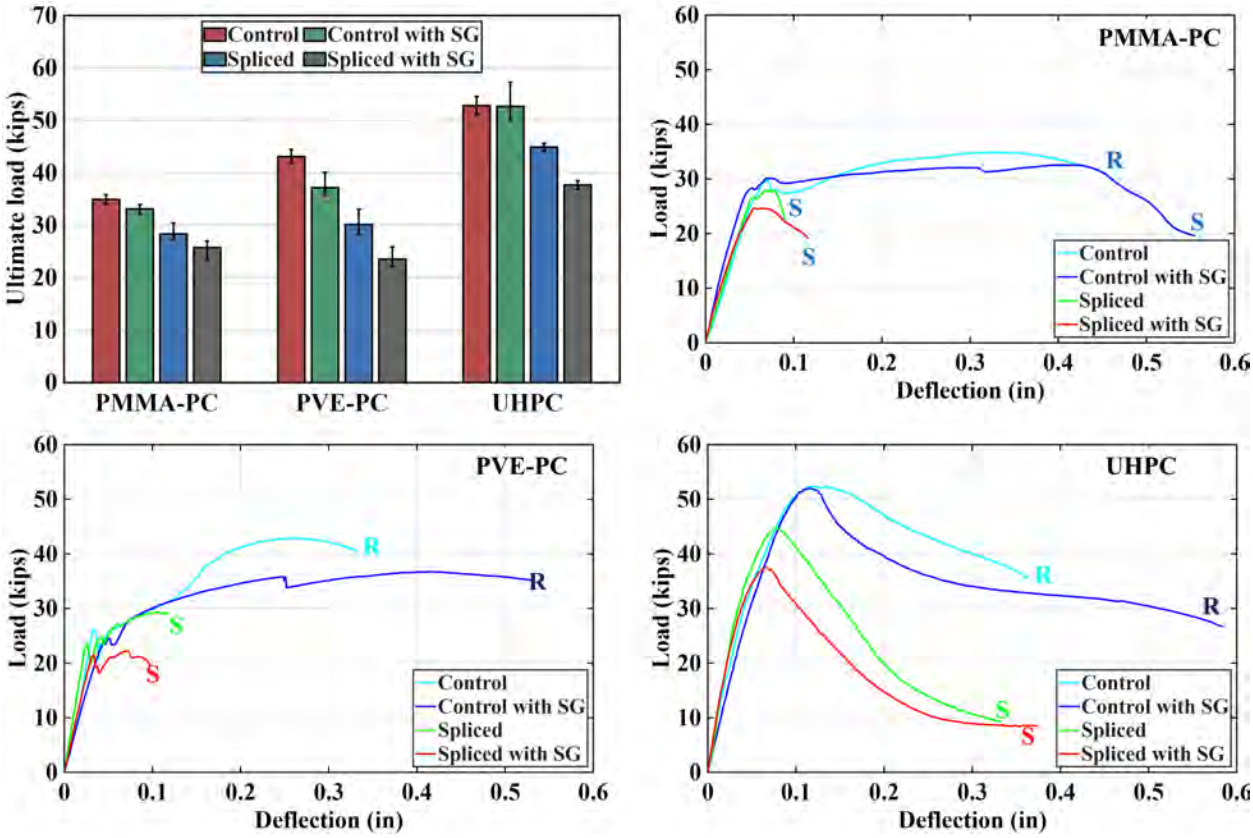

Figure 4.9. Ultimate load capacity of control and spliced beams with and without strain gauge and their load deflection relationship

It can also be observed that the failure mechanism of PVE-PC and UHPC beams were the same, rebar rupture for control specimens and rebar slippage for spliced specimens, with and without strain gauge. However, in the case of PMMA-PC, control specimens with strain gauges also failed in rebar slippage from one of the ends.

The maximum strain in the spliced rebars and the average force-rebar strain relationship in control beams have been presented in Figure 4.10a and b respectively. It can be observed that the maximum strain in spliced rebars of all PVE-PC and UHPC beams exceeded 0.2% yield strain

while in the case of PMMA-PC, a spliced rebar of only one specimen out of three exceeded the 0.2% yield strain. From the force-rebar strain relationship, the force value at 0.20% rebar strain was determined to be 27.68 kips, 24.70 kips, and 31.75 kips for PMMA-PC, PVE-PC, and UHPC, respectively. These values are considered as the elastic capacity of the beams for determining the appropriate splice length.

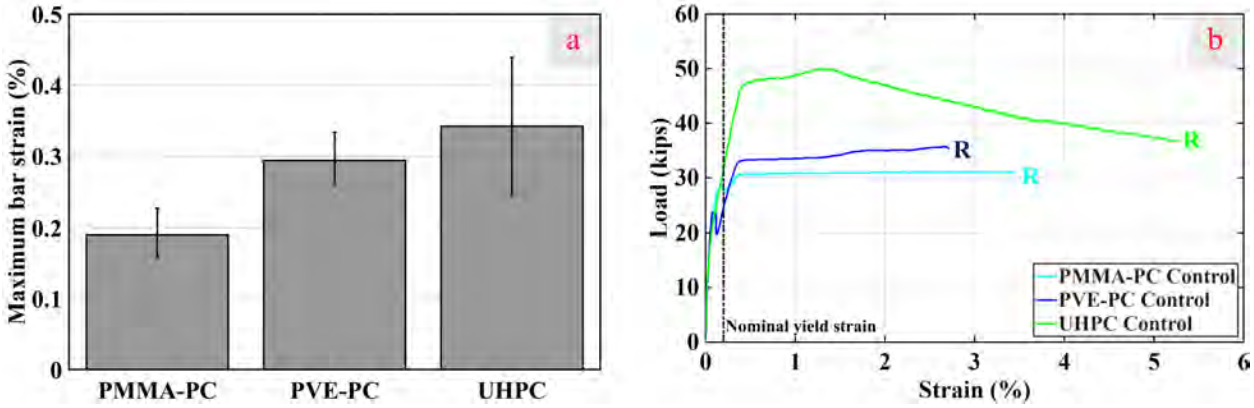

Figure 4.10.a) Rebar strain for beams with rebar splice length of $8d_b$ b) Force – rebar strain relationship for control beams

4.1.3 Bond with conventional concrete

The bond strength of PCs with conventional concrete was evaluated using four types of specimens, categorized based on the state of surface preparation and use of bonding agent: i.no surface preparation without a bonding agent, ii. surface preparation by sandpapering without a bonding agent, iii. no surface preparation but with a bonding agent, and iv. surface preparation by sandpapering in addition to using a bonding agent. For UHPC, specimens without bonding agent were used. Specimens after testing and the representative pictures of two observed failure mechanisms: pure bond failure and bond failure with substrate cracking are shown in Figure 4.12. All the test specimens had bond failure except for PVE-PC specimens with primer, in which failure of the conventional concrete substrate was observed for some specimens. This mode failure with substrate cracking signifies that the observed peak strength was less than actual bond strength as

the substrate failed earlier than the bond between the two wedge pieces.

Figure 4.11 shows the bond strength of PCs and UHPC with conventional concrete. It can be seen that, for both PC combinations of sandpapering the surface along with the use of a primer as a bonding agent leads to the highest bond strength of 3400 psi for PVE-PC and 2430 psi for PMMA-PC whereas for UHPC the highest bond strength of 2330 psi was obtained when no surface preparation was performed. A line representing the minimum bond strength of 2000 psi required for the repair and rehabilitation of structures as per ACI 546.3R [54] has also been plotted where it can be observed that surface preparation by sandpapering with the bonding agent can satisfy the required bond strength for both PMMA-PC and PVE-PC .

Observing the effect of surface preparation, in the case of PMMA-PC without using a bonding agent, the bond strength increased by 7.88% when the conventional concrete surface was sandpapered while for the same materials bonded using a bonding agent, the bond strength increased by 51.37%. Similarly, in the case of PVE-PC with and without a bonding agent, the increase in bond strength was found to be 88.12% and 6.87%, respectively. However, in the case of UHPC, an opposite effect was observed where sandpapering the conventional concrete surface decreased the bond strength by 63.88%. This opposite effect of surface preparation on PC and UHPC can be attributed to the consistency of the PC and UHPC mix. UHPC is pastier than PC mix and does not bleed upon tamping whereas PC has a greater flow value and bleeds like conventional concrete upon tamping. This allowed the polymer resin itself or the bonding agent to infiltrate inside the micro surface indentations as shown in Figure 4.13 created by sand papering, which increased the bond strength. However, in the case of UHPC, the pastier UHPC mix could not infiltrate the micro indentations, leading to the opposite effect. It can also be observed that, when no surface preparation was performed, the bond strength of UHPC with CC was found to be

higher than that of PCs with CC. Figure 4.13 also shows the enlarged view of the CC surface without any surface preparation on the same scale, in which the surface indentations due to the mold are larger than when the surface was sandpapered. As a result, both UHPC and PC mix were able to seep inside the indentations. This resulted in higher bond strength for UHPC due to its superior strength.

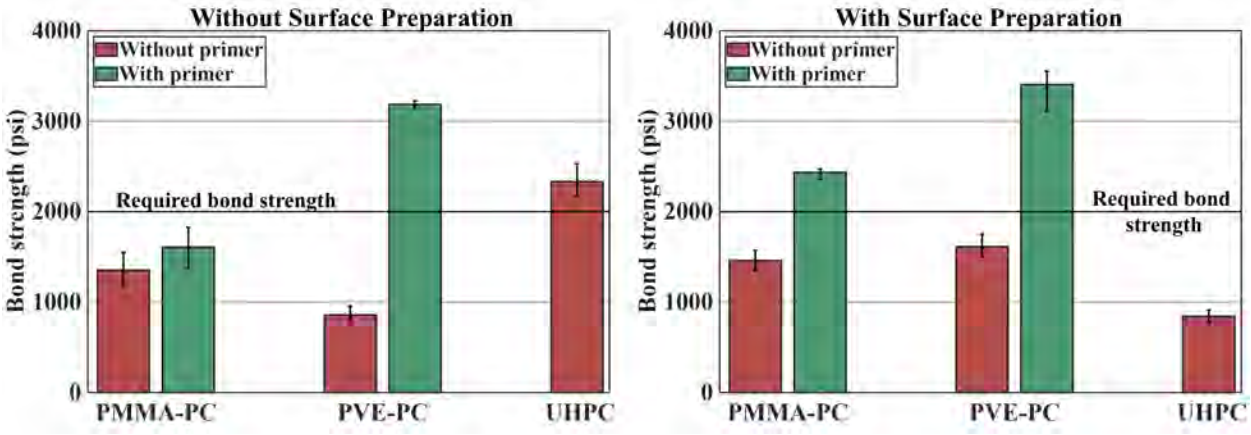

Figure 4.11. Bond strength of PMMA-PC and PVE-PC with conventional concrete

Figure 4.12. a) PVE-PC specimens after testing b) Typical example of bond failure with substrate cracking c) Typical example of pure bond failure

Comparing the effect of the primer as a bonding agent in PCs, the bond strength increased by 18.90% and 66.83% for PMMA-PC without and with surface preparation respectively, and by 271.64% and 111.13% for PVE-PC without and with surface preparation. respectively. From these results, it can also be seen that among the two methods to improve the bond strength between

polymer concrete and conventional concrete, using a bonding agent was more effective than surface preparation.

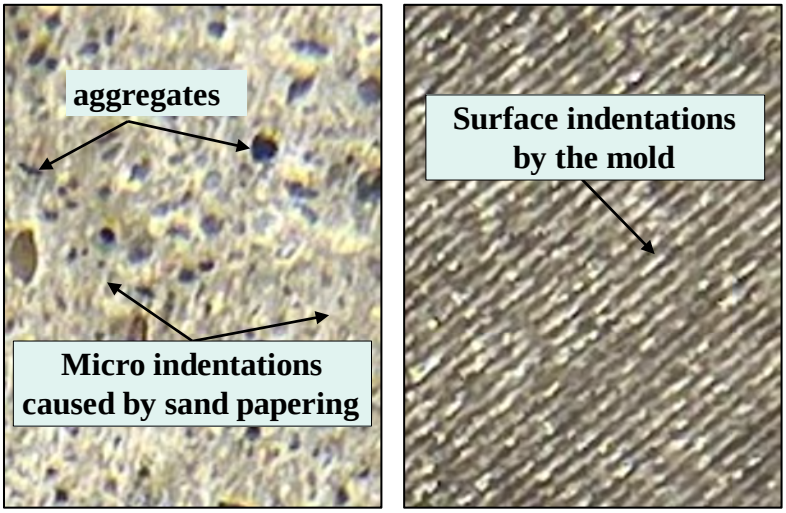

Figure 4.13. Magnified view of the conventional concrete surface with and without sand papering

4.2 Analysis and recommendations

4.2.1 Bond with rebar upon direct pullout

The average bond strength between the rebar and concrete was calculated using **Error! Reference source not found.** suggested by Graybeal et al. in a previous study [18] and summarized in Table 4.3. In this equation μ_{test} is the calculated bond strength, $f_{s,max}$ is the bar stress at failure, d_b is the diameter of the rebar and l_d is the embedment length.

$$\mu_{test} = \frac{f_{s,max} * d_b}{4 l_d} \tag{4.1}$$

Table 4.3. Average bond strength obtained from pullout test (ksi)

Concrete / Rebar type	Grade 60		Grade 100
	#4	#5	#4
PMMA-PC	3.31	3.53	2.68
PVE-PC	3.88	3.18	3.42
UHPC	4.07	-	3.60

The minimum embedment length in terms of rebar diameter (l_d/d_b) required to achieve

yield and ultimate strength in the rebar was calculated using **Error! Reference source not found.** and summarized in Table 4.4. In this equation, μ_{avg} is the average bond strength and f_s is the nominal yield or the ultimate strength of rebar taken as 60 ksi and 90 ksi for grade 60 rebar and 100 ksi and 115 ksi for grade 100 rebar, respectively.

$$\frac{l_d}{d_b} = \frac{f_s}{4 * \mu_{avg}} \tag{4.2}$$

Table 4.4. Embedment length (l_d/d_b) for yield and ultimate strength

Concrete / Rebar type	Based on yield strength			Based on ultimate strength		
	Grade 60		Grade 100	Grade 60		Grade 100
	#4	#5	#4	#4	#5	#4
PMMA-PC	4.53	4.25	9.33	6.79	6.38	10.73
PVE-PC	3.92	4.72	7.30	5.88	7.08	8.39
UHPC	3.69	-	6.94	5.53	-	7.99

4.2.2 Bond with rebar upon flexural loading

Building on the results presented in the previous section, this section evaluates the influence of splice length and splice configuration by comparing the performance of spliced beams with the elastic and ultimate load capacities determined previously.

The load capacity of PVE-PC beams with splice lengths of $8d_b$ and greater exceeded the elastic capacity of the control PVE-PC beam, measured at 24.70 kips. Also, in PVE-PC beams the strain in spliced rebar exceeded the design yield strain of 0.20%. Similarly, UHPC beams with the same splice length also exceeded the corresponding elastic capacity of 31.75 kips with the strain in rebar exceeding the design yield strain of 0.20%. In contrast, for PMMA-PC beams, the load capacity of two of the specimens with a non-contact splice length of $8d_b$ was found to be lower than the obtained elastic capacity of the control beam, which is 27.68 kips. Additionally, not all rebars in these beams achieve their maximum strain greater than the design yield strain of 0.20%. However, the load capacity of the PMMA-PC beams with non-contact splice lengths of $10d_b$ and

higher exceeded the corresponding elastic capacity of control beams. Based on these findings, it is recommended to use non-contact splice lengths of $10d_b$, $8d_b$, and $8d_b$ for PMMA-PC, PVE-PC, and UHPC beams respectively to achieve the elastic capacity of their control counterparts.

The ultimate load capacity of PVE-PC and PMMA-PC beams increased by 23.18% and 2.59% respectively on providing contact splice. Although the increase in ultimate strength by 2.59% in PMMA-PC seems insignificant, the ultimate capacity of the spliced PMMA-PC beam with contact splice measured at 29.08 kips is higher than the elastic capacity of the control beam measured at 27.68 kips. Therefore, a contact splice length of $8d_b$ is sufficient in both PMMA-PC and PVE-PC beams to achieve the elastic capacity of corresponding control beams. When comparing the ultimate capacity of the control PC beams with their spliced counterparts, the spliced PVE-PC beams with a splice length of $10d_b$ achieved an ultimate load capacity of 40.70 kips which is slightly lower than the corresponding ultimate capacity of control beams at 43.10 kips. However, the failure of all the PVE-PC beams with splice lengths of $10d_b$ and higher is governed by rebar rupture. So, a non-contact splice length of $10d_b$ can be deemed sufficient for PVE-PC beams to achieve their ultimate capacity.

In the case of PMMA-PC, the ultimate load as well as the displacement capacity of the spliced PMMA-PC beams with a splice length of $12d_b$, which was the longest splice length considered in this study, remained lower than that of control beams. It was not feasible to further increase the splice length from $12d_b$ due to the dimensional limitations of the beam specimens used. On comparing the recommendations of this study with existing literature, the $4.1d_b$ lap splice length recommended by [21]in PMMA-PC beam with #4 rebar and $3d_b$ cover to achieve yield in the spliced rebar is found to be insufficient when the clear cover of $2d_b$ (1 in) is used.

5 RESULTS AND ANALYSIS: THERMAL PERFORMANCE OF POLYMER CONCRETE

This section presents and analyzes the results of study on mechanical and bond behavior of PC subjected to thermal stresses. For brevity, polymer concrete specimens subjected to ten heating and cooling thermal shocks between 55° C - 0° C, similar thermal shocks between 110° C - 0° C, and constant temperature of -25° C are referred as T55, T110 and T-25 specimens, respectively.

5.1 Compressive strength and modulus of elasticity

The compressive strength and the compressive stress-strain relationships of PMMA-PC and PVE-PC cylinders subjected to thermal shocks are presented in Figure 5.1 . Additionally, the modulus of elasticity of these cylinders has been presented in Figure 5.2. It can be observed that the thermal shocks at 55 °C (T55) and 110 °C (T110) had minimal influence on the compressive strength of both PMMA-PC and PVE-PC when compared to the control specimens of the same age. However, the compressive stiffness of both materials, expressed in terms of the modulus of elasticity, was significantly affected by the same thermal shocks. As summarized in Table 5.1, the MOE of both PMMA-PC and PVE-PC decreased relative to their late age (test day) reference values when subjected to T55 and T110 conditions. For PMMA-PC, at T55 condition, the modulus of elasticity reduced from 2870 ksi at late age to 2350 ksi and further to 1740 ksi at T110. Similarly, the modulus decreased from 2575 ksi to 2035 ksi at T55 and to 1500 ksi at T110.

Table 5.1. Compressive strength and modulus of elasticity of PC subjected to thermal stress

Test condition		**Compressive strength (psi)**		**Modulus of elasticity (ksi)**	
		PMMA-PC	**PVE-PC**	**PMMA-PC**	**PVE-PC**
Reference	Early age	9,460	8,620	2,700	1,970
	Late age	9,420	11,360	2,870	2,575
Thermal conditions	T55	9,980	11,340	2,350	2,035
	T110	9,020	11,310	1,740	1,500
	T-25	14,750	15,300	3,160	3,330

This softening behavior can be attributed to the onset of resin chain mobility resulting from

thermal exposure and the impact of thermal variations. Resin chain mobility refers to the phenomenon in which the long chains of polymer gain freedom to slide and rotate relative to each other, near and beyond the glass transition temperature. While the resin chain mobility reduces the stiffness of the resin temporarily at the elevated temperature, the observed results indicate that, with repeated exposure in terms of thermal shocks, this temporary softening can leave irreversible changes. Nevertheless, the preservation of compressive strength indicates that the resin-aggregate bond, and thus the overall structural integrity of the concrete remained intact despite the thermal shocks beyond the glass transition temperature. Although the compressive strength of PMMA-PC and PVE-PC was preserved, the reduction in modulus of elasticity observed after exposure to thermal cycles, most notably under T110 conditions, implies increased potential of greater deflection at service load. Combined with inherently lower MOE of PC compared to conventional concrete, this reduced stiffness under extreme thermal exposure may contribute to deflection incompatibility with conventional concrete in bridge joints.

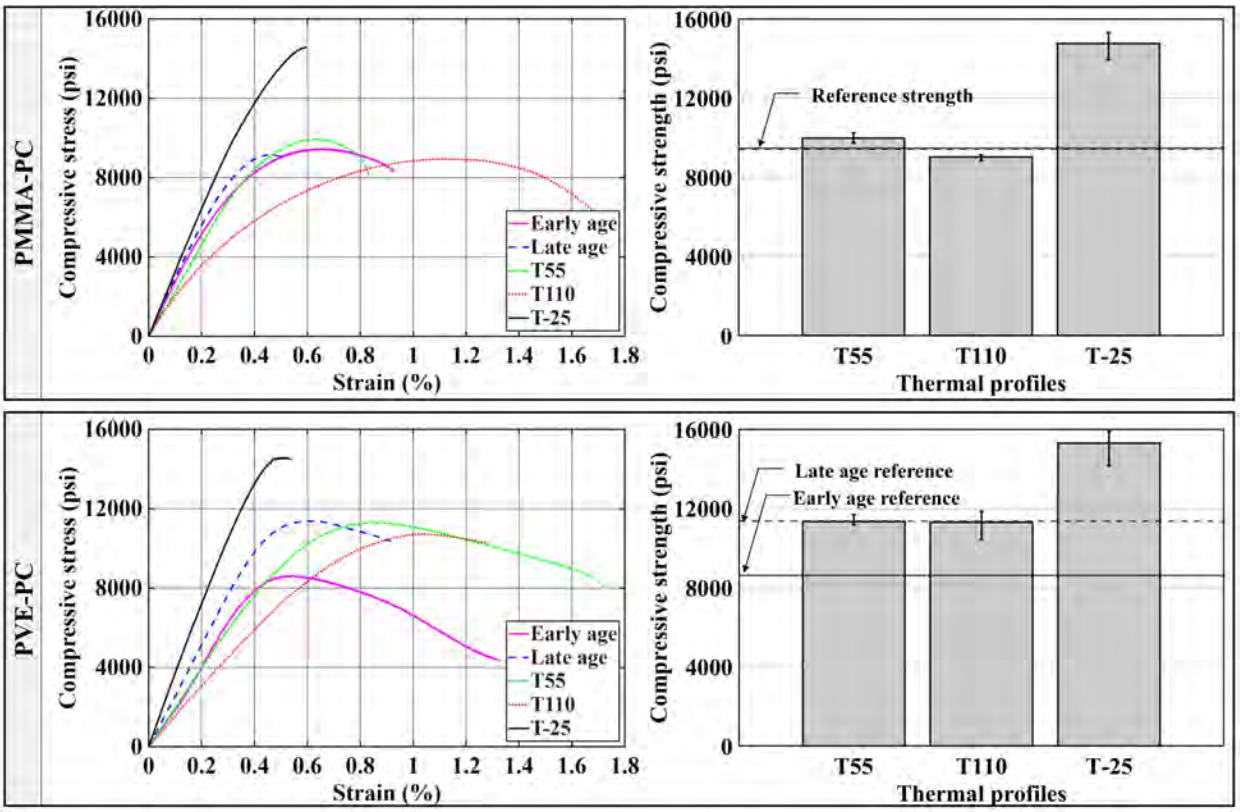

Figure 5.1. Average compressive stress – strain relationship and compressive strength of PC subjected to the three thermal conditions.

In contrast, when the PC specimens were subjected to prolonged subzero conditions at -25°C and tested at the same temperature, pronounced increase in both compressive strength as well as modulus of elasticity was observed. The compressive strength of PMMA-PC and PVE-PC specimens reached 14,750 psi and 15,300 psi respectively which is 56.65% and 34.65% higher than that of control specimens of same age. Similarly, the modulus of elasticity of the same specimens of those PC increased to 3,160 ksi and 3,330 ksi which is 10.90% and 30.05% higher than those of control specimens. The compressive stress-strain curves, which show higher peaks with steeper initial slope, also confirm the same observations.

This increased strength and stiffness is consistent with the concept of reduced free volume in the polymer matrix and the resulting restriction of mobility of polymer chains at subzero temperature. At reduced temperature, the intermolecular voids in the polymer chain commonly

referred as free volume shrink, because of which the molecular chains that make up the polymer are tightly packed within the matrix and their ability to slide and rotate relative to each other gets reduced. Hence, the reduced temperature causes increase in the compressive strength of the polymer resin itself due to compact packing and increase in stiffness due to loss of mobility which explains the observed increase in compressive strength and modulus of elasticity. Although this increased compressive strength can be beneficial, corresponding reduction in ability to accommodate larger strain can lead to brittle failure, which is also evident in the stress-strain relations.

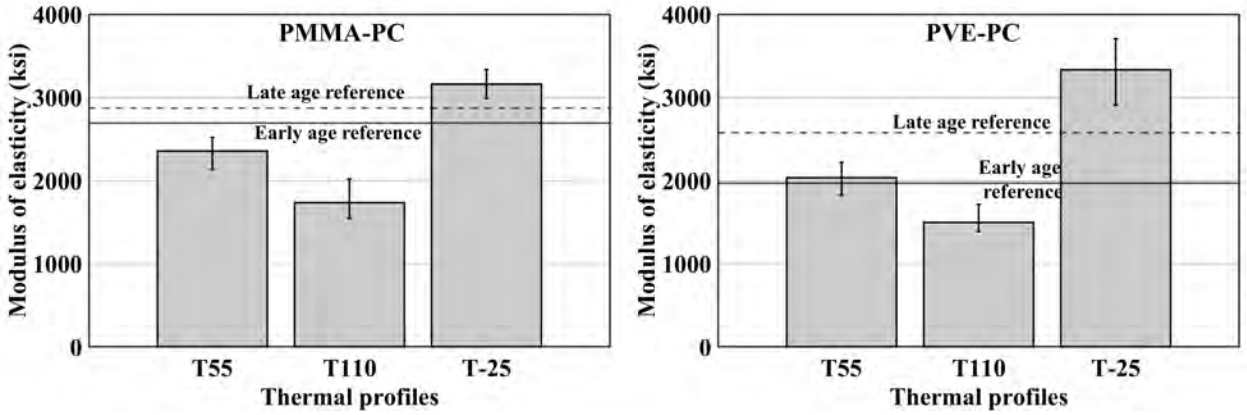

Figure 5.2. Modulus of elasticity of PC subjected to the three thermal conditions.

5.2 Flexural strength

The force deflection curves obtained from the flexural tests and the modulus of rupture (MOR) of the control polymer concrete beams along with the beams subjected to thermal shocks T55, T110, and T-25 are presented in Figure 5.3 and the modulus of rupture (MOR) is presented in Table 5.2. The MOR of T55 PMMA-PC and PVE-PC beams were found to be 2.49 ksi and 2.91 ksi, respectively. These were marginally lower than or equal to that of corresponding control beams of same age measured at 2.73 ksi and 2.88 ksi, respectively. In contrast, the T110 PC beams had significantly higher MOR of 2.93 ksi and 3.38 ksi for PMMA-PC and PVE-PC beams respectively, exceeding the MOR of the control beams. The force deflection curve showed that the flexural

stiffness, indicated by the initial slope of the curve, decreased under both thermal shocks for both PC types when compared to that of control specimens of the same age. However, in the case of PVE-PC, even the reduced stiffness remained comparable with the control specimen tested at the age of seven days.

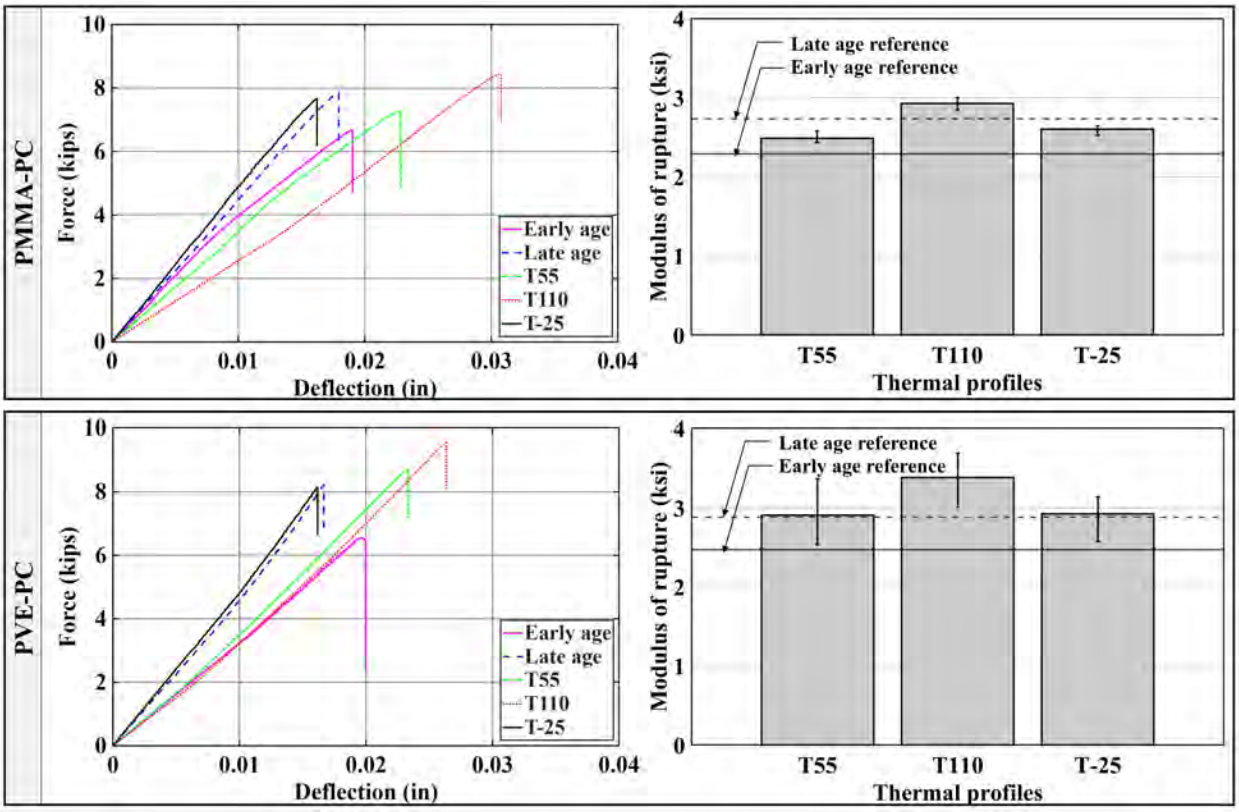

Figure 5.3. Average Force-Deflection curve and modulus of rupture obtained from third point bending test of specimens subjected to thermal conditions.

Table 5.2. Modulus of rupture of PC subjected to thermal conditions

Test condition		**Modulus of Rupture (ksi)**	
		PMMA-PC	**PVE-PC**
Reference	Early age	2.29	2.47
	Late age	2.73	2.88
Thermal conditions	T55	2.49	2.91
	T110	2.93	3.38
	T-25	2.60	2.92

The reduction in stiffness observed in the flexural response of these PC beams is consistent with chain mobility effects that were identified in the compression tests. However, the paradoxical

increase in the MOR of T110 beams can be explained by the increase in the ultimate deflection capacity also consistent with the effect of chain mobility of the polymer resin with increased temperature. Similar to that explained in compression behavior, these effects are expected to be temporary. However, repeated thermal shocks rendered those changes irreversible. The increased tensile strain capacity coupled with reduction of stiffness negated each other in the case of T55 cases which resulted in the MOR comparable to the control cases but in the case of T110, the enhanced tensile strain capacity outweighed the softening, leading to higher MOR.

This dependence of the ultimate strain capacity and stiffness on the temperature also explains the improvement in flexural behavior of T-25 specimens whose MOR was found to be 2.60 ksi and 2.92 ksi for PMMA-PC and PVE-PC, comparable to the control specimens of same age. In contrary to T55 and T110 cases, tensile strain capacity i.e. the ultimate deflection decreased for T-25 cases and the force-deflection behavior showed increase in flexural stiffness whose combined effect resulted in MOR similar to control cases.

5.3 Bond strength with rebar

The tensile stress strain response obtained from pullout test of rebar embedded in PMMA-PC and PVE-PC and their corresponding maximum rebar stress are presented in Figure 5.4. For PMMA-PC, specimens subjected to service level thermal cycling (T55) and prolonged exposure to subzero temperature (T-25) demonstrated similar or slightly better performance than the control specimen tested on day seven. In contrast, extreme thermal cycling resulted in reduced bond capacity indicating deterioration in bond performance. However, even with the reduced performance, the peak stress was still significantly higher than the rebar yield stress indicating that the bond between rebar and PMMA-PC was sufficient for the design point of view. For PVE-PC, the stress strain curves show stable stress strain curves with minimal sensitivity to all kinds of thermal exposure.

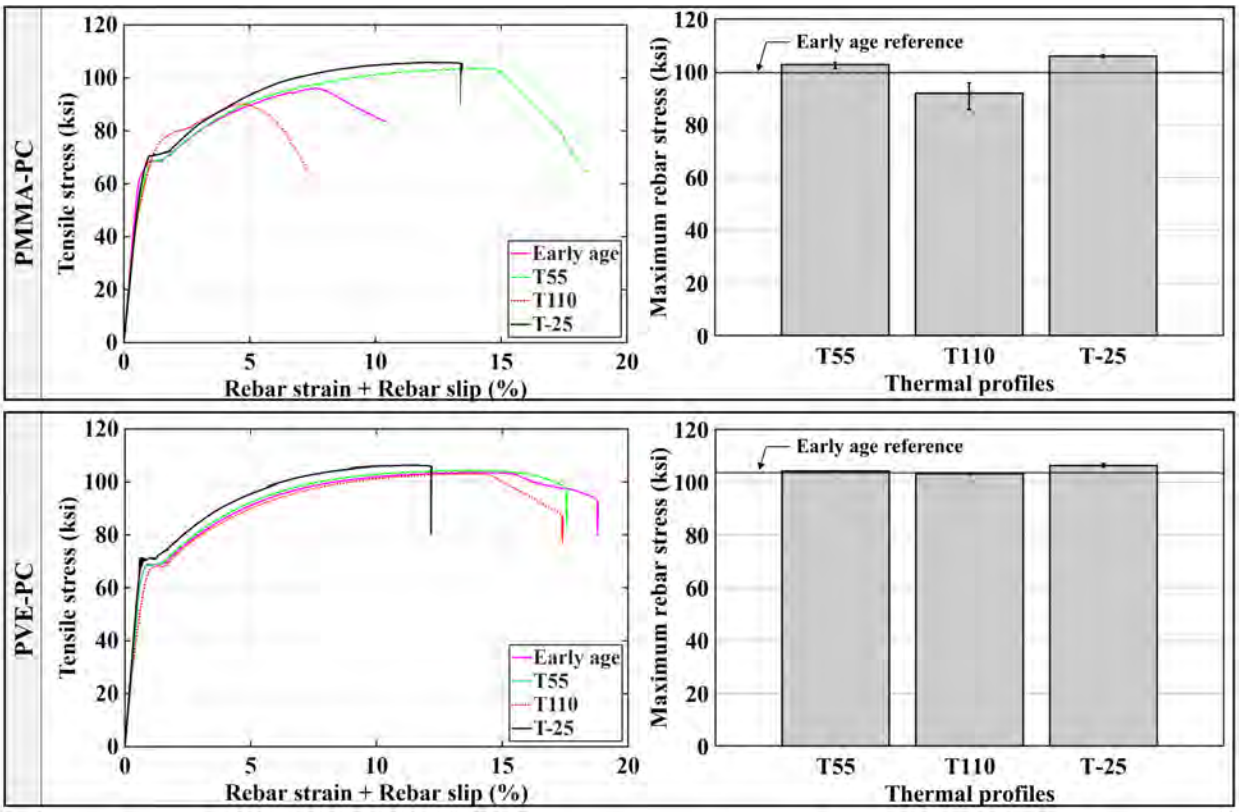

Figure 5.4. Stress strain relationship and maximum rebar stress during pullout test of thermally conditioned PC specimens.

5.4 Bond strength with conventional concrete

The peak load obtained from the test of slant shear specimens performed to characterize the bond between polymer concrete (PC) and conventional concrete (CC) subjected to various thermal conditions is summarized in Figure 5.5 and tabulated in . For PMMA-PC, the bond increased with age regardless of primer application. For PVE-PC such increase was observed only without primer. Yet, the absolute value of bond strength in this case remained significantly lower than when primer was used. Notably, the aging induced increased bond strength for PMMA-PC without primer exceeded the bond strength of PMMA-PC with primer measured at seven days.

Table 5.3. PC-CC bond strength (in psi) subjected to thermal conditions

PC / Primer Use	Reference		Thermal conditions		
	Early age	Late age	T55	T110	T-25

PMMA-PC	With primer	2435	3160	2560	155	3660
	Without primer	1460	2750	2205	1035	3240
PVE-PC	With primer	3405	3420	2840	2190	5230
	Without primer	1610	1995	700	235	3015

Thermal shocks significantly impacted the PC-CC bond, and all the specimens suffered a PC-CC bond failure. In the case of T55 thermal shocks, which were intended to mimic service level conditions, the reduction of bond strength in PMMA-PC was relatively smaller. These specimens had bond strength of 2560 psi (with primer) and 2205 psi (without primer) compared to 3160 psi and 2750 psi for the corresponding control specimens tested at the same age. It must be noted that despite this reduction, the bond strength remained higher than that of seven days old control specimens. Similarly, the bond strength of T55 PVE-PC specimens with primer was 2840 psi which is a minimal reduction from the bond strength of 3420 psi of the control specimen. In contrast, the bond strength of PVE-PC T55 specimens without bonding agent was significantly lower measured at 700 psi. This sharp reduction in bond strength was attributed to interfacial cracks developed during the thermal shocks as shown in Figure 5.6. These cracks were first observed during the eighth cycle of thermal shocks in PVE-PC T55 specimens.

Under the T110 thermal shock scenario, which was intended to mimic extreme events, the reduction of bond strength was drastic with almost no bond strength in T110 PMMA-PC specimens with primer and PVE-PC without primer. Cracks similar to those in T55 cases were visible in the initial cycles and complete separation of the two wedge pieces took place in the subsequent cycles in some of these specimens as shown by the zero as the lower values of bond strength. The bond strength of T110 PMMA-PC specimens without primer was considerably low measured at 1035 psi, however, no signs of damage were visible in the specimens. In contrast, the T110 PVE-PC specimens with primer maintained a considerable bond strength of 2190 psi.

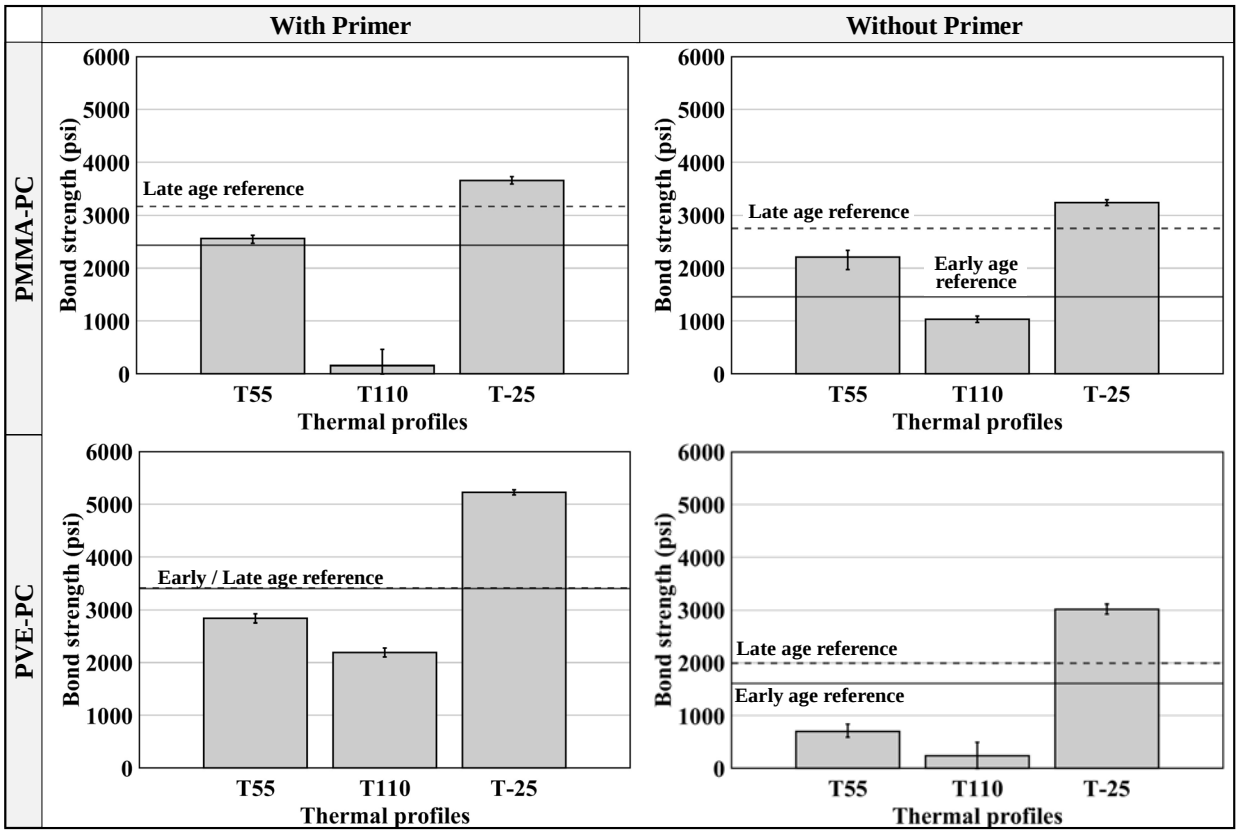

Figure 5.5. Bond strength of thermally conditioned specimens obtained from slant shear test.

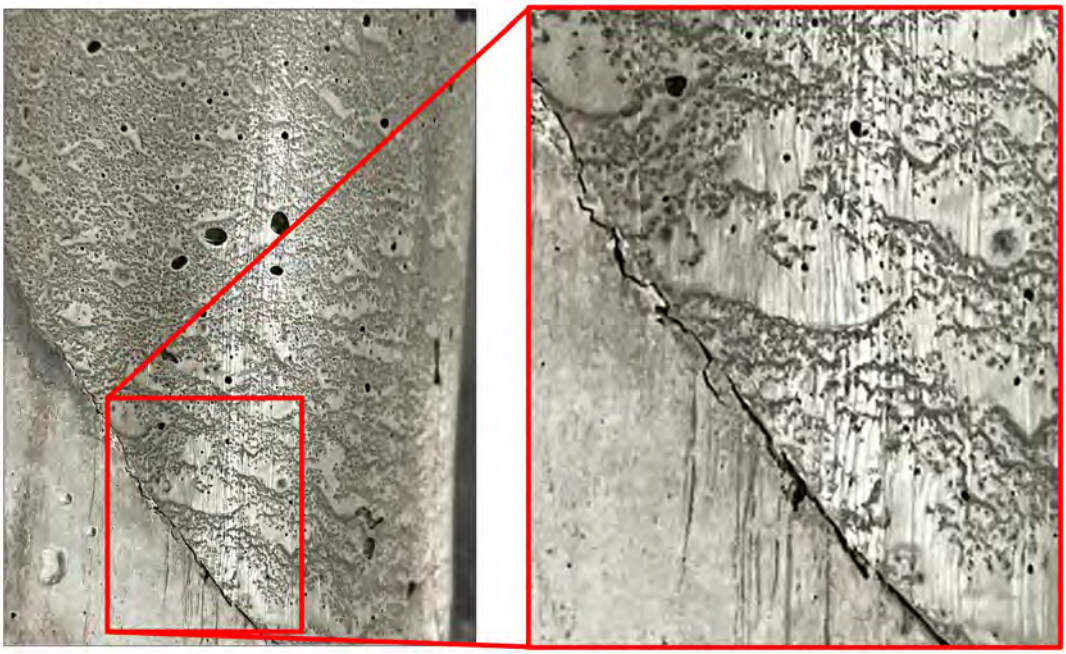

Figure 5.6. Crack developed in PVE-PC specimen without primer during T110 shocks.

In T-25 conditions, the bond strength of both PMMA-PC and PVE-PC specimens were higher than the control specimens. In all cases, all the T-25 bond strengths exceeded 3000 psi indicating that prolonged exposure to subzero temperatures does not negatively affect the bond performance of polymer concrete rather enhances its bond strength.

The bond performance of PC under thermal shocks can be explained considering the polymer chemistry and the mismatch in coefficient of thermal expansion. The measured CTE of PMMA-PC and PVE-PC was $(2.87 \pm 0.05) \times 10^{-5}$ /°C and $(2.10 \pm 0.07) \times 10^{-5}$ /°C. These values are two to three times the CTE of conventional concrete which is usually between 1.0 to 1.2×10^{-5} /°C. This mismatch in the CTE with repeated thermal cycling consisting of rapid drop in temperature induced interfacial stress in the bond. In the case of T55 condition, the peak temperature approached but did not exceed the T_g and the difference in the temperature was also smaller as a result of which the specimens retained their bond strength in most conditions. In the case of T110 shocks, the peak temperature exceeded the glass transition temperature, and the range of temperature was also higher which led to higher thermal stresses causing a drastic drop in the bond strength. Although primer generally improves bond strength, the complete loss of bond strength in PMMA-PC specimens with primer can be attributed to thermal deterioration of the primer at 110 °C as the same failure mode was not observed in the specimens without primer.

6 RESULTS AND ANALYSIS: STRUCTURAL PERFORMANCE OF POLYMER CONCRETE

The experimental results from the test of four bridge slabs with four different PC types as longitudinal closure joint material are presented and discussed in this section. Before delving into detailed observations, a summary of key results is presented in Table 6.1. The table reports the peak load capacity of each specimen, the initial stiffness, and the differential midspan deflection between the panels at either side of the closure joint. The initial stiffness was determined using the midspan deflections recorded by two string potentiometers positioned at east and west side of the closure joint in the midspan (SP Mid E and SP Mid W). The line of best fit was fit between 2.25 kips and 22.5 kips (10 and 100 kN) through the load deflection curve and the slope of the line has been presented as the initial stiffness. This summary provides a consistent measure of the structural response of the specimens and has been used as a basis for the comparative discussion presented in the subsequent sections. The remainder of this section presents the results in the three sections: Observed damage progression, load deflection relationship, and water leakage performance. For clarity and brevity, throughout this section, each slab specimen is identified by type of PC used as the closure joint material.

Table 6.1. Summary of test results

Specimen ID	Peak Load (kips)	Initial Stiffness (kips/in)		Differential Midspan Deflection at: (in)		
		East	West	Service load	Ultimate Load	Peak Load
PMMA-PC	142.29	384.46	407.59	0.033	0.070	0.763
PPC	142.00	172.22	175.13	0.019	0.051	0.858
EPC	142.39	246.91	266.84	0.023	0.025	0.043
PVE-PC	165.97	324.05	337.47	0.007	0.001	0.207

6.1 Observed damage progression.

The crack and damage patterns observed during and after the test have been described in this

section. For test orientation, the slabs spanned in the north – south direction with longitudinal joint running parallel to the span length. In the asymmetrically loaded specimens i.e. PMMA-PC and PPC specimens, the actuator load was applied on the east panel, directly adjacent to the closure joint.

6.1.1 PMMA-PC Specimen

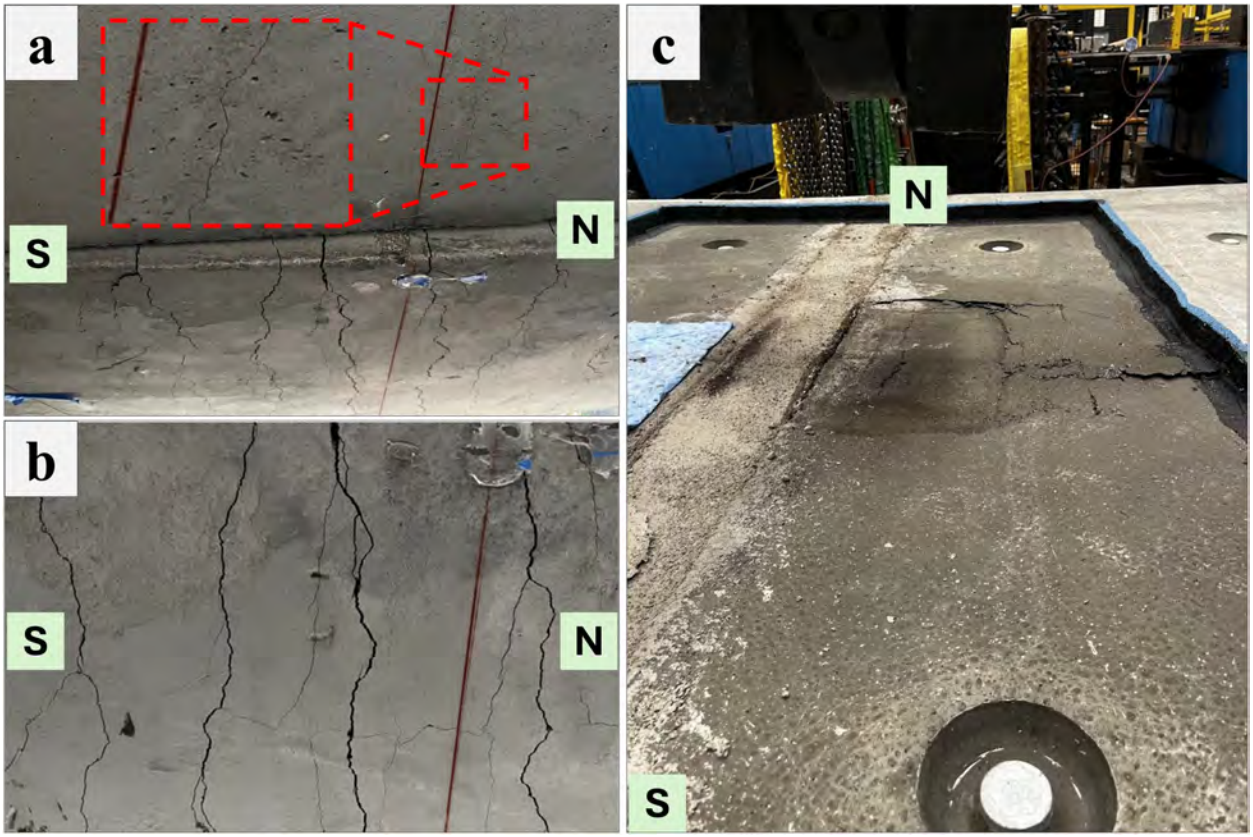

Figure 6.1. Crack pattern at a) bottom b) bottom east panel and c) top of PMMA-PC specimen.

The crack pattern observed in the slab specimen with PMMA-PC as longitudinal closure joint material is presented in Figure 6.1 and Figure 6.2. No visible cracks occurred prior to reaching the code compliant ultimate load. First crack was observed on the north and south face of the west panel, near the longitudinal joint. The widened form of this crack along with similar crack towards the western edge formed towards the end of the test is presented in Figure 6.2a. During the displacement-controlled phase of the test, flexural cracks oriented in the east-west direction as well

as fine vertical hairline cracks on the eastern face of the specimen were observed. These cracks widened with increasing actuator load and similar hairline cracks started to form in the adjacent, unloaded west slab.

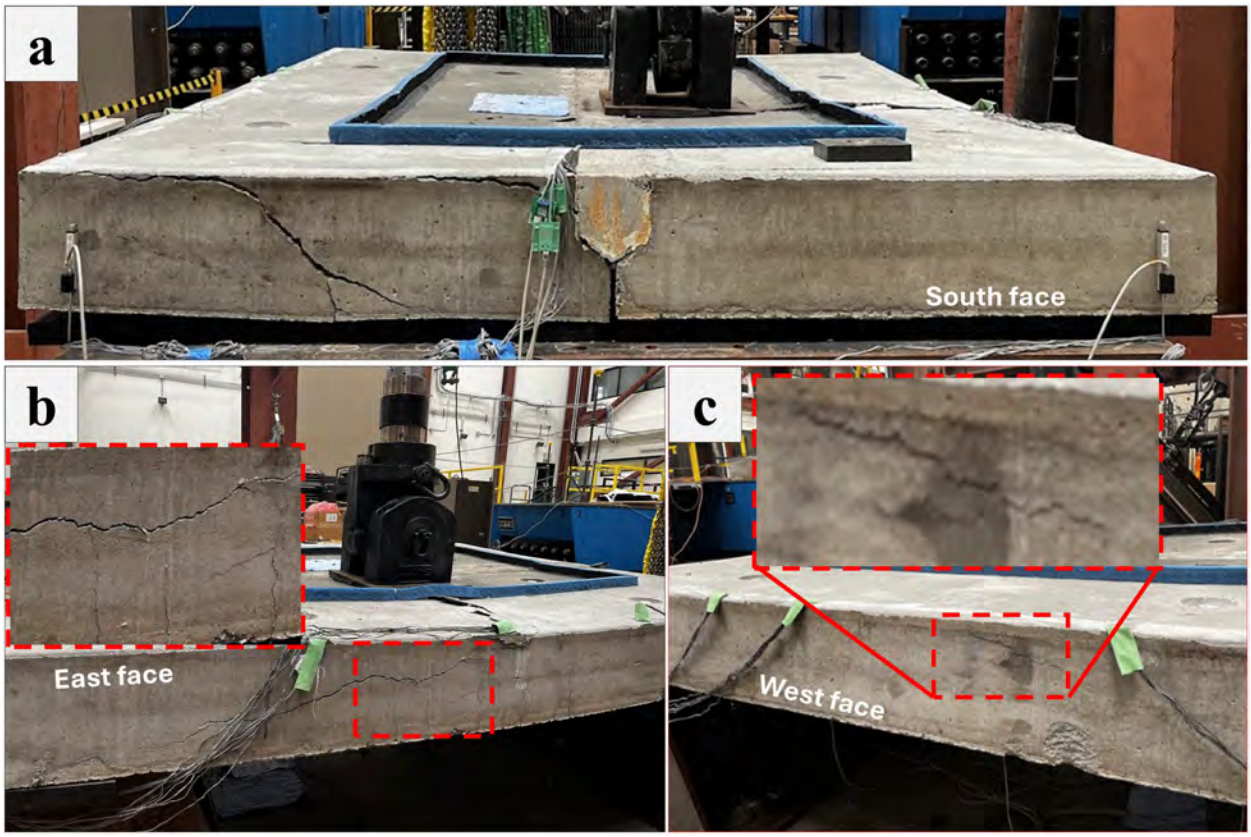

Figure 6.2. Crack pattern at a) south face b) east face c) west face of PMMA-PC specimen.

The specimen ultimately failed by concrete compression crushing at the top surface of the loaded, precast panel accompanied by yielding of bottom main longitudinal rebar in addition to localized compression failure directly beneath the loading pad as illustrated in Figure 6.1c. Deep and wide flexural cracks were observed in the bottom of the loaded east slab whereas a few flexural cracks towards the midspan were observed in the bottom of the adjacent west slab as shown in Figure 6.1 a and b. In addition to the flexural cracks, diagonal shear cracks were observed in the east face of the loaded panel. In the adjacent west panel, shear cracks were seen in all three north, south and west faces as shown in Figure 6.2 a and c. Additionally, no flexural cracks propagated

through the PMMA-PC closure joint itself and interfacial debonding was limited to a small localized area beneath the loading plate on the east slab side.

6.1.2 PPC Specimen

The crack pattern in the slab specimen with PPC as longitudinal joint material, is presented in Figure 6.3. Unlike other specimens, the PPC specimen had cracks in the longitudinal joint, well before the structural testing. Hours after the PPC closure joint pour, shrinkage cracks developed along the longitudinal joint as shown in Figure 6.3a. These early cracks were attributed to resin bleeding towards the top of the freshly poured joint, due to accumulation of the excess primer that didn't adhere to the vertical joint surface and collected in the joint. Additional coarse aggregate was placed on the joint surface after such bleeding to prevent shrinkage cracking. However, this measure was not fully effective, hence the specimen had surface cracks prior to testing. To access if these cracks penetrated deep into the joint, water was pooled at the top and leakage was monitored from the sides and the bottom of the specimen. On doing so, no leakage was observed, indicating that the cracks were superficial and did not extend deep into the closure joint.

The cracks progression observed during the tests of PPC specimen followed trend similar to that of PMMA-PC specimen. No additional cracking was observed before reaching the code specified ultimate load and the first test induced cracks were observed in the north and south face of the west unloaded panel, near the longitudinal joint. The widened form of this crack photographed after the completion of the test is shown in Figure 6.3b. As actuator load increased, flexural cracks were observed in the bottom surface of the loaded slab which propagated upwards and were seen in the east face of the loaded panel. By the completion of the test, wide flexural cracks oriented in the east west direction were present at the bottom of the loaded panel, while finer cracks of the same orientation appeared in the unloaded panel. In addition to the vertical

flexural cracks, diagonal shear cracks were formed in the east face of the specimen, as shown in Figure 6.3c.

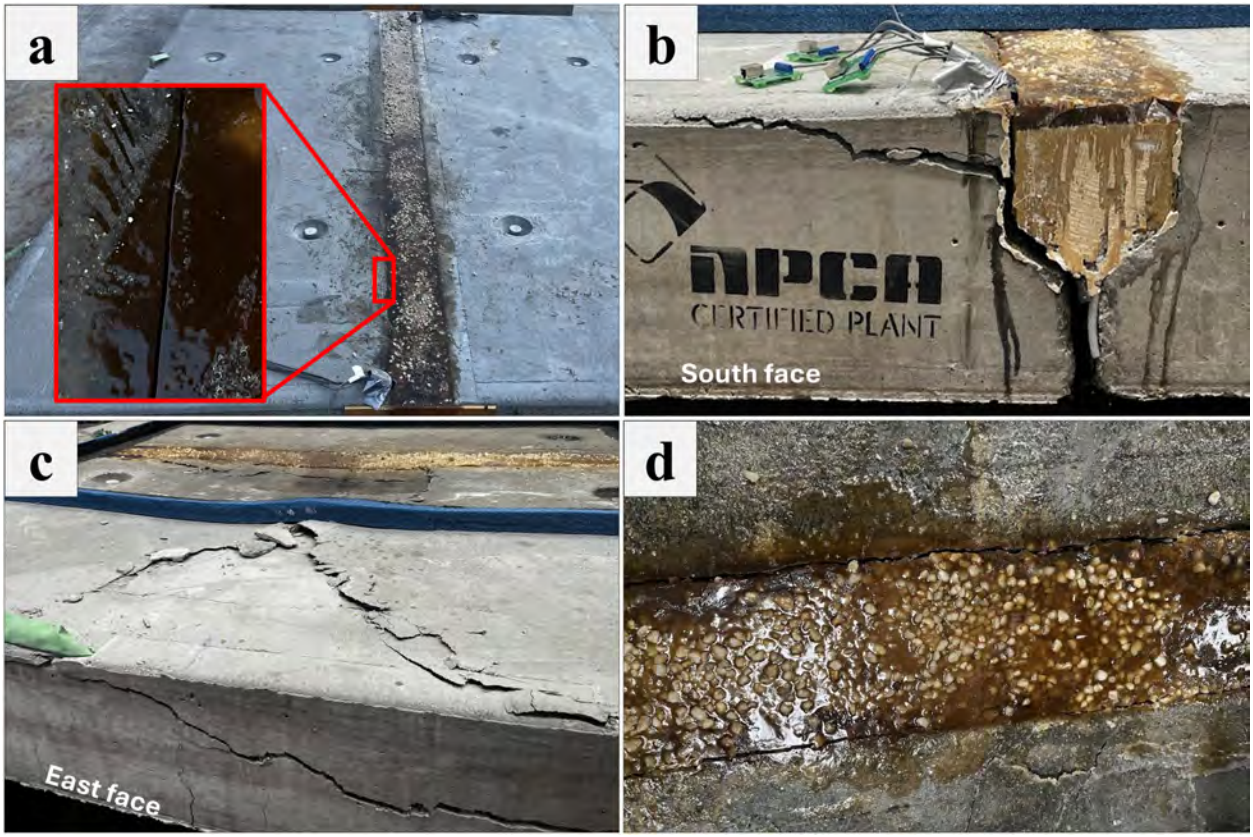

Figure 6.3. a) Crack formed in the PPC material before test b) Shear cracks formed in the south face c) Shear and diagonal cracks in the loaded slab d) Debonding of PPC from the precast slab

The specimen ultimately failed by the compression failure of the top surface accompanied by localized crushing beneath the loaded pad, consistent with the failure of PMMA-PC specimen. However, unlike PMMA-PC specimen, the shrinkage developed prior to testing, deepened causing total debonding of the closure joint material with two parallel longitudinal cracks developed at the interface between PPC and precast slab as shown in Figure 6.3d. Importantly, no compression related damage was observed at the closure joint itself.

6.1.3 EPC Specimen

The crack patterns observed during and after the test of the precast slab with EPC as longitudinal

closure joint material is presented in Figure 6.4. This specimen was loaded symmetrically, with the actuator positioned exactly in the midspan at the closure joint. Similar to the previous specimens, the first visible crack developed on the north and south faces above the support, near the longitudinal joint. These fine hairline cracks near the joint were formed at the moment of sudden increase in the deflection which is described later in the load deflection relationship discussion. This crack photographed after the completion of the test is shown in highlighted portion of Figure 6.4a. Aside from this, no major cracks were visible until the code specified ultimate load. However, major water leakage was observed unlike other specimens at the second cycle to 50 kips, signifying debonding of EPC and precast concrete at some locations.

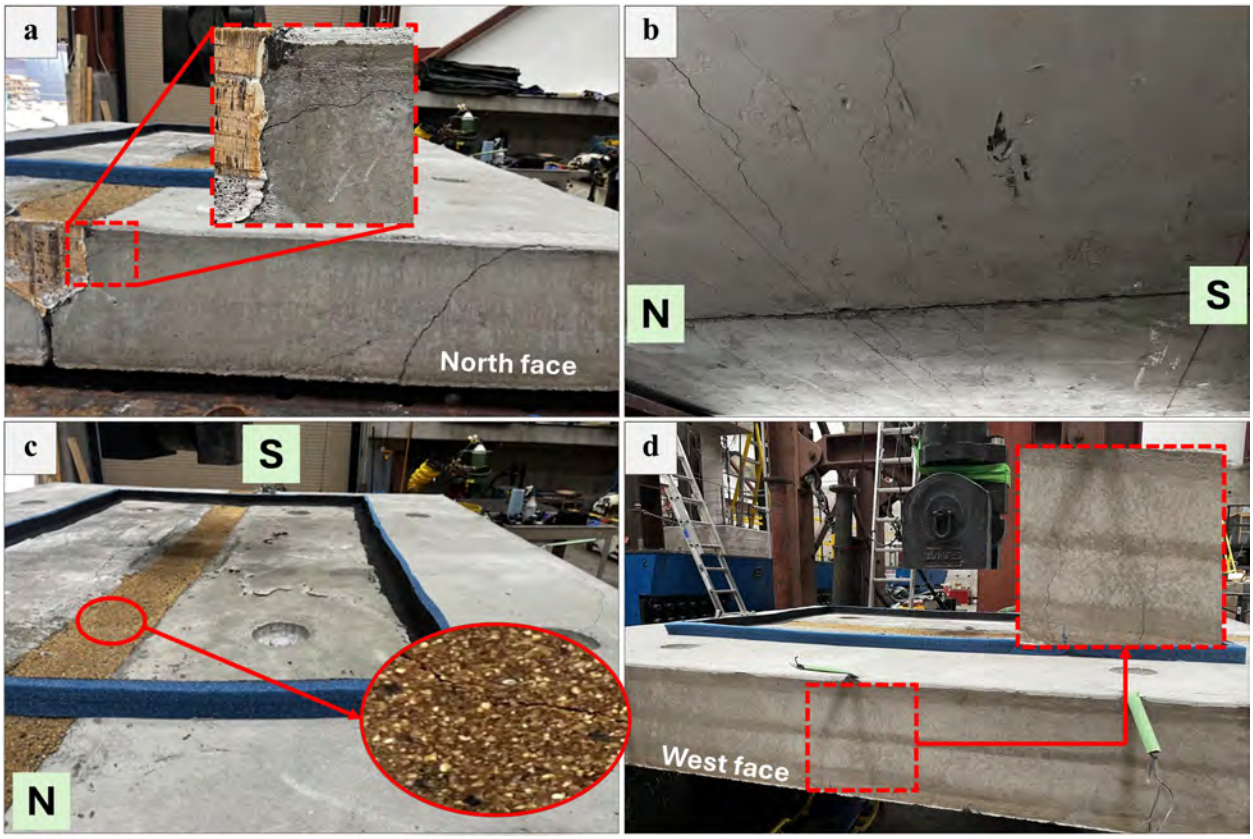

Figure 6.4. Crack patterns in a) North face of west panel b) Bottom surface of the slab c) Top of the slab and d) West face of the EPC specimen.

On continuation of load beyond 50 kips, flexural cracks oriented in the east west direction (Figure 6.4b) started to develop in both panels which widened and progressed upward gradually

which could be observed in the east and west face of the specimen as shown in Figure 6.4d. The specimen ultimately failed due to compression failure of precast concrete accompanied by longitudinal rebar yielding consistent with the failure modes of the previous specimens. In contrast to PMMA-PC and PPC specimens, the flexural cracks propagated through the closure joint material. In addition to the global compression failure at the top surface, localized crushing was also observed directly beneath the loading pad.

6.1.4 PVE-PC Specimen

The crack pattern observed in the PVE-PC specimen is presented in Figure 6.5. Similar to the EPC specimen, the first visible crack formed near the joint at the support section when there was a sudden increase in the deflection. Unlike the EPC specimen, no water leakage was observed until later in the test in the case of PVE-PC specimen. Other than this hairline crack, no major cracks were observed until the code prescribed ultimate load.

On further loading, flexural cracks similar to the previous specimens developed on the bottom surface of both east and west panels oriented in the east west direction and gradually progressed towards the top of the specimen. A significant difference observed in this specimen was that the shear cracks observed at the support were developed on both east and west panels and the diagonal shear cracks observed in the east and west face were replaced by nearly horizontal cracks around mid-depth of the specimen.

The specimen ultimately failed due to compression concrete failure and localized crushing beneath the loading pad after significant yielding of the longitudinal rebar. Apart from the loaded area, no cracks were observed in the closure joint material.

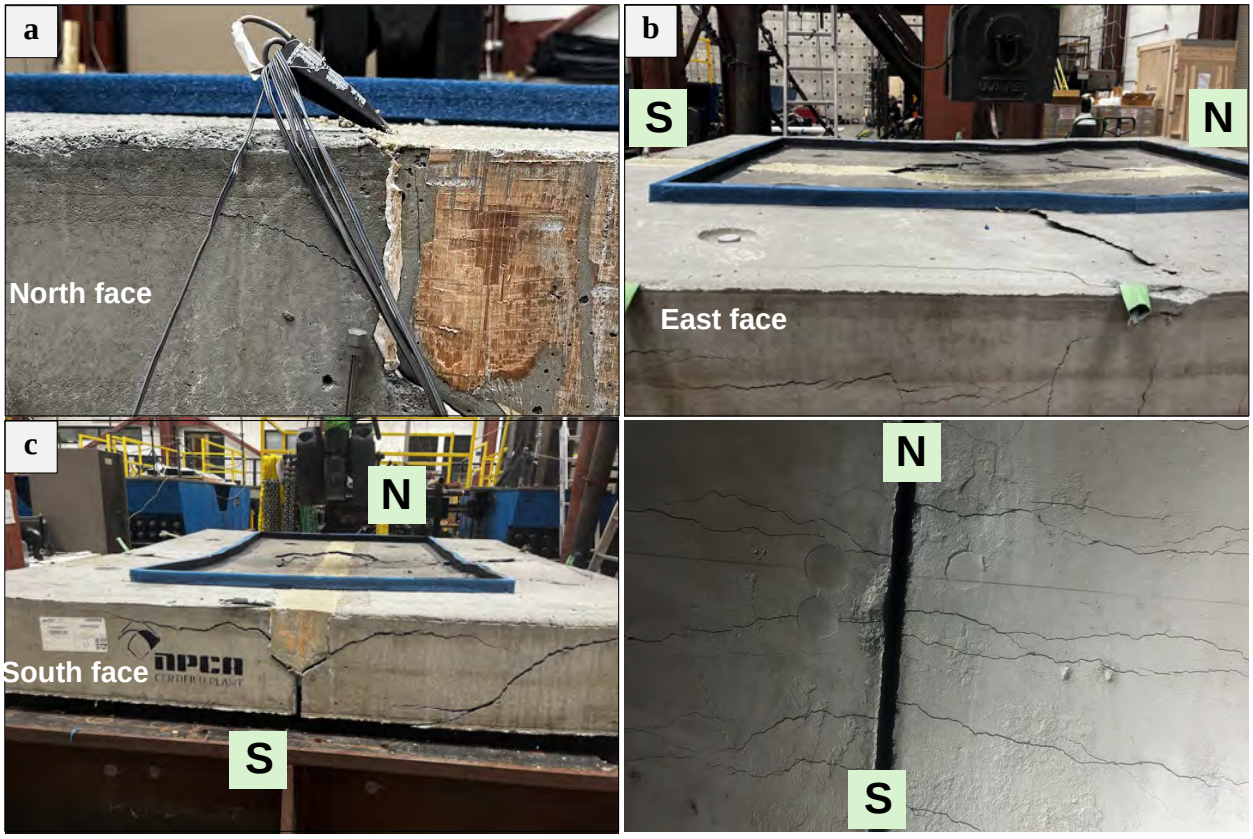

Figure 6.5. Crack patterns in a) North face of west panel b) East face and top surface c) South face and d) Bottom surface of the PVE-PC specimen.

6.2 Load deflection relationships.

The load deflection relationship results are presented in two subsections: Asymmetric loading: PMMA-PC and PPC, and Symmetric loading: PVE-PC and EPC.

6.2.1 Asymmetric loading: PMMA-PC and PPC

The load vs midspan deflection of PMMA-PC and PPC slabs loaded asymmetrically adjacent to the joint is presented in Figure 6.6 and Figure 6.7 respectively. It can be observed that the PMMA-PC and PPC specimen had the same ultimate load capacity of around 142 kips and similar load deflection relationship towards the peak load. However, a major difference in the load deflection behavior can be observed in the first few cycles. The PMMA-PC specimen had a greater initial stiffness than the PPC specimen with measured values at 384.46 kips/in and 172.22 kips/in in the

loaded panels. This lower stiffness in PPC can be attributed to two factors: preexisting drying shrinkage cracks in PPC closure section, the details of which have been explained in the earlier section and inherent lower modulus of elasticity (MOE) of PPC. The MOE of PPC on the day of testing was found to be 1650 ksi which is significantly lower than the test date MOE of PMMA-PC measured at 2584 ksi.

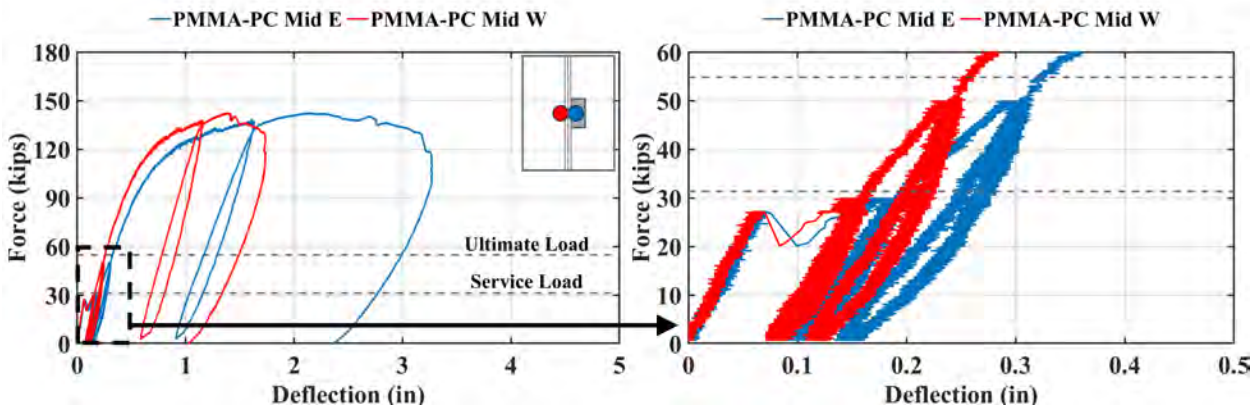

Figure 6.6. Actuator force vs deflection at the mid pan (SP Mid E and SP Mid E) for PMMA-PC slab

In the PMMA-PC specimen, during the first cycle of loading to 30 kips, a sudden increase in deflection in both the slab panels accompanied by a brief drop in actuator force and a single audible pop was noticed. This drop is actuator load does not reflect loss in structural capacity of the slab rather was triggered due to a fail-safe mechanism embedded in the control software, which stopped the actuator pressure when the actual displacement of the actuator varied largely from the software anticipated deflection in that instance. The actuator was manually restarted instantly, continuing the loading cycle. No visible cracks were observed during this event. This sudden jump observed in the load deflection relationship is attributed to the start of full engagement of joint. Due to this a permanent deformation of 0.091 in (loaded slab) and 0.081 in (adjacent slab) and was obtained at the end of first cycle when the load was reduced to 0.77 kips. It must be noted that a small seating load was intentionally maintained to avoid complete loss of contact between the actuator and the specimen. In contrary, no such sudden jump was observed in the PPC slab.

Nevertheless, the residual displacement of the PPC after the end of first loading cycle was 0.787 in (loaded slab) and 0.779 in (adjacent slab), which is comparable to the residual displacement in PMMA-PC specimen.

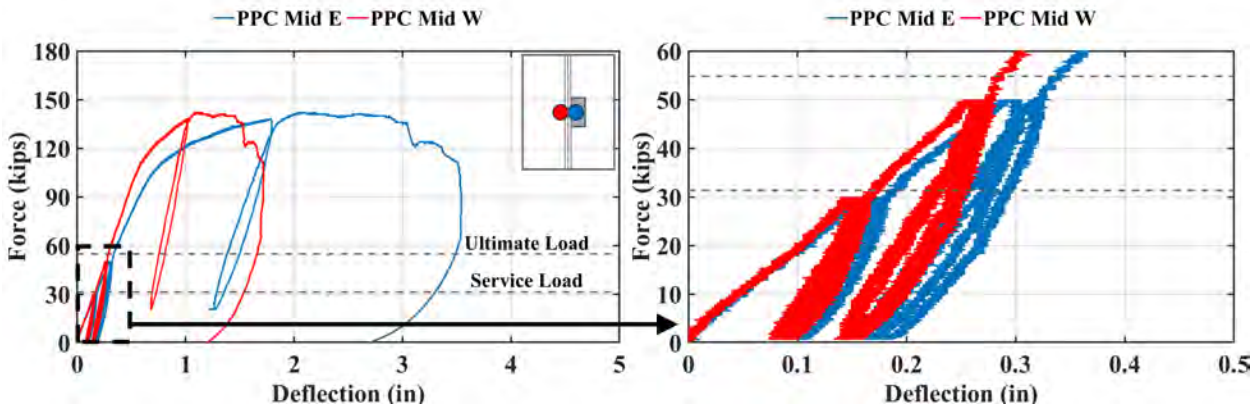

Figure 6.7. Force vs deflection at the mid span (SP Mid E and SP Mid W) for PPC slab.

Apart from that sudden jump in load – displacement curve during the first cycle in PMMA-PC specimen, the load deflection relationship remained linear past the ultimate load capacity and no additional cracks were visible in both the specimens. The gradual onset of non-linearity at around 100 kips coincided with the formation of shear and flexural cracks in the test specimen. Comparing the differential deflection of the two slab panels in midspan at either side of the closure joint, both PMMA-PC and PVE-PC specimens had considerably lower differential deflection within the ultimate load measured at 0.07 in and 0.05 in at the ultimate load condition. However, after the ultimate load level, the differential displacement in both PMMA-PC and PVE-slab increased gradually up to around 100 kips and increased drastically to 0.763 in and 0.858 in respectively at the peak load. This increased differential displacement is due to the asymmetric nature of the load as well as the loss of stiffness caused due to crack formation in the loaded slab. The load deflection relationship of the PMMA-PC and PPC slabs at four different representative string-potentiometer locations: NNE, NNW, East and West are presented in Figure 6.8 and Figure 6.9 respectively. Comparing the measurements adjacent to the joint at NNE and NNW with those

at the midspan, it can be observed that in the case of PPC slab the differential deflection is higher in the north than at the midspan. Taking the deflections at the ultimate load level as reference for this discussion, the differential deflection for PMMA-PC slabs at midspan was found to be higher than that at north string pot location measured at 0.070 in and 0.039 in, respectively. Conversely, the differential deflection for PPC slab at north string pot location was found to be higher than that at midspan measured at 0.094 in and 0.051 in, respectively.

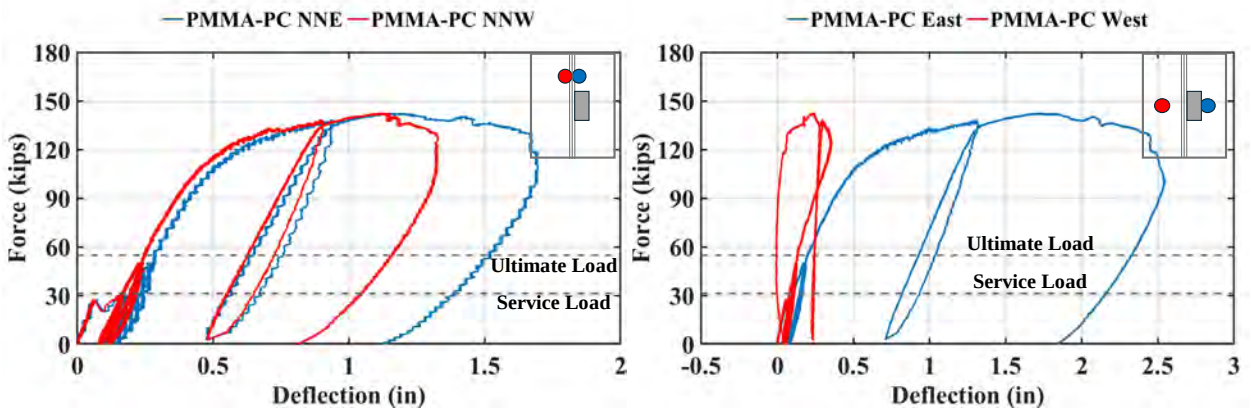

Figure 6.8. Force vs deflection for PMMA-PC slab at locations NNW, NNE, East, and West

This reverse phenomenon indicates that the adjacent west slab, which was not loaded, was going through rigid body rotation rather than meaningful flexural deformation during the early stages of loading. This behavior becomes clearer by observing the load deflection relationships at the string potentiometer locations East and West, which are the center of the individual east and west panels. It can be seen that the deflection at the center of west panel remained almost constant until the applied load reached approximately 120 kips. Such almost constant deflection despite increasing actuator force suggests that any flexural deformation was counteracted by the geometric rotation of the slab panel.

Near the peak load, center of west panel of PMMA-PC and PPC slab moved upward with nearly 1 in upward movement at the peak load in PPC slab. The upward movement in PMMA-PC slab, however, does not cause a net negative deflection. Figure 6.10 provides a visual corroboration

of this uplift during the peak load. The south view of the PPC slab clearly shows a rotated west panel consistent with the behavior inferred from the load deflection curves.

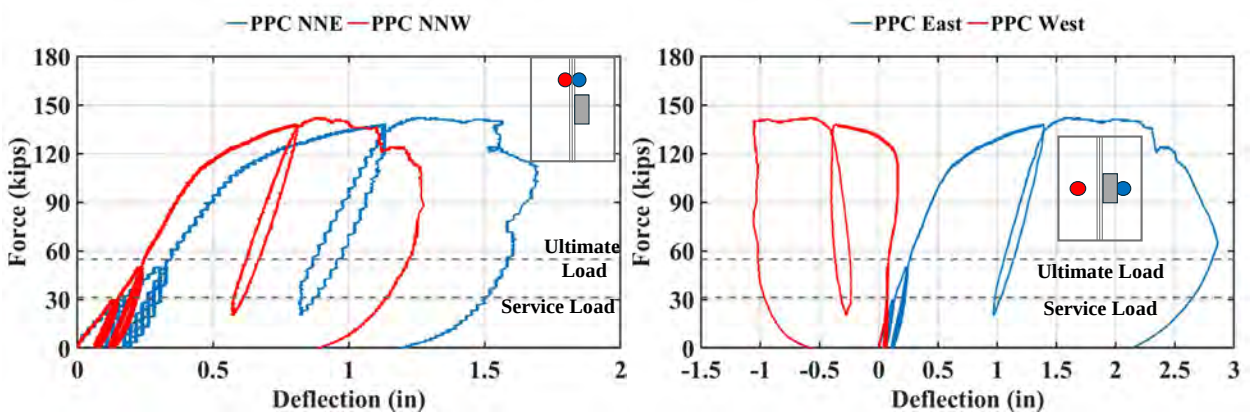

Figure 6.9. Force vs deflection for PPC slab at locations NNW, NNE, East, and West

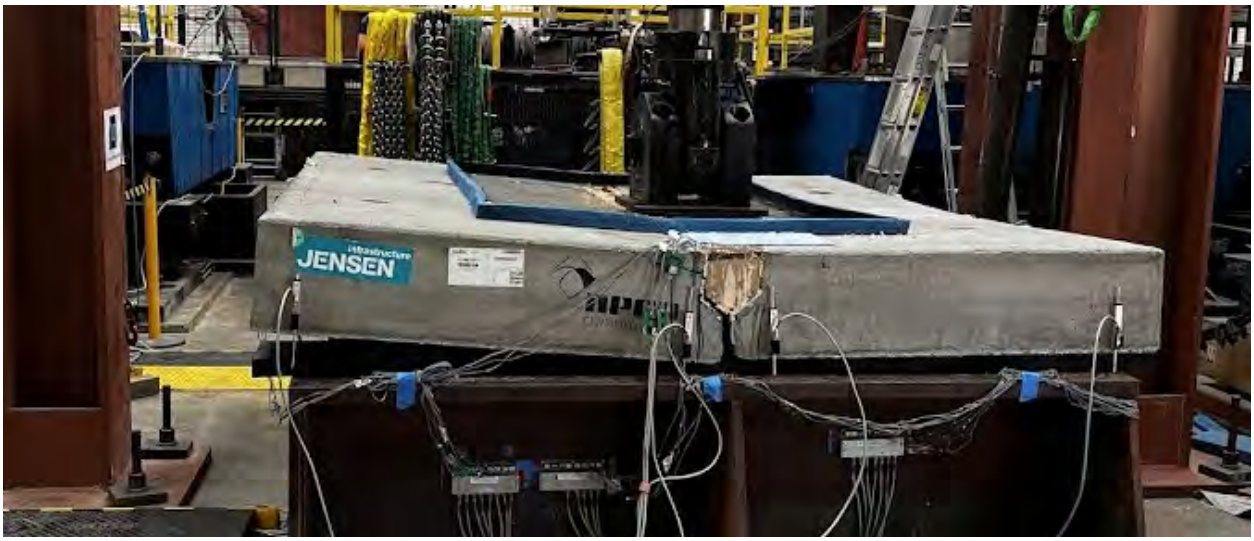

Figure 6.10. Deflected shape of PPC slab near the ultimate load.

6.2.2 Symmetric loading: EPC and PVE-PC

The load vs midspan deflection relationship of EPC and PVE-PC slabs subjected to symmetric loading at the joint are presented in Figure 6.11 and Figure 6.12 respectively. As summarized in Table 6.1, the PVE-PC specimen had a higher peak load capacity of 165.97 kips as opposed to 142.39 kips of EPC slab. In addition to that, the initial stiffness of PVE-PC specimen, measured at 324.05 kips/in (east panel) and 337.47 kips/in (west panel), was higher than that of EPC specimen,

measured at 246.91 kips/in and 266.84 kips/in at the same locations. This lower stiffness of EPC specimen aligns with the lower modulus of elasticity of epoxy polymer concrete which was found to be 1624 ksi as opposed to 2331 ksi modulus of elasticity of PVE-PC at the test day. In both the specimens, a sudden increase in the deflection can be observed at around 28 kips similar to that observed in PMM-PC specimen subjected to asymmetric loading. However, a difference observed in this case is that, in the EPC specimen, it occurred during the second loading cycle up to 30 kip as opposed to first loading cycle in PVE-PC and PMMA-PC specimens.

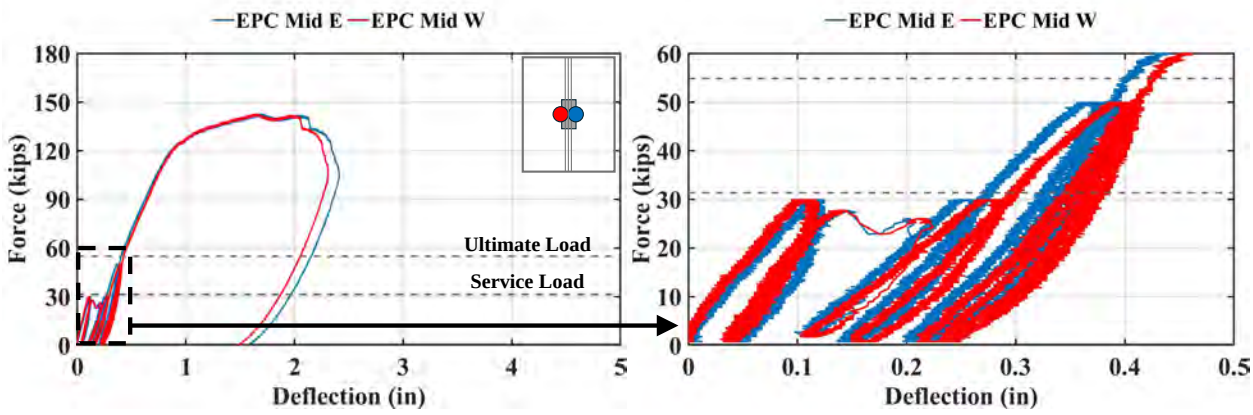

Figure 6.11. Actuator force vs deflection at the mid pan (SP Mid E and SP Mid E) for EPC slab

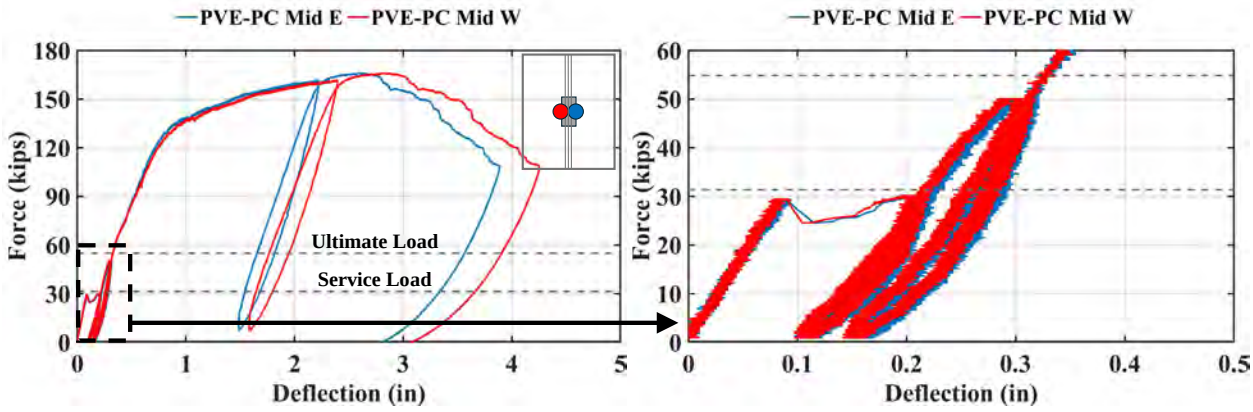

Figure 6.12. Actuator force vs deflection at the mid pan (SP Mid E and SP Mid E) for PVE-PC slab

Comparing the residual deflection at the end of the first cycle, the residual deflection was 0.04 in (west panel) and 0.05 in (east panel) in the EPC slab while the same was 0.11 in both panels of the PVE-PC specimen. However, at the end of second 30 kips cycle, the residual deflection was

similar in both the specimens measured at 0.11 in. This increase in residual displacement, despite repetition of the same loading cycle, was due to the sudden increase in the deflection. Observing the differential deflection between the individual panels at midspan, both EPC and PVE-PC specimens had negligible differential deflection measured at 0.043 in and 0.207 in at the peak load. Similar to that of the asymmetrically loaded specimens, the load deflection relationship remained linear until the ultimate load limit after which a gradual onset of non-linearity was observed consistent with the formation of shear and flexural cracks in the concrete. The actuator force vs deflection at other representative locations of EPC and PVE-PC slabs are presented in Figure 6.13 and Figure 6.14.

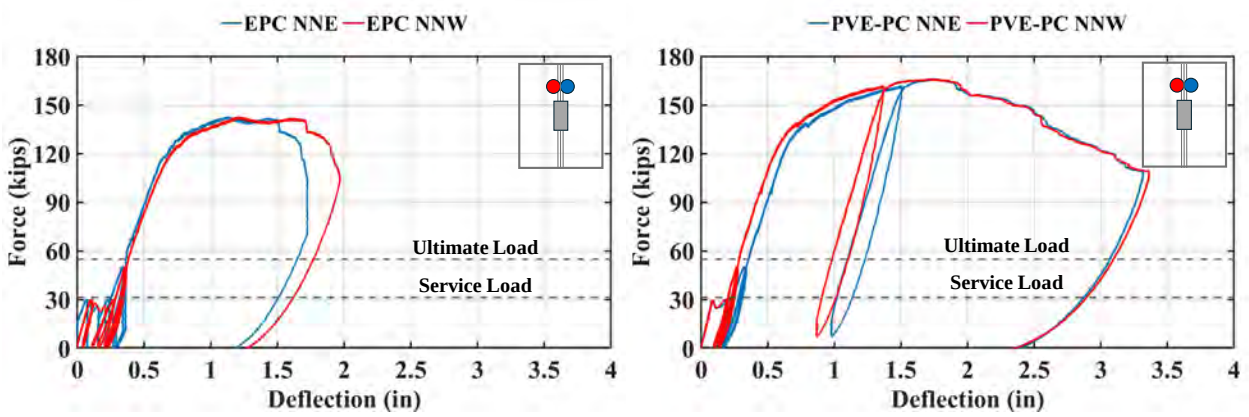

Figure 6.13. Actuator force vs deflection of EPC and PVE-PC slabs at locations NNW and NNE

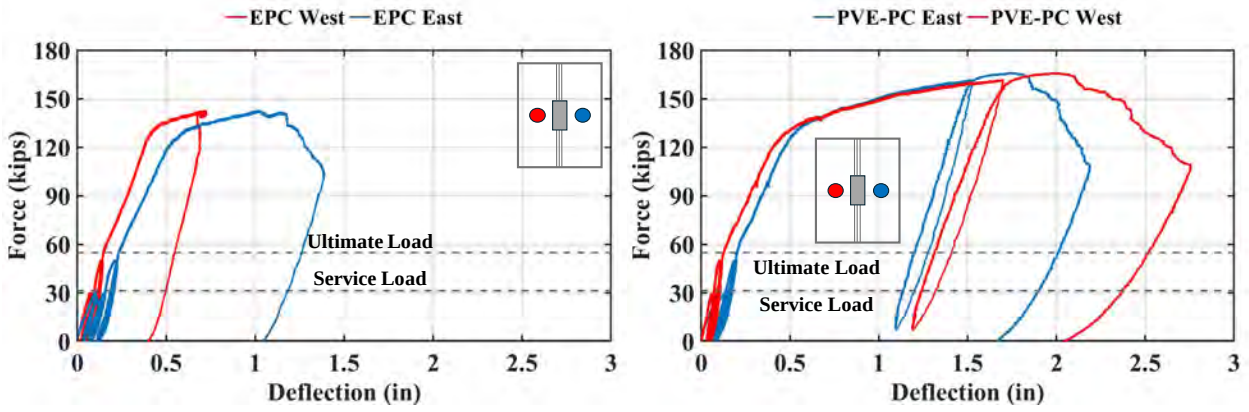

Figure 6.14. Actuator force vs deflection of EPC and PVE-PC slabs at locations East, and West

In both slabs, the deflection at either side of the joint at the north string potentiometer locations (SP NNE and SP NNW) were almost equal throughout the test. The same observation was made at the south string potentiometer locations. A small difference up to 0.1 in between the deflections at the center of the panels (SP East and SP West) of both specimens can be observed until the peak load and then increases drastically post peak load.

6.3 Water leakage

Water leakage was monitored throughout testing as an indicator of interfacial debonding at the joint. Four moisture sensors were installed in the joint region: two below the joint in between the butt faces of the two precast panels and two placed at the joint surface. The sensors at the joint reason were expected to be compromised by the polymer resin, but the sensors below the joint were also coated and rendered ineffective. Accordingly, water leakage was instead tracked through direct visual observation during the test and by reviewing the video footage captured by camera positioned below the test specimen.

Table 6.2 summarizes the load levels and location at which leakage was first detected along with the points of major leakage. This observation closely aligned with the information obtained from the crack patterns and load deflection curves provides an additional means to access joint behavior. It is important to note that the unplanned unloading observed near the peak load in the load-deflection curves corresponds to the onset of major water leakage, at which point the specimens were temporarily unloaded to allow removal of water in order to protect the laboratory equipment and instrument from potential damage.

For the PMMA-PC specimen, the first sign of water leakage was observed during the second loading cycle to 30 kips, originating at the joint interface. This early leakage in the form of few drops per minute was not accompanied by any visible cracks in the closure material and was

likely caused due to minor interfacial gaps too small to detect visually. This leakage did not exacerbate until a sudden major leakage occurred at 137.05 kips from one the shear cracks formed at the top surface of the specimen which is the continuation of shear cracks formed in the southern face of the west slab. This observation aligns with the analysis of crack patterns, which showed that no interfacial debonding or compression cracks were developed in the closure material. The localized debonding and crushing failure beneath the loading pad developed past this point during the test.

Table 6.2. Load and location corresponding to water leakage.

Specimen ID	**First sign of water leak**		**Major water leak**	
	Load	**Location of leak**	**Load**	**Location of leak**
PMMA-PC	On second cycle to 30 kips	Joint	137.05 kips	Shear crack in the precast slab
PPC	137.87 kips	Joint	137.87 kips	Joint
EPC	On second cycle to 50 kips	Joint	On second cycle to 50 kips	Joint
PVE-PC	160.56 kips	Joint	160.56 kips	Joint

In PPC specimen, the first and major leakage occurred near the peak load at 137.87 kips originating at the joint. Unlike PMMA-PC specimen this specimen had preexisting shrinkage cracks developed prior to the tests, despite that, the leakage occurred at higher load. The increased load deepened the preexisting cracks causing debonding of the PPC-precast slab interface. As a result, the leakage occurred at the joint region.

The EPC specimen had the most pronounced and the earliest leakage among all the specimens. Major water leakage occurred during the second cycle to 50 kips signifying debonding between the closure joint material and the precast slab.

For the case of PVE-PC specimen, the first and major water leakage occurred at a load of 160.56 kips, which is significantly higher than that of other specimens, signifying proper bonding

between the closure material and the precast slab. This observation is consistent crack analysis which revealed that no joint interface failure was observed apart from the localized failure directly beneath the loading pad. At such a higher load, several cracks had developed throughout the slabs and properly evaluating the path of leakage was challenging. Nonetheless, the water leakage could be attributed to localized bond failure below the loading pad.

7 SUMMARY AND CONCLUSIONS

7.1 Summary

This study was undertaken to evaluate the feasibility of polymer concrete (PC) as the closure material for longitudinal joints in prefabricated slab bridge. A predominantly experimental approach was used throughout the study with tests performed at material, component, and structural level to ensure comprehensive evaluation under representative field conditions. The overall research program was executed in four interconnected phases, each targeting a key performance aspect on field application of PC. Phase I focused on evaluating the mechanical properties of six different types of commercially available polymer concrete to identify viable PC types based on strength, stiffness, and durability. An additional exercise on engineering the stiffness property of one of the types of PC was also performed in this phase. Phased II focused on the bond behavior of two selected PC types: PMMA-PC and PVE-PC with reinforcing steel and conventional concrete, including the effect of surface preparation and splice detailing of the reinforcement. Phase III investigated the residual mechanical and bond behavior of PMMA-PC and PVE-PC when subjected to thermal cycles and exposed to subzero temperatures. In phase IV, global behavior of large-scale bridge slabs with four different PC types as closure joints was evaluated with realistic loading and reinforcement configuration. The summary of the outcomes of each phase of this study has been presented in the following sections, establishing a foundation for use of PC as closure joint material.

7.1.1 Material Behavior of Polymer Concrete

The material level study demonstrated that PC exhibits rapid early age strength, with gain of more than 58% of its ultimate strength and modulus of elasticity in the first 24 hours. This strength gain is due to the instantaneous nature of the polymerization reaction.

The results show that the compressive behavior of PC is dependent on the resin class, with PMMA-PC and PVE-PC consistently achieving higher compressive strength and stiffness than EPC and PPC. Additionally, the compressive strength of two-inch cubes were found to be 95.60 % of compressive strength of 3 in x 6 in cylinders, indicating that two inch cubes can be reliably used to measure compressive strength.

Although the class of resin determines its compressive behavior, commercial PC of same class namely EPC 1 and EPC 2 exhibited different stress strain behavior. This emphasizes the role of proprietary formulations in the resin and the type and gradation of the aggregate.

Across all PC types, the modulus of elasticity was found to be consistently lower than that of conventional concrete of same compressive strength and the modulus of elasticity of PC can be approximated by **Error! Reference source not found.**. Note that the modulus of elasticity of PC is calculated in ksi for compressive strength provided in psi in Equation 7.1.

$$\mathbf{E = 20\sqrt{f_c'}} \tag{7.1}$$

Flexural strength of PC also develops rapidly with most of the strength gain in the first 24 hours. However, the flexural stiffness continues to increase even though flexural strength does not show proportion increment. Among the different classes of PC, the distinction of higher compressive strength in PMMA-PC and PVE-PC was not observed in the case of flexural strength. Among the PC of same class, EPC 1 and EPC 2 showed significantly different load-deflection response when subjected to flexural loading. This difference is consistent with their behavior under compressive loading, further reinforcing the idea that resin formulation can have significant influence on the mechanical properties of PC. The regression model established in this study estimates the flexural strength of PC as presented in **Error! Reference source not found.**. Note that the modulus of rupture of PC in Equation 7.2 is calculated in psi for compressive strength provided in psi.

$$\mathbf{MOR} = \mathbf{25.60}\sqrt{\mathbf{f_C}'} \quad (7.2)$$

All PC types had a minimum direct tensile strength of 990 psi which is significantly greater than that of conventional concrete of similar compressive strength. The tensile strength of PC (calculated in psi) can be approximated as a function of compressive strength (in psi) as shown in **Error! Reference source not found.**.

$$\mathbf{TS} = \mathbf{15.60}\sqrt{\mathbf{f_C}'} \quad (7.3)$$

Polymer concrete shrinks at a higher rate during the first seven days and the rate of shrinkage decreases after that. PMMA-PC has the least shrinkage among the PC classes used and the maximum shrinkage of polymer concrete is limited to 0.09% after 28 days of construction.

The evaluation of PMMA-PC mixes with different gradation of local aggregates from Reno showed that PC properties can be influenced by the gradation and the quality of aggregates used in the mix. The results indicate that the source of aggregate plays a significant impact on the mechanical properties of PMMA-PC. While larger size of coarse aggregate can lead to higher compressive strength and modulus of elasticity, these improvements depend equally on appropriate gradation of aggregates.

7.1.2 Bond Behavior of Polymer Concrete

The pullout tests results suggest that, within the parametrical limits of tests performed, a minimum embedment length of 3.92 to 4.72 and 7.30 to 9.33 times the diameter of the rebar is required to achieve yield stress in the grade 60 rebars and grade 100 rebars respectively embedded in PC which is higher than that required for UHPC at 3.69 and 6.94 times the diameter of rebar. Similarly, a minimum embedment length of 5.88 to 7.08 and 8.39 to 10.73 times the diameter of rebar is required to achieve ultimate stress in grade 60 and grade 100 rebars embedded in PC respectively

which is also higher than that required for UHPC at 5.53 and 7.99 times the diameter of rebar. Based on the flexural test of PC and UHPC beams with continuous and spliced #4 reinforcement, a non-contact splice length of 10db, 8db, and 8db splice length with 2db clear cover is sufficient in PMMA-PC, PVE-PC, and UHPC respectively to obtain the elastic capacity of the control beams. Additionally, a splice length of 10db is sufficient to achieve the same ultimate strength as control PVE-PC beams. On observing the difference in results from pull out tests and flexural tests, it can also be concluded that the pullout tests with rebar positioned at the center of the specimen cannot accurately predict the required splice length in flexural members where reinforcement is usually placed at the bottom or top of the member with a minimum cover concrete. However, the pull-out test can provide a starting point for flexural studies.

Additionally, contact splices can be used to improve the performance of PC beams. In doing so, the minimum splice length required for lap splice with #4 rebar and 2db clear cover can be reduced to 8db for PMMA-PC. Also, the use of rebar instrumentation can significantly reduce the bond between rebar and polymer concrete.

The bond strength of PMMA-PC and PVE-PC with conventional concrete obtained from the slant shear test is 1350 and 860 psi respectively which is less than that of UHPC measured at 2330 psi. However, the bond strength can be improved significantly by surface preparation and the use of bonding agent up to 2430 psi and 3400 psi, respectively.

A single type of surface preparation, sandpapering in this case, does not necessarily increase bond strength. Sandpapering increases PMMA-CC bond up to 51.36% and PVE-CC bond up to 88.12%. However, on the same surface preparation, the UHPC-CC bond decreased by 63.88%. Among the two bond improvement methods, the use of a bonding agent is more effective than surface preparation and can increase the bond strength up to 66.83% and 271.64% for PMMA-

CC and PVE-CC joints.

7.1.3 Thermal performance of Polymer Concrete

This phase of study investigated the mechanical and bond properties of two types of polymer concrete: PMMA-PC and PVE-PC when subjected to three thermal conditions representing seasonal variation of temperature under service conditions, extreme temperature variation beyond the glass transition temperature and extreme subzero temperature. The summary of the findings of this research is as follows:

Repeated thermal shocks have minimal effect on the compressive strength of both polymethyl methacrylate polymer concrete and polyvinyl ester polymer concrete. However, prolonged exposure to subzero temperature (-25°C) enhances the compressive strength of both PMMA-PC and PVE-PC. Specifically, PMMA-PC and PVE-PC specimens subjected to -25°C had compressive strength of 14,750 psi and 15,300 psi respectively which is an increase of 56.65% and 34.65% over the control specimens of the same age.

The modulus of elasticity (MOE) of both PMMA-PC and PVE-PC is significantly reduced when subjected to thermal shocks. The MOE of PMMA-PC reduced to 2350 ksi and 1740 ksi under T55 and T110 conditions respectively from 2870 ksi of the control specimen. Similarly, the MOE of PVE-PC reduced to 2035 ksi and 1500 ksi under the same conditions from 2575 ksi of the control specimen. Similar to compressive strength, the MOE of PC specimens increase when subjected to prolonged exposure to -25°C. The MOE of PMMA-PC and PVE-PC specimens increased by 10.90% and 30.05% respectively on doing so.

The flexural behavior of polymer concrete has mixed response when subjected to thermal conditions. The T55 and T-25 conditions had minimal effect on the flexural strength of both polymer concrete and surprisingly, the flexural strength of both the PCs increased under T110

conditions. However, the thermal conditions influence the flexural stiffness of both the PCs. Similar to the compressive stiffness, the thermal shocks reduced the flexural stiffness of both the PCs with greater effect due to T110 conditions and exposure to -25°C increased the flexural stiffness.

The bond strength between both PCs and rebar remains largely unaffected by all the thermal conditions. The only notable reduction in the bond strength was on PMMA-PC subjected to T110 conditions, where the maximum rebar stress reduced to 91.82 ksi compared to 102.65 ksi in the control specimen.

The bond between both the PCs and conventional concrete is reduced due to the thermal variations. Although reduced, the PMMA-PC specimens with and without bonding agent along with PVE-PC specimens with bonding agent had a considerable bond strength equal to or greater than 2000 psi under T55 thermal shocks representing service conditions. However, under the same condition, the PVE-PC specimens without primer had severe degradation of bond strength measured at 700 psi with visible cracks developed during the thermal shocks. A further reduction in bond strength was observed at T110 conditions mimicking extreme events, with almost zero strength in PMMA-PC specimen with primer and PVE-PC without primer. In the T-25 condition, both PC had higher bond strength than their control counterparts, suggesting the bond strength is enhanced when exposed to subzero temperatures.

7.1.4 Structural performance of Polymer Concrete

The structural phase of this study evaluated the performance of four large-scale bridge slabs with four types of PC namely PMMA-PC, PPC, EPC and PVE-PC as the closure joint material. All specimens developed flexural capacities higher than the code prescribed ultimate load limit and failed by concrete compression of the top surface of the loaded panel under asymmetric loading

condition and in both the panels under symmetric loading, accompanied by yielding of main longitudinal rebars indicating ductile, flexure-controlled failure. The peak load capacity was about 142 kips for PMMA-PC, PPC and EPC specimens, while the PVE-PC specimen reached around 166 kips. Across all specimens, the presence of shear cracks in the unloaded panels and the flexure-controlled failure of the precast slab demonstrate that the load transferred across the joint up to the peak load confirming that the joints were not the weak link in the system.

In the asymmetrically loaded panels, there was a clear distinction in the initial stiffness between the two specimens with comparable peak load capacities. The PMMA-PC exhibited higher stiffness than the PPC specimen which has been attributed to lower modulus of elasticity and preexisting shrinkage cracks in the PPC specimen. Both specimens remained linear and maintained small differential deflection till the code specified ultimate load after which the differential deflection increased significantly. The uplift of the unloaded panel, which was more pronounced in the PPC slab, indicated that the response of the adjacent slab was governed by the geometric rotation than flexural deformation during the higher load stage of the test.

Under the symmetric loading conditions, both EPC and PVE-PC slabs demonstrated linear load deflection relationship up to onset of cracking past the code specified ultimate load while the peak load capacity of PVE-PC slab was significantly higher than that of the EPC specimen. In both specimens, the differential deflection remained minimal throughout the majority of testing, indicating compatible deformation and effective load transfer across the closure joint.

Observing the water leakage behavior, PMMA-PC and PVE-PC specimens showed major water leakage at relatively high load level and leakage originating from shear cracks in the case of PMMA-PC and localized bond failure beneath the loading pad rather than widespread joint debonding. In contrast, the water leakage in PPC occurred from longitudinal interfacial cracks near

the peak load while the EPC specimen leaked early at around 50 kips. These observations highlight that PMMA-PC and PVE-PC maintained stronger joint integrity while EPC and PPC were more susceptible to interfacial failure, especially at higher load levels.

7.2 Conclusions

This study evaluated the feasibility of polymer concrete as closure joint material with a special focus on longitudinal joints of prefabricated slab bridges through a comprehensive experimental program consisting of PC characterization at material and component level along with large-scale structural testing. The results collectively demonstrate the viability of PC as an alternative to cementitious and ultra-high performance concrete (UHPC) for prefabricated bridge element system (PBES) applications and draw the following main conclusions:

- At the material level, PC exhibited rapid strength and stiffness growth in addition to high tensile and flexural capacity. Among the PC classes, PMMA-PC and PVE-PC consistently achieved higher or comparable performance to EPC and PPC. EPC and PPC showed variability in their performance based on resin formulation and proprietary composition. Based on the extended material study focused on compressive strength and modulus of elasticity of PMMA-PC, its performance can be enhanced by carefully selecting the type and generation of the coarse aggregates.
- Based on component level tests performed on PMMA-PC and PVE-PC, PC develops adequate bond strength with rebar although required lengths are slightly greater than UHPC. A non-contact splice length in the range of eight to ten times the diameter of rebar is required to provide sufficient load transfer between the rebars, while contact splicing can further enhance the performance. The bond between PC and conventional concrete is adequate for joint applications and can be significantly increased by using proper surface preparation and

appropriate primer as a bonding agent.

- Thermal studies on PMMA-PC and PVE-PC showed that PC maintains stable compressive strength and rebar bond capacity when subjected to service and extreme level thermal shocks with increased flexural strength in some cases under similar conditions. However, compressive, and flexural stiffness of PC decrease when subjected to such thermal variations. With appropriate selection of primer and surface preparation, the bond between PC and conventional concrete can be preserved despite these thermal variations. Under prolonged exposure to subzero temperature, PC performance improved across all measured properties.
- The large-scale structural tests confirmed that PC closure joints provide effective load transfer and maintained deformation capacities up to and beyond code specified capacities. All specimens achieved flexure dominated failure governed by failure of the precast panels, confirming that joints were not the weak link in the structure. The load deflection relationships, water leakage pattern and the crack patterns further showed that PMMA-PC and PVE-PC offered greater stiffness and better overall performance in terms of load transfer and water retention whereas the EPC specimen experienced early water leakage indicating interfacial bond failure and both EPC and PPC displayed comparatively lower stiffness.

7.3 Recommendations for Future Work

While this study addresses the material, component and structural behavior of PC for bridge joint application, additional research is needed further to refine its performance characterization and support broader implementation. Key areas that require further exploration at material & component level as well as structural level are summarized below:

- The material level characterization may be expanded to include time dependent properties such as creep and shrinkage under realistic restraint conditions where PC is bonded to conventional

concrete at joint interface.

- The influence of surface preparation on PC-Conventional concrete bond may be studied across the thermal exposure conditions.
- The distinction between residual and in-situ material properties after thermal exposure can be further explored to better understand the temperature dependent behavior.
- Experimental study separating the effect of peak exposure temperature and cyclic thermal variation may help clarify whether the reduced bond strength is primarily associated with material degradation or due to thermal stresses arising from variation in coefficient of thermal expansion thereby informing whether mitigation efforts should be more appropriate in material development level or through structural detailing.
    - The combined influence of joint geometry and surface preparation on load transfer may be further studied under service and environmental loads.
    - The large-scale testing may be extended to include effects of prestressing to access the joint performance at field conditions.
    - The applicability of PC in other bridge applications such as girder connections, and segmental bridge systems may be explored.
    - Field evaluation can be considered in pilot projects with embedded instrumentation and sensors to monitor joint performance under realistic service and environmental loads with use of innovative methods like digital image correlation.
    - Evaluation of a larger population of existing bridge decks incorporating PC as overlay material from a structural perspective can provide a valuable insight into long term bond performance at PC-Conventional concrete interface under environmental exposure.

REFERENCES

[1] “Tables of Frequently Requested NBI Information - National Bridge Inventory - Bridge Inspection - Safety Inspection - Bridges & Structures - Federal Highway Administration.” Accessed: Jan. 05, 2025. [Online]. Available: https://www.fhwa.dot.gov/bridge/britab.cfm

[2] “A comprehensive assessment of America’s infrastructure.” [Online]. Available: www.infrastructurereportcard.org

[3] “Environmental Review Toolkit.” Accessed: Dec. 17, 2025. [Online]. Available: https://www.environment.fhwa.dot.gov/env_topics/historic_pres/post1945_engineering/this_bridge.aspx

[4] “NCDOT: Reinforced Concrete Slab Bridges.” Accessed: Dec. 17, 2025. [Online]. Available: https://www.ncdot.gov/initiatives-policies/Transportation/bridges/historic-bridges/bridge-types/Pages/reinforced-slab.aspx?utm_source=chatgpt.com

[5] “Bespoke Concrete Bridges | Easy Bridge Building | Poundfield Precast.” Accessed: Feb. 03, 2025. [Online]. Available: https://poundfield.com/bespoke-precast-concrete/civils-infrastructure/bridges/

[6] C. Vipulanandan, N. Dharmarajan, and E. Ching, “Mechanical behaviour of polymer concrete systems,” 1988.

[7] C. Vipulanandan and N. Dharmarajan, “Flexural behavior of polyester polymer concrete,” Cem Concr Res, vol. 17, no. 2, pp. 219–230, Mar. 1987, doi: 10.1016/0008-8846(87)90105-0.

[8] S. Acharya, M. A. Moustafa, and S. Shoaib, “Tensile characteristics of polymethyl methacrylate polymer concrete under different strain rates,” Case Studies in Construction Materials, vol. 22, p. e04759, Jul. 2025, doi: 10.1016/J.CSCM.2025.E04759.

[9] M. Abokifa, M. A. Moustafa, and A. M. Itani, “Comparative structural behavior of bridge deck panels with polymer concrete and UHPC transverse field joints,” Eng Struct, vol. 247, Nov. 2021, doi: 10.1016/j.engstruct.2021.113195.

[10] M. Abokifa and M. A. Moustafa, “Experimental behavior of poly methyl methacrylate polymer concrete for bridge deck bulb tee girders longitudinal field joints,” Constr Build

Mater, vol. 270, Feb. 2021, doi: 10.1016/j.conbuildmat.2020.121840.

[11] J. T. San-José, I. J. Vegas, and Moisés Frías, “Mechanical expectations of a high performance concrete based on a polymer binder and reinforced with non-metallic rebars,” Constr Build Mater, vol. 22, no. 10, pp. 2031–2041, Oct. 2008, doi: 10.1016/j.conbuildmat.2007.08.001.

[12] W. Ferdous et al., “Optimal design for epoxy polymer concrete based on mechanical properties and durability aspects,” Constr Build Mater, vol. 232, Jan. 2020, doi: 10.1016/j.conbuildmat.2019.117229.

[13] N. J. Jin, J. Yeon, S. H. Min, and K. S. Yeon, “Strength Developments and Deformation Characteristics of MMA-Modified Vinyl Ester Polymer Concrete,” Int J Concr Struct Mater, vol. 12, no. 1, Dec. 2018, doi: 10.1186/s40069-018-0232-0.

[14] J. P. Gorninski, D. C. Dal Molin, and C. S. Kazmierczak, “Comparative assessment of isophtalic and orthophtalic polyester polymer concrete: Different costs, similar mechanical properties and durability,” Constr Build Mater, vol. 21, no. 3, pp. 546–555, Mar. 2007, doi: 10.1016/j.conbuildmat.2005.09.003.

[15] M. Nodehi, “Epoxy, polyester and vinyl ester based polymer concrete: a review,” Innovative Infrastructure Solutions, vol. 7, no. 1, Feb. 2022, doi: 10.1007/s41062-021-00661-3.

[16] “Polymer Concrete: Guidelines for Structural Applications,” 2019, [Online]. Available: www.concrete.org

[17] M. A. Saleem, A. Mirmiran, J. Xia, and K. Mackie, “Development Length of High-Strength Steel Rebar in Ultrahigh Performance Concrete,” Journal of Materials in Civil Engineering, vol. 25, no. 8, pp. 991–998, Aug. 2013, doi: 10.1061/(ASCE)MT.1943-5533.0000571/ASSET/E942C7BD-C6C1-4B83-9AE7-2FF35532A2C1/ASSETS/IMAGES/LARGE/FIGURE13.JPG.

[18] B. Graybeal, “Bond Behavior of Reinforcing Steel in Ultra-High Performance Concrete,” 2014.

[19] B. Zhang, J. Yu, W. Chen, J. Chen, H. Li, and J. Niu, “Interface Shear Failure Behavior Between Normal Concrete (NC) and Ultra-High Performance Concrete (UHPC),” Int J Concr Struct Mater, vol. 18, no. 1, Dec. 2024, doi: 10.1186/s40069-023-00657-6.

[20] S. Feng, H. Xiao, and Y. Li, “Influence of interfacial parameters and testing methods on UHPC–NSC bond strength: Slant shear vs. direct tensile testing,” Cem Concr Compos, vol. 131, Aug. 2022, doi: 10.1016/j.cemconcomp.2022.104568.

[21] I. Mantawy, R. Chennareddy, M. Genedy, and M. R. Taha, “Polymer concrete for bridge deck closure joints in accelerated bridge construction,” Infrastructures (Basel), vol. 4, no. 2, Jun. 2019, doi: 10.3390/infrastructures4020031.

[22] R. H. Haddad and R. M. Abendeh, “Effect of thermal cycling on bond between reinforcement and fiber reinforced concrete,” Cem Concr Compos, vol. 26, no. 6, pp. 743–752, Aug. 2004, doi: 10.1016/S0958-9465(03)00083-0.

[23] M. S. Khan, J. Prasad, and H. Abbas, “Bond strength of RC beams subjected to cyclic thermal loading,” Constr Build Mater, vol. 38, pp. 644–657, Jan. 2013, doi: 10.1016/J.CONBUILDMAT.2012.09.018.

[24] M. S. Khan, J. Prasad, and H. Abbas, “Shear strength of RC beams subjected to cyclic thermal loading,” Constr Build Mater, vol. 24, no. 10, pp. 1869–1877, Oct. 2010, doi: 10.1016/J.CONBUILDMAT.2010.04.016.

[25] M. An, H. Huang, Y. Wang, and G. Zhao, “Effect of thermal cycling on the properties of high-performance concrete: Microstructure and mechanism,” Constr Build Mater, vol. 243, p. 118310, May 2020, doi: 10.1016/J.CONBUILDMAT.2020.118310.

[26] H. Ma, S. Zhang, H. Fu, S. Li, M. Su, and C. Wu, “Effect of thermal cycling on the mechanics and microstructure of ultra-high performance concrete,” Constr Build Mater, vol. 424, p. 135878, Apr. 2024, doi: 10.1016/J.CONBUILDMAT.2024.135878.

[27] B. G. C Lee, T. S. Shih, K. C. Chang, and A. Member, “Mechanical Properties of High-Strength Concrete at Low Temperature,” Journal of Cold Regions Engineering, vol. 2, no. 4, pp. 169–178, Dec. 1988, doi: 10.1061/(ASCE)0887-381X(1988)2:4(169).

[28] F. S. Rostásy, U. Schneider, and G. Wiedemann, “Behaviour of mortar and concrete at extremely low temperatures,” Cem Concr Res, vol. 9, no. 3, pp. 365–376, May 1979, doi: 10.1016/0008-8846(79)90129-7.

[29] S. Yamane, H. Kasami, and T. Okuno, “Properties of Concrete at Very Low Temperatures,” Special Publication, vol. 55, pp. 207–222, Aug. 1978, doi: 10.14359/6615.

[30] F. S. Rostásy and G. Wiedemann, “Stress-strain-behaviour of concrete at extremely low temperature,” Cem Concr Res, vol. 10, no. 4, pp. 565–572, Jul. 1980, doi: 10.1016/0008-8846(80)90100-3.

[31] T. Miura, “The properties of concrete at very low temperatures,” Mater Struct, vol. 22, no. 4, pp. 243–254, Jul. 1989, doi: 10.1007/BF02472556/METRICS.

[32] Y. Huo, H. Sun, D. Lu, Z. Chen, and Y. Yang, “Mechanical properties of concrete at low and ultra-low temperatures- a review,” Journal of Infrastructure Preservation and Resilience, vol. 3, no. 1, pp. 1–15, Dec. 2022, doi: 10.1186/S43065-022-00063-4/FIGURES/9.

[33] I. T. Roh, K. C. Jung, S. H. Chang, and Y. H. Cho, “Characterization of compliant polymer concretes for rapid repair of runways,” Constr Build Mater, vol. 78, pp. 77–84, Mar. 2015, doi: 10.1016/j.conbuildmat.2014.12.121.

[34] J. M. L. Dos Reis, “Effect of temperature on the mechanical properties of polymer mortars,” Materials Research, vol. 15, no. 4, pp. 645–649, Jul. 2012, doi: 10.1590/S1516-14392012005000091.

[35] R. Letsch, “Polymer concrete with metallic and non-metallic reinforcement,” in 110th International congress on polymers in concrete, Honolulu, Hawaii, 2001.

[36] M. C. S. Ribeiro, P. R. Nóvoa, A. J. M. Ferreira, and A. T. Marques, “Flexural performance of polyester and epoxy polymer mortars under severe thermal conditions,” Cem Concr Compos, vol. 26, no. 7, pp. 803–809, Oct. 2004, doi: 10.1016/S0958-9465(03)00162-8.

[37] M. M. Shokrieh, M. Heidari-Rarani, M. Shakouri, and E. Kashizadeh, “Effects of thermal cycles on mechanical properties of an optimized polymer concrete,” Constr Build Mater, vol. 25, no. 8, pp. 3540–3549, Aug. 2011, doi: 10.1016/J.CONBUILDMAT.2011.03.047.

[38] K. Jafari, F. Heidarnezhad, O. Moammer, and M. Jarrah, “Experimental investigation on freeze-thaw durability of polymer concrete,” Frontiers of Structural and Civil Engineering, vol. 15, no. 4, pp. 1038–1046, Aug. 2021, doi: 10.1007/s11709-021-0748-2.

[39] Y. Tan, K. Freeseman, and K. Wang, “Long-Term Performance of Overlays: Thin Epoxy vs. Traditional Rigid Overlay,” Ames, Iowa, 2020. [Online]. Available: https://www.cptechcenter.org/wp-content/uploads/2020/02/long_term_perf_of_overlays_thin_epoxy_vs_traditional_rigid_w

_cvr.pdf

[40] M. Abokifa and M. A. Moustafa, “Mechanical characterization and material variability effects of emerging non-proprietary UHPC mixes for accelerated bridge construction field joints,” Constr Build Mater, vol. 308, Nov. 2021, doi: 10.1016/j.conbuildmat.2021.125064.

[41] M. Abokifa and M. A. Moustafa, “Full-scale testing of non-proprietary ultra-high performance concrete for deck bulb tee longitudinal field joints,” Eng Struct, vol. 243, Sep. 2021, doi: 10.1016/j.engstruct.2021.112696.

[42] M. Abokifa and M. A. Moustafa, “Mechanical characterization and material variability effects of emerging non-proprietary UHPC mixes for accelerated bridge construction field joints,” Constr Build Mater, vol. 308, p. 125064, Nov. 2021, doi: 10.1016/J.CONBUILDMAT.2021.125064.

[43] M. Aboukifa, M. A. Moustafa, and M. S. Saiidi, “Seismic response of precast bridge columns with composite non-proprietary UHPC filled ducts ABC connections,” Compos Struct, vol. 274, Oct. 2021, doi: 10.1016/j.compstruct.2021.114376.

[44] M. Tazarv and M. S. Saiidi, “UHPC-filled duct connections for accelerated bridge construction of RC columns in high seismic zones,” Eng Struct, vol. 99, pp. 413–422, Sep. 2015, doi: 10.1016/j.engstruct.2015.05.018.

[45] M. Aboukifa, M. Abokifa, S. Shoaib, and M. A. Moustafa, “Seismic performance of precast columns with polymer concrete filled ducts accelerated bridge construction connections: An experimental study,” Eng Struct, vol. 335, p. 120358, Jul. 2025, doi: 10.1016/J.ENGSTRUCT.2025.120358.

[46] T. Thonstad and C. Donohoe, “Exploring Fiber-Reinforced Polymer Concrete for Accelerated Bridge Construction Applications,” May 2024.

[47] “Test Methods for Compressive Strength of Chemical-Resistant Mortars, Grouts, Monolithic Surfacings, and Polymer Concretes,” Jun. 01, 2023, ASTM International, West Conshohocken, PA. doi: 10.1520/C0579-23.

[48] “Test Method for Static Modulus of Elasticity and Poissons Ratio of Concrete in Compression,” Apr. 01, 2022, ASTM International, West Conshohocken, PA. doi: 10.1520/C0469_C0469M-22.

[49] “Test Method for Flexural Strength of Concrete (Using Simple Beam with Third-Point Loading),” Mar. 01, 2022, ASTM International, West Conshohocken, PA. doi: 10.1520/C0078_C0078M-22.

[50] “Test Method for Linear Shrinkage and Coefficient of Thermal Expansion of Chemical-Resistant Mortars, Grouts, Monolithic Surfacings, and Polymer Concretes,” Jul. 01, 2018, ASTM International, West Conshohocken, PA. doi: 10.1520/C0531-18.

[51] “Test Method for Abrasion Resistance of Concrete or Mortar Surfaces by the Rotating-Cutter Method,” Oct. 01, 2019, ASTM International, West Conshohocken, PA. doi: 10.1520/C0944_C0944M-19.

[52] “AASHTO LRFD Bridge Design Specifications, 9th Edition,” American Association of State Highway and Transportation Officials, 2020, Accessed: Nov. 13, 2024. [Online]. Available: www.transportation.org

[53] “Test Method for Bond Strength of Epoxy-Resin Systems Used With Concrete By Slant Shear,” Jun. 01, 2020, ASTM International, West Conshohocken, PA. doi: 10.1520/C0882_C0882M-20.

[54] “American Concrete Institute (ACI), Guide for the selection of materials for the repair of concrete,” ACI 546.3R-06, Farmington Hills, MI, 2006.